UNIVERSIDADE ESTADUAL PAULISTA
Instituto de Geociências e Ciências Exatas
Câmpus de Rio Claro

ANA CAROLINA FRANCIOSI LUCHETTI

Vulcanologia e Petrologia das Rochas Vulcânicas Ácidas da Província Magmática do Paraná.

Tese de Doutorado apresentada ao Instituto de Geociências e Ciências Exatas do Câmpus de Rio Claro, da Universidade Estadual Paulista "Júlio de Mesquita Filho", para obtenção do título de Doutor em Geologia Regional.

Orientador: Prof. Dr. Antonio José Ranalli Nardy

RIO CLARO – SP
2015

551.21 Luchetti, Ana Carolina Franciosi
L936v Vulcanologia e petrologia das rochas vulcânicas ácidas da Província Magmática do Paraná / Ana Carolina Franciosi Luchetti. - Rio Claro, 2015
118 f. : il., figs., tabs.

Tese (doutorado) - Universidade Estadual Paulista, Instituto de Geociências e Ciências Exatas
Orientador: Antonio José Ranally Nardy

1. Vulcões. 2. Erupções ácidas. 3. Formação Serra Geral. 4. Vulcanismo ácido. 5. Membro Chapecó. 6. Membro Palmas. I. Título.

Ficha Catalográfica elaborada pela STATI - Biblioteca da UNESP
Campus de Rio Claro/SP

AGRADECIMENTOS

Muito especialmente, desejo agradecer ao meu orientador Prof. Antonio José Nardy, pela disponibilidade, atenção dispensada, paciência, dedicação e profissionalismo ... um Muito Obrigada.

A todos os Professores pesquisadores colaboradores com esse projeto, Fábio Machado, José Madeira, Marcelo Arnósio, Guilherme Gualda, Darren Gravley e Francisco Negri, obrigada pelo grande conhecimento passado.

À minha família, pelo incentivo, compreensão e encorajamento, durante todo este período.

Ao meu namorado Douglas, pela paciência e ajuda em muitos momentos.

Ao colega Nuno, pela grande ajuda com questões da tese.

Aos alunos da graduação, Juliane, Vítor, Juan, Taís, Rômulo, Letícia e Isabela, pelos trabalhos desenvolvidos e que fizeram parte desta tese.

A todos os técnicos do Depto de Petrologia e Metalogenia, sem os quais o trabalho ficaria inviável.

Aos meus amigos de sempre e aos que conquistei durante a pós-graduação, obrigada pela força e momentos de descontração.

Resumo

Os traquitos e dacitos do tipo Chapecó (ATC) e dacitos e riolitos do tipo Palmas (ATP), de idade cretácica, compõem 2,5% dos ~ 800.000 km^3 de lavas da Província Magmática do Paraná (PMP) geradas anteriormente à quebra do Gondwana. Seções colunares estudadas ao longo da PMP mostram que as rochas ácidas encontram-se na parte superior das sequências, sobrepostas aos basaltos toleíticos e, em alguns perfis da região central da PMP, entre os municípios de Guarapuava (PR) e Campina da Alegria (SC), as rochas ATC se sobrepõem às ATP. Na região sul, entre os municípios de Sobradinho e Soledade (RS), e ao longo da rodovia Rota do Sol (BR-453) (RS), assim como na região central, os depósitos revelam ignimbritos de alto a extremamente alto grau de soldadura (reoignimbritos). Esses reoignimbritos (*sheet-like*) formam extensos platôs (dezenas a centenas de km) de depósitos maciços, monótonos, variavelmente desplacados (juntas) e com brechas peperíticas locais. Bandamento por *blobs* de vidro (lentes escuras microcristalinas) dispostos em material esbranquiçado é característico dos depósitos ATC e ATP. A matriz está intensamente devitrificada, localmente com raros *fiammes* e *glass shards* extremamente deformados. Na região sul, subjacentes aos reoignimbritos, também ocorrem lava-domos e/ou *coulées*, em cujos afloramentos há aglomerados de pitchstones com base e exterior autobrechados, separados localmente por peperitos, e/ou corpos devitrificados com juntas cerradas (*sheeting joints*) concêntricas. Ainda na região sul, depósitos bandados a complexamente dobrados de rochas ATP ocorrem na base da sequência ácida. Esses depósitos podem representar lava-domos, ignimbritos *lava-like* ou mesmo fluxos de lava *fountain-feed*. Além disso, esses alforamentos, assim como os dos lava-domos ocorrem alinhados em uma mesma direção, podendo indicar fissuras que alimentaram o vulcanismo ácido na PMP, cuja direção é paralela à linha de costa, possivelmente refletindo a tectônica extensional que levou à quebra do Gondwana. Temperaturas de cristalização estimadas para plagioclásio e piroxênios indicam valores elevados (ATC: 1030 ±4°C – plagioclásio, 969 ±18°C – piroxênio; ATP: 976 ±2°C a 1040 ±2°C – plagioclásio), estando os piroxênios das rochas ATP em equilíbrio com magma básico a andesítico, com T de cristalização de 1134 ±18°C e 1100 ±11°C respectivamente. Além

disso, as profundidades de cristalização dos mesmos revelam um sistema *plumbing* raso abaixo da Bacia do Paraná (ATC: 4.3 ±0.9 kbar – plagioclásio, 3.3 ±2.4 kbar – piroxênio; ATP: 2.6 ±0.7 a 1.1 ±1.5 – plagioclásio, 2.8 ±1.1 a 1.0 ±1 kbar – piroxênio). Assim, os dados obtidos mostram que os lava-domos representam fluxos degaseificados de pequeno volume, intermitentes, limitados por corpos magmáticos iniciais, de pequeno volume. Os reoignimbritos extensos e volumosos expressam erupções que drenaram corpos magmáticos maiores, regidas por processos rasos resultantes de descompressão rápida. As altas temperaturas foram responsáveis pelas baixas viscosidades e consequente aglutinação/coalescência dos piroclastos (viscosidades magmáticas estimadas em $10^{4.31\text{-}6.39}$ Pa s para ATC, e $10^{4.27\text{-}7.22}$ Pa s para ATP) e, aliado ao baixo conteúdo de água (médias de 0.6 ±0.2 e 1.2 ±0.3 %H_2O), originaram erupções do tipo *boil-over* (baixas colunas de colapso e eficiente retenção de calor) e correntes piroclásitcas quentes e progressivas durante a deposição.

Palavras-chave: Formação Serra Geral, Vulcanismo Ácido, Membro Chapecó, Membro Palmas

Abstract

The Cretaceous Chapecó trachydacites-dacites (ATC) and Palmas dacites-rhyolites (ATP) make up 2.5% of the ~ 800.000 km^3 of lava of the Paraná Magmatic Province (PMP), prior to Gondwana breakup. Columnar sections along PMP show the silicic rocks lying on top of the volcanic sequences, overlapping tholeiitic basalts. Furthermore, in some sections of central PMP, between the Guarapuava (PR) and Campina da Alegria (SC) towns, the ATC rocks overlap those of ATP. In the southern region, between the Sobradinho and Soledad (RS) towns, and along the Rota do Sol highway (BR-453) (RS), as well as in the central region, the deposits comprise high to extremely high grade ignimbrites (rheoignimbrites). They form extensive plateaus (tens to hundreds of km) of sheet-like, monotonous, variably horizontally jointed and with local peperitic breccia deposits. Glass blobs (microcrystalline dark lenses) arranged in whitish material make up an intrinsic eutaxitic texture (or banding). The groundmass is through devitrified, with local rare flattened and/or extremely stretched fiamme and shards. In the southern area lava domes and/or coulées also appear underlying rheoignimbrites. Pitchstones clusters with brecciated base and exterior, locally separated by peperites, and/or concentrically sheeting jointed, devitrified outcrops. Flow banded to complexly folded ATP rocks occur at the base of the silicic sequence. These rocks are ambiguous and may represent lava domes, lava-like ignimbrites or, even, fountain-feed lava flows. Moreover, its outcrops, as well as those of lava domes follow a northeast-trend, parallel to the coastline, which may indicate feeder fissures and also reflect the extensional setting that led to the Gondwana breakup. Crystallization temperatures estimated for plagioclase and pyroxene indicate high values (ATC: 1030 ±4°C – plagioclase, 969 ±18°C – pyroxene; ATP: 976 ±2°C a 1040 ±2°C – plagioclase), with the ATP pyroxenes in equilibrium with basic-to-intermediate magma (1134 ±18°C e 1100 ±11°C, respectively). Furthermore, its crystallization depths reveal a shallow plumbing system beneath the Paraná Basin (ATC: 4.3 ±0.9 kbar – plagioclase, 3.3 ±2.4 kbar – pyroxene; ATP: 2.6 ±0.7 a 1.1 ±1.5 – plagioclase, 2.8 ±1.1 a 1.0 ±1 kbar – pyroxene). Thus, in a proposed model, the lava domes represent small volume, intermittent, degassed flows, limited by small initial magmatic bodies. The extensive and voluminous rheoignimbrites

express eruptions driven by shallow processes resulting from rapid decompression, draining largest magmatic bodies. High temperatures were responsible for the low viscosities and consequent agglutination/coalescence of the pyroclasts (magmatic viscosities estimated in $10^{4.31-6.39}$ Pa s for ATC, and $10^{4.27-7.22}$ Pa s for ATP). This, coupled with low water contents (average 0.6 ±0.2 and 1.2 ±0.3% H_2O), originated boil-over eruptions (low collapse columns and little heat loss) and hot pyroclastic density currents.

Keywords: Serra Geral Formation, Silicic Volcanism, Chapecó Member, Palmas Member.

Ana Carolina Franciosi
Luchetti

Vulcanologia e Petrologia das Rochas Vulcânicas Ácidas da Província Magmática do Paraná.

Tese de Doutorado apresentada ao Instituto de Geociências e Ciências Exatas do Câmpus de Rio Claro, da Universidade Estadual Paulista "Júlio de Mesquita Filho", como parte dos requisitos para obtenção do título de Doutor em Geologia Regional.

Comissão Examinadora

Prof. Dr. Antonio J. R. Nardy

Prof. Dr. Marcos Aurélio F. De Oliveira

Prof. Dr. Valdecir de Assis Janasi

Profa. Dra. Cristina Maria Pinheiros de Campos

Prof. Dr. José Eduardo de Oliveira Madeira

Rio Claro, SP, 30 de Outubro de 2015

SUMÁRIO

Chapter 1: Peperites and sedimentary deposits within the silicic volcanic sequences of the Paraná Magmatic Province, Brazil

(published in Solid Earth, 5, 121-130, 2014)

A. C. F. Luchetti[1], A. J. R. Nardy[1], F. B. Machado[2], J. E. O. Madeira[3], J. M. Arnosio[4]

1 Instituto de Geociências e Ciências Exatas, Universidade Estadual Paulista, Rio Claro, SP, 13506-900, Brazil, caroluch@rc.unesp.br, nardy@rc.unesp.br

[2] Departamento de Ciências Exatas e da Terra, Universidade Federal de São Paulo, São Paulo, SP, 09920-540, Brazil, fabio.machado@unifesp.br

[3] Departamento de Geologia da Faculdade de Ciências (GeoFCUL), Instituto Dom Luiz, Universidade de Lisboa, Portugal, jmadeira@fc.ul.pt

[4] Instituto Geonorte, Facultad de Ciencias Naturales, Universidad Nacional de Salta, Salta, Argentina, marnosio@unsa.edu.ar

Abstract

The PMP (Paraná Magmatic Province) is characterized by lava flows of the Early Cretaceous Serra Geral Formation which covers about 75 % of the Paraná Basin (southern and southeastern Brazil), composed of a thick (up to 1600 m) volcanic sequence formed by a succession of petrographically and geochemically distinct units of basic and silicic composition. The whole package must have been emplaced during approximately 3 million years of nearly uninterrupted activity. A few aeolian sandstone layers, indicating arid environmental conditions (the Botucatu Formation), are interlayered in the lower basalts. Above the basalts, the Palmas and Chapecó Members are composed of silicic volcanic rocks (quartz latites, dacites, rhyodacites and rhyolites) and basalts. This paper presents new evidence of sedimentation episodes separating silicic volcanic events, expressed by the occurrence of sedimentary deposits. Interaction between the volcanic bodies and the coeval unconsolidated sediments formed peperites. The sediments were observed between basaltic lava flows and silicic rocks or interlayered in the Palmas-type rocks, between the Chapecó-type rocks and overlying basaltic flows, between silicic bodies of the Palmas and Chapecó types, and interlayered within Palmas-type units. The observed structures indicate that the sediments were still wet and unconsolidated, or weakly consolidated, at the time of volcanism, which, coupled with the sediment features, reflect environmental conditions that are different from those characterizing the Botucatu arid conditions.

1 INTRODUCTION

The Early Cretaceous Serra Geral Formation is the result of a major volcanic phase that covered about 917,000 km^2, about 60% of the surface of the Paraná Basin (FRANK *et al*., 2009; Fig. 1). Three main petrographic types can be distinguished from macroscopic observation of these rocks. The most common corresponds to basalt presenting predominant intergranular texture and its variations (subofitic, intersertal, hialofitic, etc). The other two types, corresponding to silicic rocks, present massive and aphiric textures (Palmas type - ATP) and porphyritic textures (Chapecó type - ATC).

Macroscopic characteristics allowed easy separation in the field of these two members of the Serra Geral Formation and their geological mapping (BELLIENI *et al*., 1983; PICCIRILLO et al., 1988). The Palmas and Chapecó rock-types occur in association with basaltic flows that are more frequent near the top and bottom of these two lithostratigraphic units. Geological mapping also shown that Palmas and Chapecó Members cover 63,000 km^2, in the states of Paraná, Santa Catarina, and Rio Grande do Sul. The volume of the two members amounts to approximately 14,500 km^3, which corresponds to 2.5% of the total volume of the Serra Geral Formation (NARDY *et al*., 2002, 2008). Geochronological dating by $^{40}Ar/^{39}Ar$ shows that the age of volcanic rocks of the Serra Geral Formation ranges from 133.6 to 131.5 Ma in its northern sector, and from 134.6 to 134.1 Ma in the south (RENNE *et al*., 1992, 1996a, b; TURNER *et al*., 1994; ERNEST *et al*., 1999, 2002; MINCATO *et al*., 2003; THIEDE & VASCONCELOS, 2010; PINTO *et al*., 2010). More recently, Janasi *et al*. (2011), using U/Pb ratios from baddeleyite/zircon crystals determined by ID-TIMS from rocks of the Chapecó Member, obtained an age of 134.3 ± 0.8 Ma, compatible with the previous age determinations. However, ages obtained in the dominant basaltic flows indicate duration of the volcanism of around 3 Ma, which is consistent with paleomagnetic data presented by Ernesto & Marques (2004).

Up to now, the presence of sediments (sandstones of the Botucatu Formation) intercalated in the volcanic sequence was only reported in the lower basaltic pile. These consist of sand bodies presenting aeolian structures such as bypass surfaces, single-dunes, sand-filled cracks, multi-dune ergs (JERRAM & STOLLHOFEN, 2002; PETRY *et al*., 2007; WAICHEL *et al*., 2008), representing a desert environment that persisted

during the voluminous initial phase of basaltic volcanism. In this work, the occurrence of sedimentation and development of associated peperites in the final stage of the PMP volcanic event, is presented. The sediments, dominantly sandy-silty, and unrelated to the Botucatu Formation, indicate a change in the environmental conditions in the Paraná Basin, and attest to the occurrence of significant periods of quiescence during the final stages of the magmatic activity.

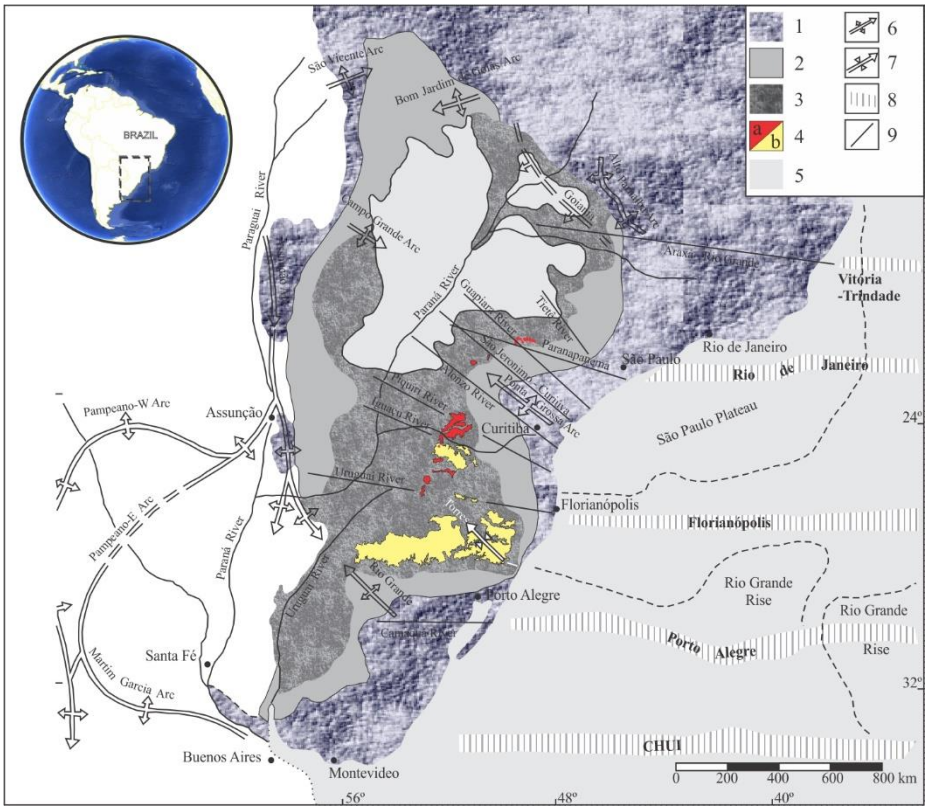

Fig. 1 **-** Map of the Paraná Basin with the location of the acidic members of the Serra Geral Formation according to Nardy *et al*. (2008). Legend: 1- Embasement; 2- Pre-volcanic sedimentary rocks; 3- Basalts (Serra Geral Formation); 4– acidic (a) Chapecó and (b) Palmas Members (Serra Geral Formation); 5- Sedimentary post-volcanic sequences (Bauru Basin); 6- Anticline structures; 7- Syncline structures; 8- Oceanic lineaments; 9- Continental lineaments.

2 PETROGRAPHIC AND GEOCHEMICAL ASPECTS OF SILICIC VOLCANIC ROCKS

The Palmas type silicic volcanic rocks (ATP) are characterized by light-gray to brownish red color, hypohyaline-holohyaline aphyric textures with a striking salt-and-pepper aspect. The mineralogy is composed of dominant *micro-phenocrysts* (granularity smaller than 0.2 mm) of plagioclase (labradorite) comprising up to 16% of the total volume of the rock, 11% of augite, 3% of pigeonite, 5% of magnetite, and less than 1% of apatite. These crystals may exhibit rapid cooling structures (quenching), developing skeletal, lath, and hollow shapes, or swallowtail terminations. The matrix reaches 63% of the rock volume on average, and is composed of dark-brown slightly birefringent glass, characterized by a granophyric texture of abundant microlites, and alkali feldspar and quartz intergrowth, that surrounds the crystal phases. When holohyaline (pichstone), these rocks show black color and prominent conchoidal fractures. However, due to its amorphous nature, the glass alters easily and thus in most outcrops the rock is completely weathered, presenting a brownish color and (often resembling sedimentary deposits) dotted with abundant vesicles and quartz-filled amygdales up to 10 mm in length.

The Chapecó type silicic volcanic rocks (ATC) are porphyritic, with an average of 24% of plagioclase phenocrysts up to 2 cm long, in a light gray (when fresh) to brown (when weathered) aphanitic matrix. The mineralogy consists of euhedral andesine phenocrysts in a matrix composed of 4.5% of augite, 2.2% of pigeonite, 3.7% of magnetite, and 1.7% of apatite (average composition) surrounded by quartz and alkali feldspar fabric in felsitic, locally granophyric, arrangement (vitrophyric texture).

Silicic volcanic rocks chemical compositions of the Paraná Magmatic Province, according to Nardy et al. (2008), show two main groups which may be observed in a R1xR2 diagram (Figure 2, De La Roche et al., 1980). The first one, Low-Ti suite, belongs to tholeiitic field (tholeiitic basalts, andesi-basalts and andesites) associated to Palmas type silicic volcanic rocks, the latter plot in the rhyodicite and rhyolite field. The second group, High-Ti suite is displaced towards the transitional field (transitional basalt, lati-basalt and latites). The Chapecó type silicic volcanic rocks belong to this

group in the rhyodacite and quartz latite fields (Fig. 2). The bulk-rock representative compositions for both Palmas and Chapecó types are listed in table 1.

According to Bellieni et al. (1984a) the chemistry of the volcanic rocks and their spacial distribution allow the Paraná basin to be schematically subdivided into three main regions: (1) southern, encompassing the tholeiitic suite in the southern Uruguay River alignment; (2) northern, where tholeiitic-transitional rocks occur in the northern Piquiri River alignment; and (3) central, located between Piquiri and Uruguay Rivers alignments, where both rock types are present, (Fig. 1). The spatial distribution of the tholeiitic – ATP and transitional-tholeiitic-ATC suites indicates that acidic volcanic rocks may have derived from the associated basalts, or ATC melts are derived from tholeiitic-transitional basalts and ATP from tholeiitic basalts as suggested by Bellieni et al. (1986) and Garland et al. (1995).

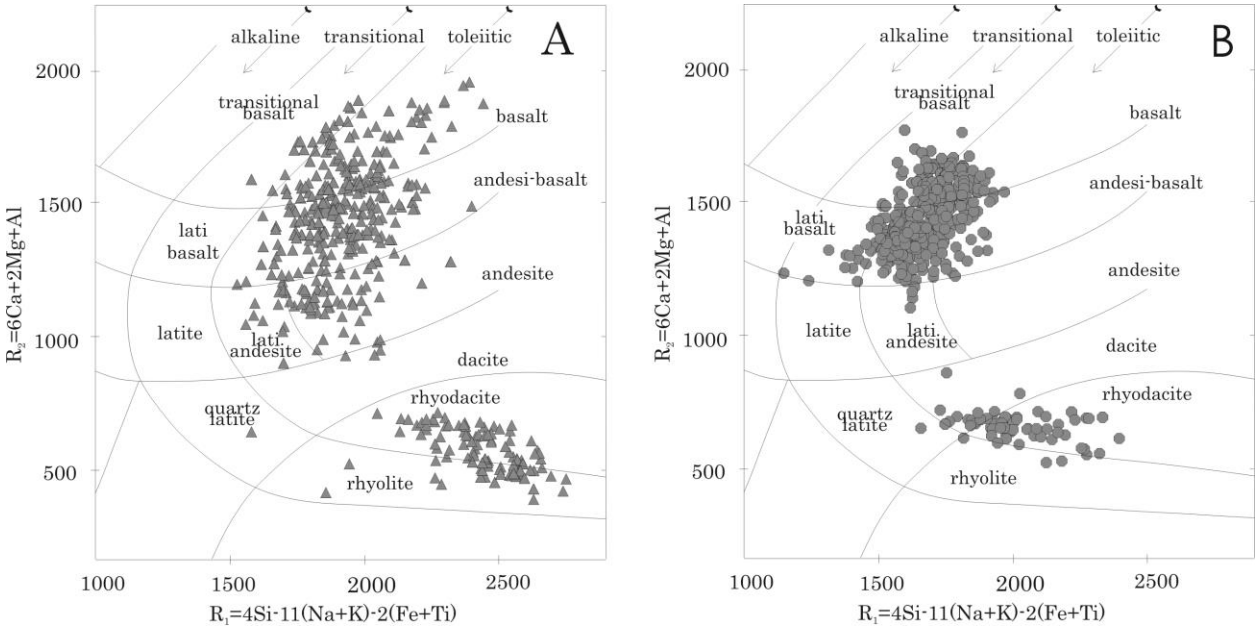

Fig. 2- R1xR2 diagram (De La Roche et al., 1980). A- tholeiitic suite (Low-Ti basalts and ATP), B- Tholeiitic-transitional suite (High-Ti basalts and ATC).

Table 1- Representative analysis of Palmas and Chapecó silicic volcanics of the PMP. (major elements- in oxide *wt%;* trace elements- in *ppm*)

	Palmas					Chapecó		
Sample	KC	KSE	KSE	KS	KSU	KC	PU	KNO
#	505	406	419	319	237	482	1011	442
SiO_2	65.48	66.44	67.58	68.70	70.46	64.38	65.44	66.93
TiO_2	1.11	0.96	0.95	0.95	0.71	1.46	1.57	1.24
Al_2O_3	12.96	12.74	12.35	12.12	12.38	12.83	13.03	13.03
Fe_2O_3	6.78	6.15	6.15	5.69	5.22	7.01	7.57	6.54
MnO	0.08	0.11	0.20	0.10	0.09	0.16	0.12	0.10
MgO	1.08	1.70	1.22	1.28	0.61	1.36	1.28	0.75
CaO	2.78	2.93	3.09	2.68	2.20	2.91	2.94	2.07
Na_2O	3.64	2.87	2.78	2.30	2.92	3.32	3.61	3.36
K_2O	4.01	3.89	4.17	4.69	4.74	4.45	4.33	4.61
P_2O_5	0.33	0.27	0.26	0.26	0.20	0.48	0.46	0.33
LOI	1.93	1.91	1.01	0.99	0.57	1.05	0.61	1.63
SUM	100.17	99.98	99.75	99.76	100.09	99.41	100.96	100.60
Cu	128	75	78	63	18	7	9	14
Ni	7	8	7	8	3	4	5	5
Ba	610	706	694	588	613	1076	1003	1199
Rb	169	160	165	175	206	100	101	136
Sr	135	143	127	137	102	360	337	318
Zr	279	258	252	266	319	633	670	592
Y	63	41	57	42	55	65	66	60
Nb	22	20	20	21	23	48	51	44
U	3.51	4.07	4.04	4.17	3.25	1.74	1.91	2.68
Th	11.53	11.30	11.64	12.09	12.25	8.76	8.62	12.69
La	42.0	35.0	36.1	36.0	43.2	60.4	63.7	67.8
Ce	88.0	76.0	78.0	73.0	95.5	144.6	147.0	145.0
Nd	46.0	36.0	34.8	34.0	42.7	68.4	71.7	70.9
Sm	9.40	7.00	7.47	7.10	8.78	15.78	15.10	14.50
Eu	2.02	1.66	1.53	1.53	1.60	3.60	3.52	3.11
Gd	9.80	7.30	7.28	8.10	8.78	14.04	13.10	11.90
Dy	8.30	6.90	7.43	7.40	8.32	10.83	11.50	10.20
Ho	1.70	1.40		1.60				
Er	4.70	4.00	4.54	4.60	5.25	5.97	6.21	5.42
Yb	4.50	3.40	3.92	3.70	4.61	4.79	5.03	4.39
Lu	0.60	0.50	0.61	0.60	0.71	0.65	0.76	0.65

3 STRATIGRAPHY

The 1600 m thick Paraná Magmatic Province (PMP) volcanic sequence consists of up to 32 lava flows of predominant basic to intermediate compositions (tholeiitic basalts, andesi-basalts, and andesites), as well as felsic volcanic rocks (dacites, rhyodacites, and rhyolites; BELLIENI *et al*., 1984, 1986).

The base of the stratigraphic column is composed of a thick sequence of basic to intermediate flows that overlap the aeolian sandstones of the Botucatu Formation. The sandstones may also occur interlayered in the first hundred meters of the basaltic pile. The Palmas and Chapecó Members overly the basalt flows. The Palmas Member is characterized by silicic volcanic bodies (ATP type) associated with a few basaltic lava flows, crops out from the central region of the basin southwards, where it may reach 270 m thickness. The Chapecó Member, composed of silicic volcanic rocks (ATC type), occurs in the northern and central regions of the Paraná Basin; the largest thickness, reaching 250 m, is present in the central region. This Member overlaps the basalts, but in the northern portion of the basin (Paranapanema River region - SP) it is found directly on the sandstones of the Botucatu Formation.

In the center of the basin the two silicic members overlap indicating that the Palmas Member is older than Chapecó, although ATP type rocks may be found interlayered in the Chapecó Member.

The last pulses of Paraná volcanism emplaced basalt flows that cover both the Palmas and Chapecó type rocks and become thicker towards the north of the basin.

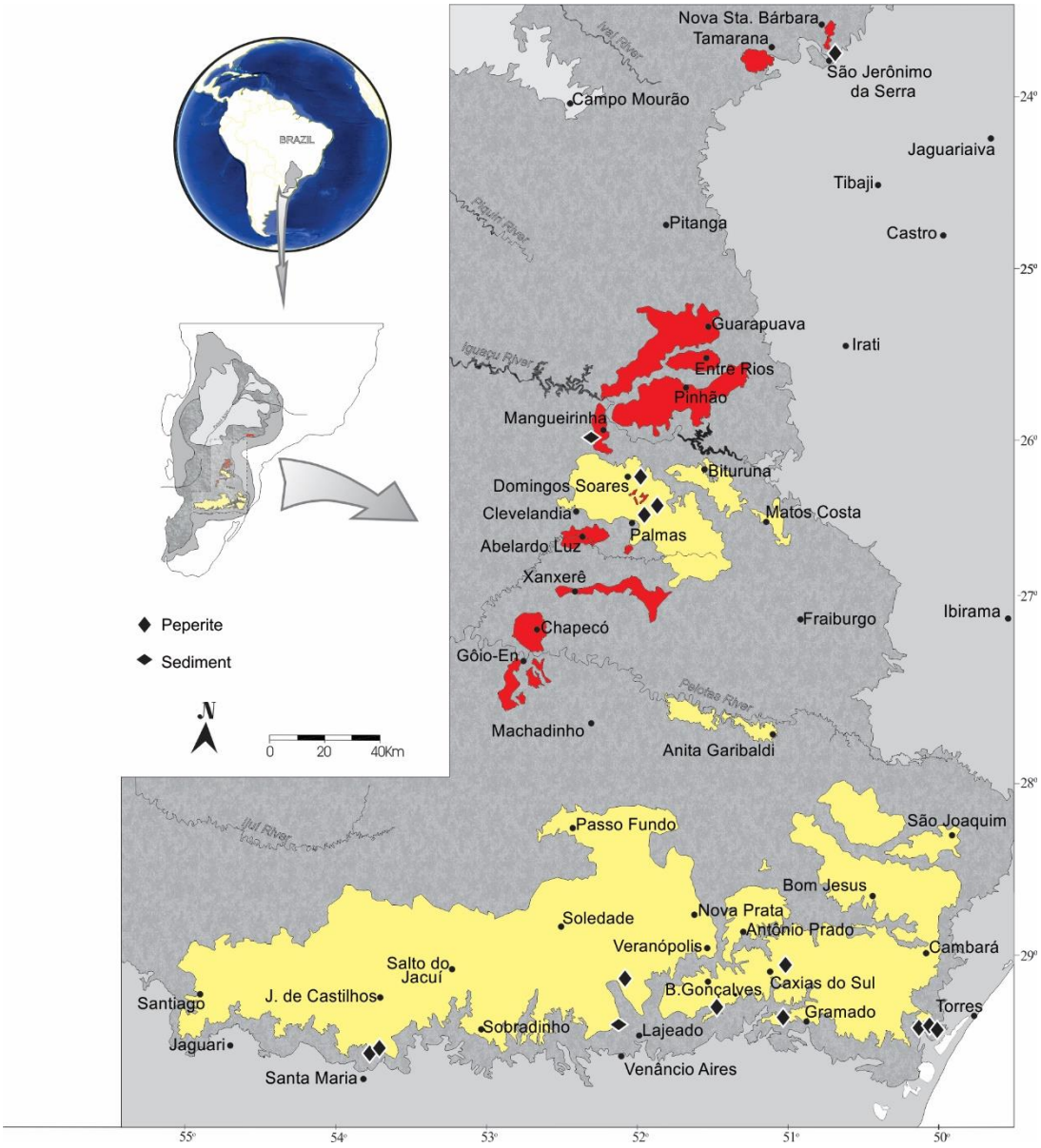

Fig. 3 - Map with the location of sediment and peperite outcrops (lozenges) within the Palmas and Chapecó Members; Yellow – Palmas units, red – Chapecó units.

3.1 Peperites and sedimentary deposit

The Literature (MARQUES & ERNESTO, 2004; THIEDE & VASCONCELLOS, 2011) indicates that the PMP magmatism occurred quickly, during a time interval that did not exceed 3 Ma, and in a rather continuous way, based on scarce observations of sedimentary intercalations or paleosoils within the volcanic sequence. However, recent

field work revealed the presence of frequent sediment lenses and peperites in various stratigraphic levels within the silicic volcanic sequence.

Peperite is a genetic term used for rocks formed in situ by the interaction between hot magma (intrusive bodies, lava or pyroclastic flows) and coeval wet sediments (FISHER, 1960; WILLIAMS & MCBIRNEY, 1979; WHITE *et al*., 2000; SKILLING *et al*., 2002). Nonetheless, interaction with dry sediments has also been described by some authors (JERRAM *et al*., 1999; JERRAM & STOLLHOFEN, 2002; PETRY et al., 2007). Peperite is classified into two basic types according to the shape of its elements (BUSBY-SPERA & WHITE, 1987): blocky, in which the volcanic clasts present angular shapes and show jigsaw-fit texture reflecting in situ quench fragmentation in a brittle state; and fluidal in which volcanic clasts present irregular, fluid (amoeboid), globular to undefined shapes, reflecting a ductile state during fragmentation, with the sediment often filling vesicles and being injected into cracks in the volcanic clasts/rocks, although more complex shapes may also be found (MCPHIE *et al*., 1993; SKILLING et al., 2002).

Sedimentary deposits and peperites found in the Chapecó and Palmas Members present a wide distribution in the Paraná Basin, as shown in Fig. 3, are described below.

In the São Jerônimo da Serra (Paraná State) region, in the northern sector of the Paraná Basin, ATC type rocks overly a sandstone forming blocky peperite (Fig. 4). It comprises few centimeters to just over 1 m thick clastic dikes (Fig. 4a) and breccias composed of matrix-supported angular to rounded volcanic blocks of variable size (Fig. 4b). The sandstone is poorly sorted with angular to rounded quartz grains (Fig. 4c and d) and it was silicified by thermal metamorphism by the overlying volcanic material.

In the region of Mangueirinha and Palmas (Paraná State), in the center of the basin, both ATC and ATP type rocks crop out, either overlying basalts or overlapping each other. A sandstone layer was observed intercalated between ATC type silicic body and an overlying basaltic lava flow. The base of the sediment is a breccia formed by vesicular ATC clasts set in a sandy matrix, implying some erosion degrees of the top of the volcanic body during sedimentation. In another location, an ATC type silicic unit overlies a vesicular ATP type silicic body, with a red clayey-silty sediment intercalated between the two units. The sediment was injected upwards into fractures in the

overlying ATC unit forming peperite with both fluidal and blocky features (Fig. 5a and b), while in the underlying ATP unit, the sediment filled cooling cracks without any peperitic interaction (Fig. 5c and d). In a third exposure, a reddish brown silty sediment, intercalated between two ATP volcanic units, formed peperite with blocky jointing morphology (Skilling *et al*., 2002), characterized by the injection of sediment into centimeter to millimeter spaced joints in the base of the overlying volcanic unit (Fig. 6).

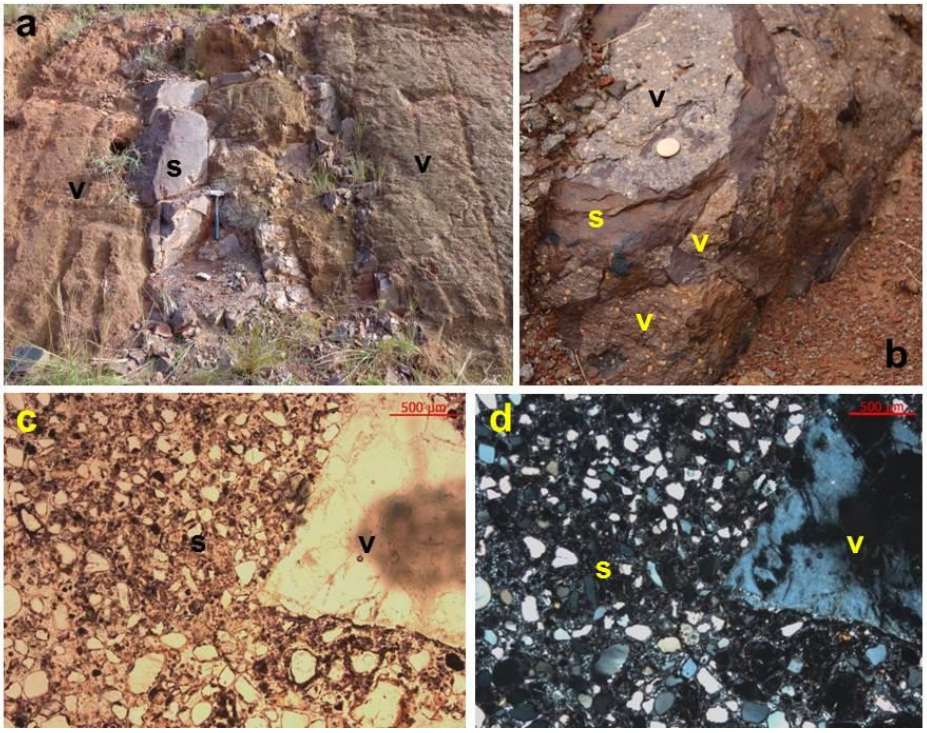

Fig. 4 – Peperite from São Jerônimo da Serra: (a) clastic dike more than 1 m thick; (b) angular to sub-angular shaped clasts set in a sandstone matrix. S –sandstone; V - volcanic rock; (c, d) photomicrographs of the immature and poorly sorted sediment (c = // pol.; d = X pol.).

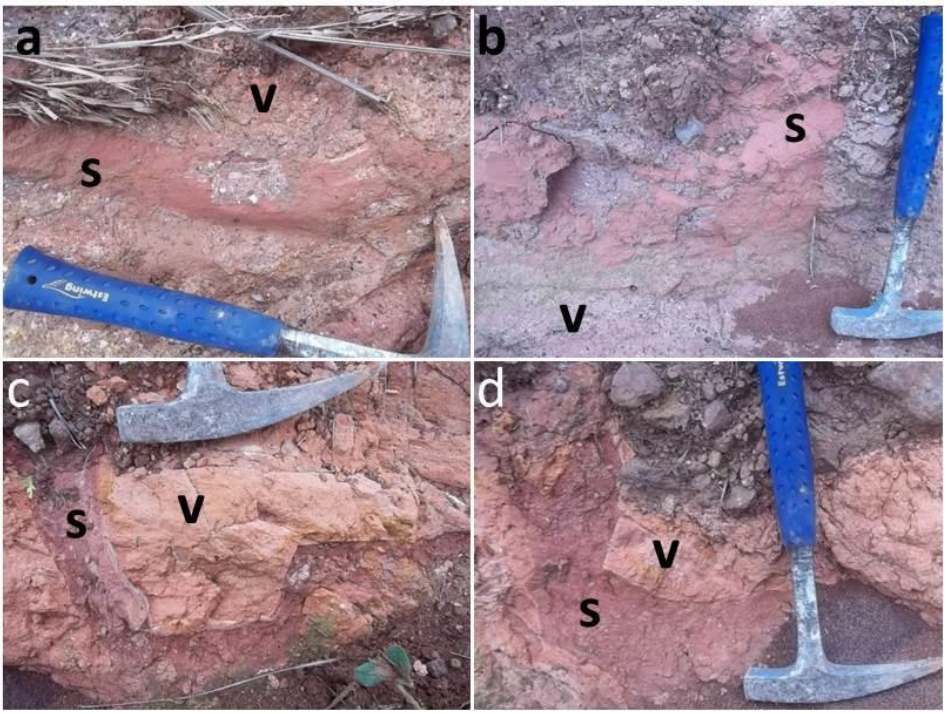

Fig. 5 – Silicic ATC and ATP type rocks (V) in contact with red clayey-siltstone (s): (a, b) peperites in the base of ATC type rocks; (c and d) fractures in the top of ATP type rock filled with sediment, in the central region of the Paraná Basin.

In the southern region of the Paraná Basin (Rio Grande do Sul State), sediments and peperites were observed between some basaltic lower units and the overlying Palmas silicic sequence. In Santa Maria region, blocky peperite was observed in the base of the lowermost silicic volcanic unit. The peperite displays a well-developed jigsaw-fit texture, and closely packed, blocky to cuneiform juvenile clast shapes of several sizes, separated by an orange colored sedimentary material (Fig. 7). The sediment exhibits a high degree of baking (thermal metamorphism) and the juvenile clasts show intense devitrification, indicating very high temperature of the volcanic material interacting with the sediment.

Near the city of Venâncio Aires, a 10 m thick sedimentary layer underlies an ATP silicic volcanic unit. The sediment is a reddish colored sandstone composed of sub-angular to rounded quartz grains (Fig. 8). The volcanic unit presents well developed horizontal jointed base and the contact with the sandstone is sharp, apparently lacking peperitic interaction (Fig. 8).

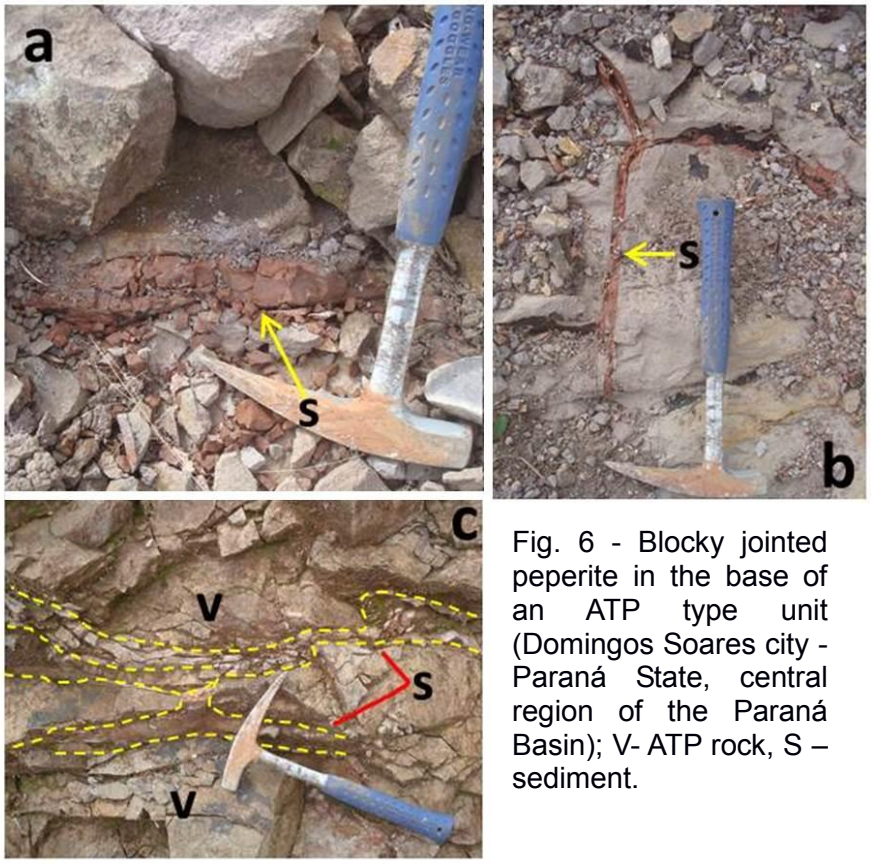

Fig. 6 - Blocky jointed peperite in the base of an ATP type unit (Domingos Soares city - Paraná State, central region of the Paraná Basin); V- ATP rock, S – sediment.

A road-cut on the Soledade to Lajeado highway exposes a peperite in the base of a 25 m thick basaltic lava flow interlayered within the ATP silicic volcanic sequence. Volcanic clasts in the peperite are vesicular and display a variety of morphologies, from blocky to fluidal. The sediment is a red poorly sorted sandstone, which partially fills vesicles in the volcanic clasts.

Fig. 7 –Blocky peperite formed by interaction of an ATP type volcanic body with sediment in Santa Maria region (Rio Grande do Sul State): well-developed jigsaw-fit texture, closely packed, gray blocky to cuneiform clasts of variable sizes, separated by orange sedimentary material, displaying intense baking.

Fig. 8 - Outcrop in the Venâncio Aires area (Rio Grande do Sul State), where a silicic volcanic unit of the ATP type (V) rests on a reddish sedimentary layer (s) lacking peperitic interaction. On the right lower corner a photomicrograph of the sandstone (X pol.).

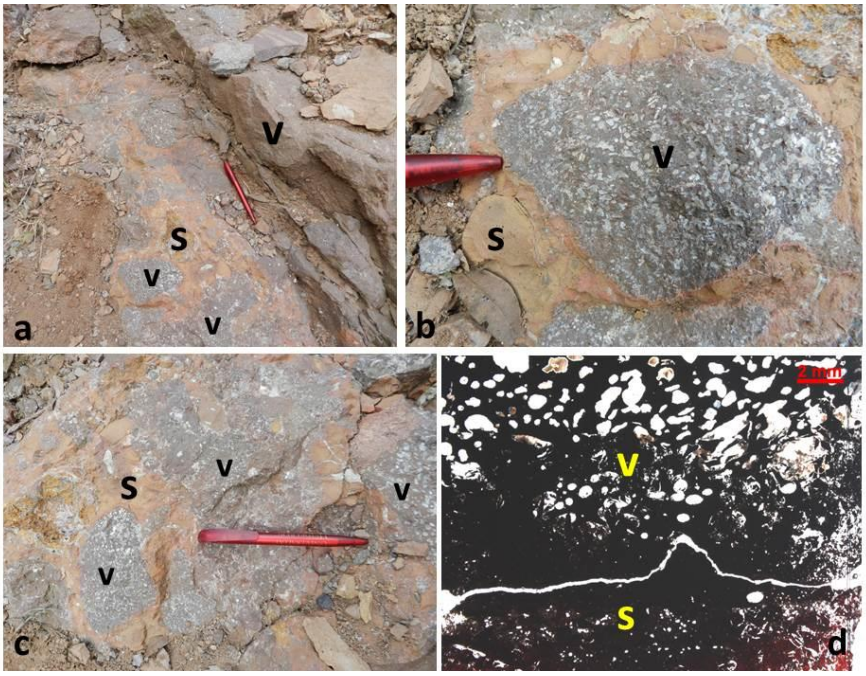

Fig. 9 – Aspects of a peperite produced by interaction of a thin basalt flow (within the silicic Palmas Member) and fine grained sediment near Nova Petrópolis (Rio Grande do Sul State), south part of the basin: (a-c) irregular blocky volcanic clasts (V) in a reddish sandstone matrix (S); (d) photomicrograph showing the amygdaloidal basalt (V) in the upper part and a poorly sorted fine-grained sandstone in the bottom (S) (// pol.).

Eastward, in the area between Bento Gonçalves and Cambará do Sul (Rio Grande do Sul), all the observed peperites are interlayered within the silicic volcanic sequence and the sedimentary material becomes finer, dominantly silty. A peperite was observed in a quarry floor in Nova Petrópolis, near Gramado city, resulting from the interaction of sediment with a thin (~ 1 m thick) amygdaloidal basalt interlayered in the silicic volcanic sequence. It displays blocky juvenile clasts with irregular shapes separated by orange to reddish, poorly-sorted fine-grained sandstone. The sediment presents vesicles that probably resulted from volatilization of sediment water by heating (Fig. 9).

On the Rota do Sol highway, connecting Caxias do Sul to the coast, three peperite levels were observed interlayered in a sequence of Palmas Member black glassy volcanic units. The stratigraphically lower two are similar and characterized by vesicular, pale to greenish glassy volcanic clasts, presenting angular to rounded irregular shapes (Fig. 10). The sedimentary material is a brown moderate to poorly sorted siltstone that also fills vesicles in volcanic clasts. The uppermost peperite presents juvenile volcanic clasts with a wide variety of morphologies, being the fluidal shapes more frequent (Fig. 11). The green and vesicular volcanic clasts are surrounded by a reddish brown siltstone, which also fills vesicles and fractures in volcanic clasts (Fig. 11d). It is slightly coarser and more poorly sorted than the previous two sediments (Fig. 12), and many clasts of the stratigraphically lower peperite display perlitic fractures (Fig. 12c).

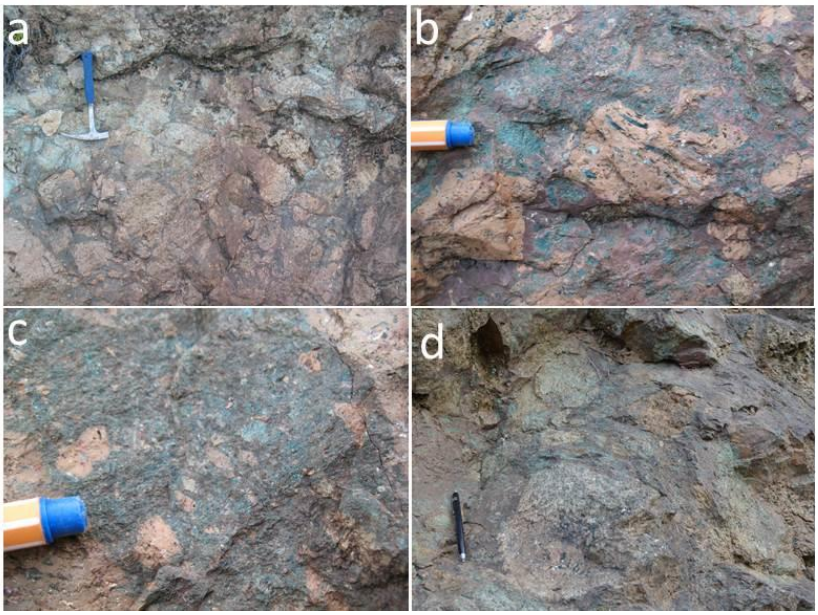

Fig. 10 - Aspects of the two lowermost peperites in the Palmas volcanic sequence, along the Rota do Sol highway (Rio Grande do Sul State): (a, b, and c) images of the lowermost peperite; and (d) photo of the middle peperite. The volcanic clasts are pale and light or dark green, while the siltstone is dark brown.

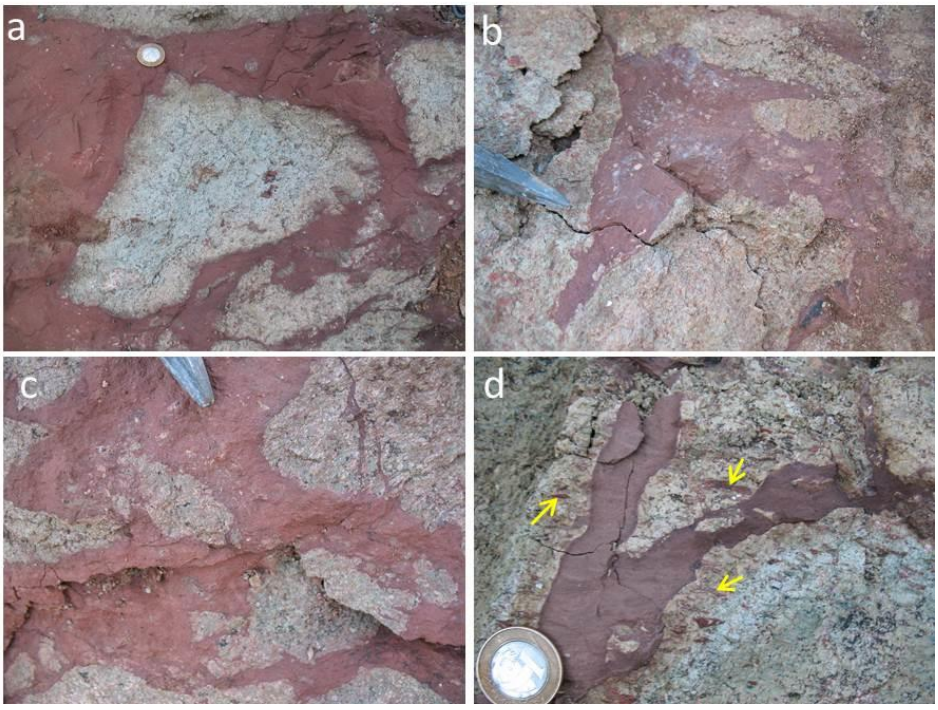

Fig. 11 - Peperite from the stratigraphically higher level on the section exposed in the Rota do Sol highway: green to pale volcanic clasts, displaying sub-angular to irregular morphologies, set in a reddish brown siltstone matrix, which also fills vesicles in volcanic clasts (yellow arrows in d).

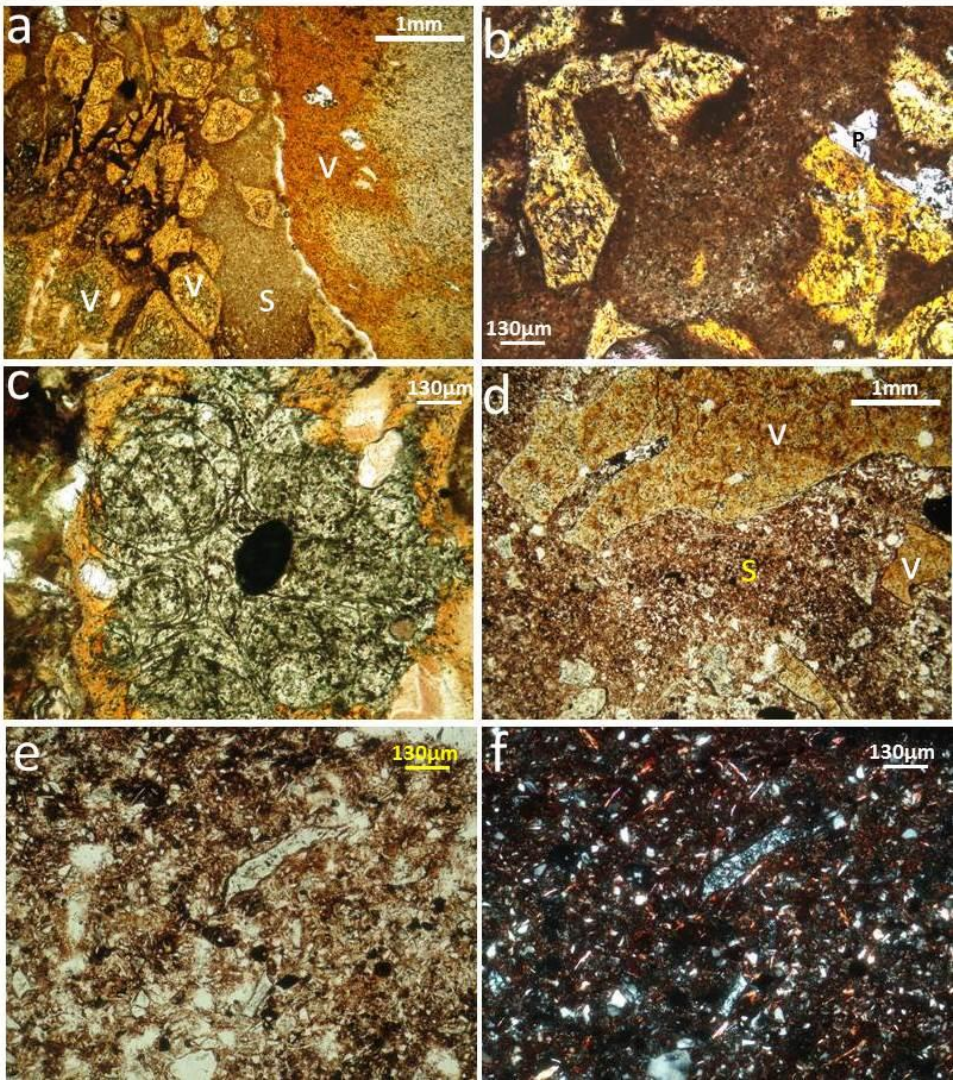

Fig. 12 - Photomicrographs of peperites from the Palmas volcanic sequence, along Rota do Sol highway: (a, b and d) volcanic glassy clasts (V) set in a brown siltstone matrix (S); (c) volcanic clast displaying concentric fractures - perlitic texture - common in the two lowermost peperites; (e and f) detail of the poorly sorted, slightly coarser siltstone from d (a, b, c, d and e - // pol.; f – X pol.; P = plagioclase).

4 DISCUSSION AND CONCLUDING REMARKS

The PEMP (Paraná-Etendeka Magmatic Province) is considered one of the largest LIPs (Large Igneous Province) in continental crust in the world, with nearly 1 million km^3 (Bryan et al, 2010). 95% of the total volume of the volcanic products is preserved in the South American continent, the Paraná Magmatic Province (PMP). All volcanic material was erupted in a short period of time (~ 3 million years) without significant interruption, as deduced from the scarcity of sediments interlayered within the volcanic sequence. In fact, and up to now, the only references to the presence of sediments interbedded within the volcanics corresponded to layers or lenses of sandstones (intertraps), a few centimeters to several meters thick, from the Botucatu Formation. These occur only in the base of the lava flow pile in both the African (JERRAM *et al*., 1999, 2000; JERRAM & STOLLHOFEN, 2002) and South American continents (PETRY *et al*., 2007; WAICHEL *et al*., 2008). Sandstone intertraps in rhyodacites of the Piraju – Ourinhos region (São Paulo State; JANASI *et al*., 2007; LUCHETTI, 2010), where the thick basaltic sequence is missing, were also known. However, until now, there were no reports of features indicating significant time breaks in the upper part of the PMP stratigraphic sequence.

New observations of the occurrence of sedimentary lenses and peperites, resulting from volcano-sedimentary interaction, at the base and within the upper silicic sequences of the PMP are presented in this paper. These were observed throughout the Paraná Basin associated with silicic and basaltic units of the Palmas and Chapecó Members.

Some works on the PMP report peperites derived from the basalt flow-sediment interaction (PETRY *et al*., 2007; WAICHEL *et al*., 2007, 2008), the most common types found in worldwide volcanic sequences. Nevertheless, structures observed in this study reveal that this interaction also occurred between silicic extrusive bodies and wet sediment. These “silicic peperites” are mostly blocky, highlighting a more viscous magma (DADD & WAGONER, 2002). However, they may also display fluidal features, which indicate less viscous melts, likely due to higher temperatures (> 1000 ^oC, PICCIRILLO & MELFI, 1988).

The sediments display immature features suggesting limited transport and, depending on the location, range from moderately to poorly-sorted sandstones to siltstones. Often, there was lava/sediment interaction producing peperites or sediment deformation by the weight of overlying volcanic units. Evidences for the presence of wet and unconsolidated or poorly consolidated sediments are the variety of morphologies found, injections of sediment into fractures, vesicles in the juvenile clast filled by sediment and vesiculated sediment (Skilling *et al*., 2002).

Paleoenvironment climatic conditions at the time of the PMP volcanism were quite dry, since the Serra Geral Formation overlies the Botucatu Formation, described as a dry aeolian system (SHERER, 2000). Sandstone lenses up to 20 m thick interlayered in the first basalt lava flows (JERRAM et al., 1999, 2000; JERRAM & STOLLHOFEN, 2002; PETRY *et al*., 2007; WAICHEL *et al*., 2008) reveal that this system remained active during the magmatic event. However, the new evidences of wet and locally silty sediment between basalt and silicic units and interlayered in the silicic units (end of the volcanic sequence) presented here reflect a paleoenvironmental change, from a dry climate in the beginning of the PMP volcanic activity to a more humid environment (fluvial-lacustrine) during the latest phases of the magmatism, as also evidenced by Waichel et al. (2007) in peperites found in some basalt units of the PMP in contact with lacustrine sediments. At São Jerônimo da Serra region, northern area of the basin, the change must have started before the volcanism. Furthermore, this seems to be common in this type of setting in which humid and dry aeolian systems may alternate over time due to climate changes (ASSINE et al., 2004).

The deposition of sediments must have taken place in depressed portions of the paleo-relief (small valleys or depressions of the original volcanic morphology), and also suggests a decrease in eruptive frequency towards the end of the volcanic activity, allowing time for the deposition of sedimentary material between individual volcanic events.

In conclusion, the PMP volcanism was not totally continuous, but presented significant pauses, mainly in the initial and terminal phases. On the other hand, the occurrence of sediments separating the top of the lower basaltic sequence and the beginning of the silicic extrusions may represent a pause in the volcanic activity that

coincides with the compositional change in the magmatism of the Paraná Magmatic Province.

Acknowledgements. This study was supported by São Paulo Research Foundation (FAPESP) and National Counsel of Technological and Scientific Development (CNPq). We thank Francisco Negri for help in field work in the central basin and Dr Scarlato, Piergiorgio, Dr Giacomoni, Pier Paolo and anonymous reviewer for valuable suggestions and review.

REFERENCES

ASSINE, M. L., PIRANHA, J. M., CARNEIRO, C. D. R.: Os paleodesertos Pirambóia e Botucatu. In: Mantesso-Neto, V., Bartorelli, A., Carneiro, C. D. R., Brito-Neves, B. B. (Eds), Geologia do Continente Sul-Americano: evolução da obra de Fernando Flávio Marques de Almeida. SP, Brasil: Beca Prod Cult Ltda, p. 77-92, 2004.

BELLIENI, G., BROTZU, P., COMIN-CHIARAMONTI, P., ERNESTO, M., ERNESTO, M., MELFI, A. J., PACCA, I. G., PICCIRILLO, E. M.: Flood basalt to rhyolites suites in the southern Paraná plateau (Brazil): paleomagnetism, petrogenis and geodynamic implications. J. Petrol., 25, 579-618, 1984.

BELLIENI, G., COMIN-CHIARAMONTI, P., MARQUES, L. S., MELFI, A. J., NARDY, A. J. R., PAPATRECHAS, C., PICCIRILLO, E. M., ROISENBERG, A.: Petrogenetic aspects of acid and basaltic lavas from the Paraná plateau (Brazil): geological, mineralogical and petrochemical relationships. J. Petrol., 27, 915-944, 1986.

BRYAN, S. E., UKSTINS-PEATE, I., PEATE, D. W., SELF, S., JERRAM, D. A., MAWBY, M. R., MARSH, J. S., MILLER, J. A.: The largest volcanic eruptions on Earth. Earth-Sci. Rev., 102, 207-229, 2010.

BUSBY-SPERA, C. J. AND WHITE, J. D. L.: Variation in peperite textures associated with differing host sediment properties. B. Volcanol., 49, 765-775, 1987.

DADD, K. A., VAN WAGONER, N. A.: Magma composition and viscosity as controls on peperite texture: an example from Passamaquoddy Bay, southeastern Canada. In: Skilling, I.P., White, J.D.L., McPhie, J. (Eds.), Peperite: Processes and Products of Magma-Sediment Mingling. J. Volcanol. Geoth. Res. 114, 63-80, 2002.

DE LA ROCHE H., LETERRIER P., GRANDCLAUDE P., MARSHAL M. A classification of volcanic and plutonic rocks using R1xR2 diagram and major element analysis. Its relationships with current nomenclature. Chem. Geol., 28: 183-210, 1980.

ERNESTO, M., RAPOSO, M. I. B., MARQUES, L. S., RENNE, P. R., DIOGO, L. A., DE MIN, A.: Paleomagnetism, geochemistry and 40ar/39ar dating of the north-eastern Paraná Magmatic Province. Tectonic implications. J. Geodyn., 28, 321-340, 1999.

FISHER, R. V.: Classification of volcanic breccias. Geol. Soc. Am. Bull., 71, 973-982, 1960.

FRANK, H. T., GOMES, M. E. B., FORMOSO, M. L. L.: Review of the areal extent and the volume of the Serra Geral Formation, Paraná Basin, South America. Pesquisas em Geociências, 36 (1), 49-57, 2009.

GARLAND, F., HAWKESWORTH, C. J., MANTOVANI, M. S. M.: Description and Petrogenesis of the Paraná Rhyolites, Southern Brazil. J. Petrol., 36 (5), 1193-1227, 1995.

JANASI, V. A., MONTANHEIRO, T. J., FREITAS, V. A., REIS, P. M., NEGRI, F. A., DANTAS, F. A.: Geology, petrography and geochemistry of the acid volcanism of the Paraná Magmatic Province in the Piraju–Ourinhos region, SE Brazilian Journal of Geosciences, 37, 745–759, 2007.

JANASI, V. A., FREITAS, V. A., HEAMAN, L. H.: The onset of flood basalt volcanism, Northern Paraná Basin, Brazil: A precise U–Pb baddeleyite/zircon age for a Chapecó-type dacite. Earth. Planet. Sc. Lett., 302, 147–153, 2011.

JERRAM, D. A., MOUNTNEY, N., STOLLHOFEN, H.: Facies architecture of the Etjo Sandstone Formation and its interaction with the Basal Etendeka flood basalts of NW Namibia: Implications for offshore analogues. in: Cameron, N., Bate, R. & Clure , V. (eds) The Oil and Gas Habitats of the South Atlantic. Geological Society, London, Special Publications, 153, 367–380, 1999.

JERRAM, D.A., MOUNTNEY, N., HOWELL, J., LONG, D., STOLLHOFEN, H.: Death of a Sand Sea: an active erg systematically buried by the Etendeka flood basalts of NW Namibia. J. Geol. Soc. London, 157, 513–516, 2000.

JERRAM, D. A. AND STOLLHOFEN, H.: Lava-sediment interaction in desert settings; are all peperite like textures the result of magma-water interaction? J. Volcanol. Geoth. Res., 114: 231-49, 2002.

LUCHETTI, A. C. F.: Aspectos vulcanológicos dos traquidacitos da região de Piraju–Ourinhos (SP) [Master Dissertation]. São Paulo, SP, Brazil, Universidade de São Paulo, 92 pp, 2010.

MALAGUTTI, M. I. A., BAHIA F, MORENO, M. M. T., NARDY, A. J. R.: Determinação de elementos terras raras e ítrio em rochas silicáticas por ICP-OES com separação em resina trocadora de íons. Geochem. Bras., 12, 2, 75-80, 1998.

MARQUES, L. S. AND ERNESTO, M.: O magmatismo toleítico da Bacia do Paraná. In: Geologia do Continente Sul-Americano, Mantesso-Neto, V.; Bartorelli, A.; Carneiro, C.D.R.; Brito-Neves, B.B. Beca Produções Culturais Ltda, 2004.

MCPHIE, J., DOYLE, M., ALLEN, R.: Volcanic textures: a guide to the interpretation of textures in volcanic rocks. University of Tasmania, 197 p, 1993.

MILNER, S. C., DUNCAN, A. R., EWART, A.: Quartz latite rheoignimbrite flows of the Etendeka Formation, north western Namibia. B. Volcanol., 54, 200- 219, 1992.

MINCATO, R. L., ENZWEILER, J., SCHRANK, A.: Novas idades 39Ar/40Ar e implicações na metalogênese dos depósitos de sulfetos magmáticos de Ni-Cu-EPG na Província Ígnea

Continental do Paraná. in: 9th Brazilian Congress of Geochemistry, Belém (Pará), Brazil, 2 – 9 November 2003, 67-92, 2003.

NARDY, A. J. R., ENZWEILER, J., BAHIA F, O., OLIVEIRA, M. A. F., PENEIRO, M. A. V.: Determinação de elementos maiores e menores em rochas silicáticas por espectometria de fluorescência de raios-x: resultados preliminares. In: 6th Brazilian Congress Of Geochemistry, Salvador (Bahia), Brazil, 346-348, 1997.

NARDY, A. J. R., OLIVEIRA, M. A. F., BETANCOURT, R. H. S., VERDUGO, D. R. H., MACHADO, F. B.: Geologia e estratigrafia da Formação Serra Geral. Revista Geociências, 21, 15-32, 2002.

NARDY, A. J. R., MACHADO, F. B., OLIVEIRA, M. A. F.: As rochas vulcânicas mesozóicas ácidas da Bacia do Paraná: litoestratigrafia e considerações geoquímico-estratigráficas. Brazilian Journal of Geosciences, 38 (1), 178-195, 2008.

PEATE, D., HAWKESWORTH, C. J., MANTOVANI, M. S. M.: Chemical Stratigraphy of the Paraná Lavas (South America): Classification of Magma Types and their Spatial Distribution. B. Volcanol., 55, 119-139, 1992.

PETRY, K., JERRAM, D. A., DE ALMEIDA, D. P. M., ZERFASS, H.: Volcanic-sedimentary features in the Serra Geral Fm., Paraná Basin, southern Brazil: Examples of dynamic lava-sediment interactions in an arid setting. J. Volcanol. Geoth. Res., 159, 313-325, 2007.

PICCIRILLO, E. M. & MELFI, A. J. (eds.): The Mesozoic Flood Volcanism of the Paraná Basin: Petrogenetic and Geophysical Aspects. Instituto Geofísico, Astronômico e Ciências Atmosféricas, Universidade de São Paulo, São Paulo, Brazil, 1988.

RENNE, P. R., ERNESTO, M., PACCA, I. G., COE, R. S., GLEN, J. M., PRÉVOT, M., PERRIN, M.: The age of Parana flood volcanism, rifting of Gondwanaland, and the Jurassic–Cretaceous boundary. Science 258, 975–979, 1992.

RENNE, P. R., DECKART, K., ERNESTO, M., FÉRAUD, G., PICCIRILLO, E. M.: Age of the Ponta Grossa dyke swarm (Brazil), and implications to Paraná flood volcanism. Earth. Planet. Sc. Lett. 144, 199–211, 1996a.

RENNE, P. R., GLEN, J. M., MILNER, S. C., DUNCAN, A. R.: Age of Etendeka flood volcanism and associated intrusions in southwestern Africa. Geology 24, 659–662, 1996b.

SANTOS, R. N., MARQUES, L. S., BRENHA-RIBEIRO, F., NICOLA, S. H. A.: Determination of uranium concentrations and activity ratios in silicate rocks by alpha spectrometry: application to volcanic rocks from Trindade and Martin Vaz Islands. Appl. Radiation and Isotopes, 56, 5, 741-750, 2002.

SANTOS, R. N., MARQUES, L. S., BRENHA-RIBEIRO, F., NICOLA, S. H. A.: Determination of thorium concentrations and activity ratios in silicate rocks by alpha spectrometry. Appl. Radiation and Isotopes, 56, 5, 741-750, 2004.

SCHERER, C.: Aeolian dunes of the Botucatu Formation (Cretaceous) in southernmost Brazil: morphology and origin. Sed. Geol., 137: 63-84, 2000.

SKILLING, I. P., WHITE, J. D. L., MCPHIE, J.: Peperite: a review of magma-sediment mingling. J. Volcanol. Geoth. Res., 114, 1-17, 2002.

SUN, S. AND MCDONOUGH, W. F.: Chemical and isotopic systematics of oceanic basalts: implications for mantle composition and processes. in: Saunders A.D. and Norry M.J. (eds.) Magmatism in the Ocean Basins. Geol. Soc. London, 1, London, 313-345, 1989.

THIEDE, D.S., VASCONCELOS, P.M.: Paraná flood basalts: rapid extrusion hypothesis confirmed by new 40Ar/39Ar results. Geology, 38 (8), 747-750, 2010.

TURNER, S., REGELOUS, M., KELLEY, S., HAWKSWORTH, C., MANTOVANI, M. M. S.: Magmatism and continental break-up in the South Atlantic: high precision 40 Ar / 39Ar geochronology. Earth Plan. Sci. Lett., 121**,** 333-348, 1994.

WAICHEL, B. L., LIMA, E. F., SOMMER, C. A., LUBACHESKY, R.: Peperite formed by lava flows over sediments: An example from the central Paraná Continental Flood Basalts, Brazil. J. Volcanol. Geoth. Res., 159, 343–354, 2007.

WAICHEL, B. L., SCHERER, C. M. S., FRANK, H. T.: Basaltic lava flows covering active aeolian dunes in the Paraná Basin in southern Brazil: Features and emplacement aspects. J. Volcanol. Geoth. Res*.,* 171, 59–72, 2008.

WAICHEL, B. L., LIMA, E. F. DE, VIANA, A. R., SCHERER, C. M., BUENO, G. V., DUTRA, G.: Stratigraphy and volcanic facies architecture of the Torres Syncline, Southern Brazil, and its role in understanding the Paraná–Etendeka Continental Flood Basalt Province. J. Volcanol. Geoth. Res., 215-216, 74–82, 2012.

WILLIAMS, H., MCBIRNEY, A. R.: Volcanoes: San Francisco, Freeman, Cooper and Company, 397 p., 1979.

WHITE, J. D. L., MCPHIE, J., SKILLING, I. P.: Peperite: a useful genetic term. B. Volcanol., 62, 65-66, 2000.

Chapter 2: Physical Volcanology of Silicic Volcanic Rocks from Paraná Magmatic Province

1 INTRODUCTION

Chapecó and Palmas silicic volcanic rocks are included in the Serra Geral Formation, in the Paraná Basin, and make up part of the Lower Cretaceous age Paraná Magmatic Province (PMP), a giant bimodal tholeiitic volcanism, with ~900,000 km^3, which preceded the Gondwana breakup and the subsequent opening of the Atlantic Ocean.

Geochronological dating by $^{40}Ar/^{39}Ar$ shows that the age of volcanic rocks of the Serra Geral Formation ranges from 133.6 to 131.5 Ma in its northern sector, and from 134.6 to 134.1 Ma in the south (RENNE et al., 1992, 1996a, b; TURNER et al., 1994; ERNESTO et al., 1999; MINCATO et al., 2003; THIEDE & VASCONCELOS, 2010; PINTO et al., 2010). More recently, Janasi et al. (2011), using U/Pb ratios from baddeleyite/zircon crystals determined by ID-TIMS from rocks of the Chapecó Member, obtained an age of 134.3 ± 0.8 Ma, compatible with the previous age determinations. These ages obtained in the dominant basaltic flows indicate duration of the volcanism of around 3 Ma, also consistent with paleomagnetic data presented by Marques & Ernesto (2004).

Chapecó type rocks (ATC) appear more northerly and include porphyritic, crystal-rich, high-Ti dacites and trachydacites, whereas Palmas type (ATP) includes fine-grained, crystal-poor, low-Ti dacites and rhyolites. Even comprising a small proportion of the total erupted volume (2.5%), these rocks correspond to an extensive and voluminous (~14,500 km^3) (NARDY et al., 2008), significant flare-up of silicic volcanism over a short period of time. Nardy (1995) noted a chemical lateral homogeneity along 45 km of a single cooling unit in the central region of the Paraná Basin, and paleomagnetic data show that a single cooling unit may be extended up to 30 km away (MARQUES & ERNESTO, 2004).

The mode of emplacement (lavas vs. pyroclastic flows) of the volcanic units has been the subject of much controversy (e.g. WHITTINGHAN, 1989; MILNER et al., 1992; GARLAND et al., 1995; WAICHEL et al., 2012). In this way, the aim of this project was

to better understand the origin and evolution of the PMP silicic rocks, in some key regions in particular, combining field information from stratigraphy, structures and textures to the thin section scale to characterize eruption dynamics and magma condictions prior to eruption.

Nevertheless the silicic eruption products seem to differ from the general pattern of worldwide registered large-volume silicic eruptions (tens to thousands km^3 of magma) which typically involve fallout layers of pumice lapilli with subordinate lithic clasts produced by Plinian explosive eruptions, accompanied by emplacement of voluminous pumice lapilli-bearing ignimbrites, ending with extrusion of relatively small-volume domes and coulées of degassed silicic lava (e.g. WHITE et al., 2009; BRYAN et al., 2010). In contrast, the silicic volcanism evolved from lava domes to extensive high to extremely high grade ignimbrites showing a lack of lithic fragments and broken phenocrysts and non preservation of vitroclastic textures and fiamme.

2 GEOLOGICAL SETTING

The Paraná Magmatic Province (PMP) comprises volcanic rocks of the Serra Geral Formation covering 917,000 km^2, with average 650 m thick sequences and corresponding to more than 600,000 km^3 of volcanic products (FRANK et al., 2009). Basalt flows make up about 90%, whereas intermediate (basaltic-andesites and andesites) and silicic compositions make up 7 and 2.5% respectively (BELLIENI et al., 1984; PICCIRILLO & MELFI, 1988). However much larger volumes must be considered, since significant erosion affected the South American Platform (GALLAGHER et al., 1994). Also part of this volcanism is preserved in the African Continent, in the Etendeka (Namibia), Kwanza and Namibe (Angola) basins (ALBERTI et al., 1992), giving rise the Paraná-Etendeka LIP. In Brazil the PMP volcanics were emplaced on aeolian sandstones of the Botucatu Formation in the Paraná Basin. The silicic rocks lie on top of the volcanic sequence, representing only 2.5% of total volume, however by no means they are negligible.

Based on volcanics chemistry and spacial distribution data Bellieni et al. (1984) proposed the Paraná basin to be schematically subdivided into three main regions: (1) southern, encompassing tholeiitic suite lying south of the Uruguay River alignment; (2) northern, with tholeiitic-transitional rocks lying north of the Piquiri River alignment; and (3) central, between Piquiri River and Uruguay River alignments (Fig. 1). Main outcrop remnants of Chapecó type silicic volcanic rocks (ATC) occur mainly north of the Uruguay River alignment, with some outcrops south of the Uruguay River alignment. They currently cover an area of ~6,000 km^2 with a total volume of ~1,000 km^3. Palmas type silicic volcanic rocks (ATP) are spatially and volumetrically more significant than ATC rocks. They lie mainly in the southern region covering a current area of ~35,000 km^2 with a total volume of ~12,000 km^3, whereas smaller units (~5,000 km^2 and ~700 km^3 total) crop out in the central region (Fig. 1).

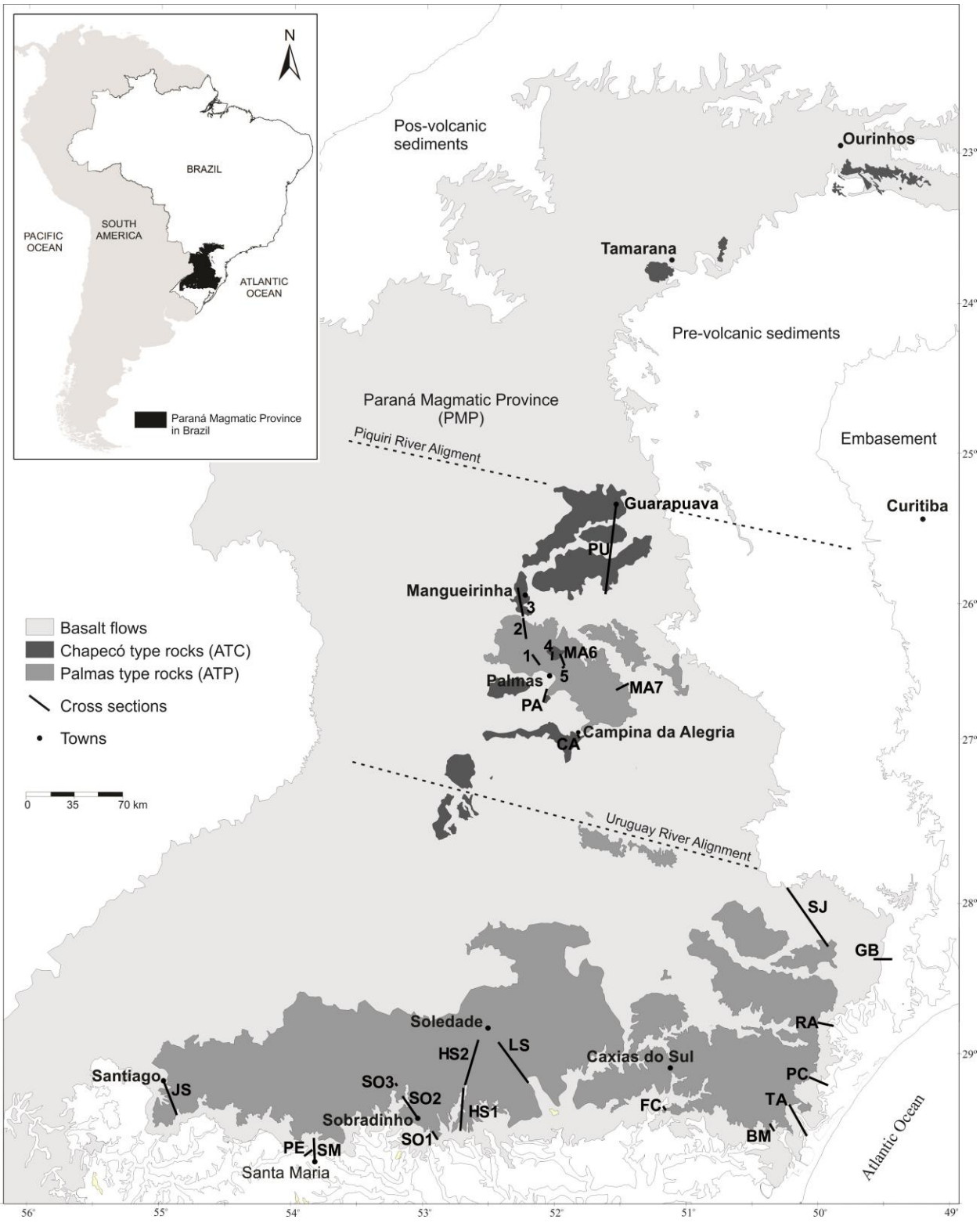

Fig. 1 - Geological and location map for the ATC and ATP units in the PMP, modified from Nardy et al. (2002). Dashed lines mark the Piquiri-Uruguay rivers lineaments which divide the Paraná Basin in northern, central and southern regions (BELLIENI et al.,1984).

3 SILICIC CHEMICAL GROUPS AND SUB-GROUPS

Geochemical data presented in this study were obtained from a set of 250 samples of fresh acidic rocks. Major and trace elements were carried out at Unesp laboratories, using X-ray fluorescence spectrometry. Major elements were analysed using fusion beads (1:10 lithium tetraborate) while trace elements were obtained using pressed (30 ton/cm^2) powder discs (mixed with 25 wt% of micropowder wax). All methodology (including errors) is described in Nardy et al (1997). REE were analysed by ICP-OES, using chromatographic concentration of elements, and the analytical approach is presented in Malagutti et al. (1998).

The silicic volcanics of the PMP are chemically quite different. The Chapecó type silicic volcanic rocks (ATC) are trachytes to dacites (Fig. 2), enriched in TiO_2, P_2O_5, Al_2O_5 and Fe_2O_3, and impoverished in CaO and MgO when compared to Palmas dacites to rhyolites (ATP). ATC rocks are also enriched in some incompatible elements (Ba, Nb, La, Ce, Zr, P, Nd, Y, Yb, Lu and K) and impoverished in Rb, Th and U relative to ATP rocks.

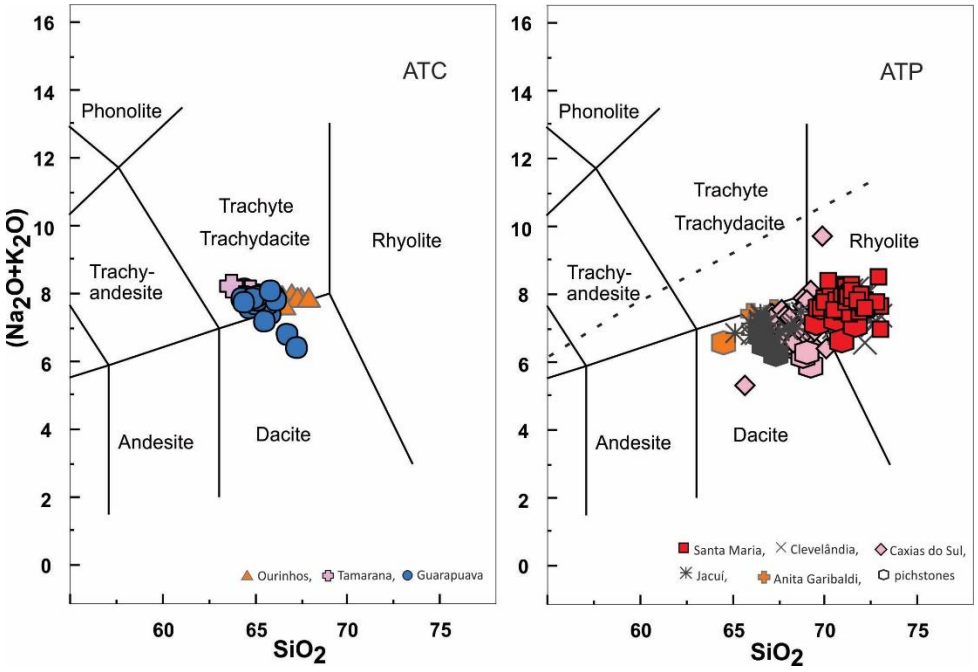

Fig. 2 – TAS diagram (LE BAS et al., 1986) for classification and nomenclature of ATC and ATP silicic volcanic rocks.

These two main silicic groups have been divided in subgroups or magma subtypes based on TiO_2 and P_2O_5 contents (PEATE et al., 1992; GARLAND et al., 1995; NARDY et al., 2008). Thus the Guarapuava ($TiO_2 \geq 1,47\%$), Ourinhos ($TiO_2 \leq 1,29\%$) and Tamarana ($1.38 \leq TiO_2 \leq 1.5\%$) subgroups comprise the ATC rocks. ATP rocks are formed by two subgroups: Low-Ti ($TiO_2 \leq 0,87\%$), composed by the Santa Maria ($P_2O_5 \leq 0,21\%$) and Clevelândia ($0,21\% < P_2O_5 \leq 0,23\%$) subtypes; and High-Ti ($TiO_2 \geq 0,90\%$), composed by the Caxias do Sul ($0,91\% < TiO_2 < 1,03\%$ and $0,25\% < P_2O_5 < 0,28\%$), Jacuí ($1,05\% < TiO_2 < 1,16\%$ and $0,28\% < P_2O_5 < 0,31\%$) and Anita Garibaldi ($1,06\% < TiO_2 < 1,25\%$ and $0,32\% < P_2O_5 < 0,36\%$) magma subtypes. Furthermore, it can be noted from the TAS diagram (Fig. 2) that Jacuí and Anita samples fall in the dacites field, Caxias do Sul in the dacites-rhyolites fields, and Santa Maria and Clevelândia in the rhyolites field.

4 VOLCANIC DEPOSITS

4.1 Stratigraphic Aspects

The silicic volcanic rocks of the PMP overlap tholeiitic basalt-to-andesite flows, lying in the top of the volcanic sucession. Interlayered basalt and/or andesite flows and silicic rocks also occur in places in the southern region.

The central region, between Guarapuava (PR) and Campina da Alegria (SC) towns, is the only place occuring both silicic rock types, ATC (Guarapuava subtype trachydacites-dacites) and ATP (Clevelândia subtype rhyolites). Geomorphologically, it is characterized by remaining flattened surfaces (plateaus) with gently undulating tabular tops and variably thick alteration mantle. 'Fresh' outcrops are rare, scattered, and the contact between units ranging up to 375 m altitude with both ATC and ATP rocks occurring in the same topographic levels in places. This reflects tectonic processes, most likely due to the resulting uplift from the Gondwana breakup, which also led to the emergence of the basement and pre-volcanic sedimentary deposits in the eastern portion. Despite this, representative columnar sections of the area (Fig. 3a-a') show ATP sheets (at least two units) underlie ATC rocks (sections: MA5 and MA6 in Fig. 3a, CA and MA4 in Fig. 3a'), in aggrement with northwest Etendeka sequences, where the Fria 'quartz latite'/Clevelândia underlies the Sarusas 'quartz latite'/Guarapuava (MARSH et al., 2001; EWART et al., 2004). Both silicic units are overlapped by basalts in places.

In the southern region, ATP rocks make up the broader silicic volcanic rock outcrops. The landscape is dominantly characterized by extensive flattened surfaces with gently undulating tabular tops, as the central region, and up-and-down surfaces toward to the base of the silicic volcanic sequence.

Columnar sections (Fig. 3b), especially those in the eastern part (TA, PC, RA, SJ and GB), show the contact with the Botucatu sandstone varying up to 980 m altitude, indicating this region was also affected by the tectonic event resulting from the separation of the South American and African plates. Nevertheless, one can observe the ATP chemical subtypes are also arranged in a stratigraphic sequence. The Santa Maria subtype magma was the latter erupted, overlapping all other ATP subtypes

(columnar sections SO2 – LS, Fig. 3b). In turn, despite the Jacuí subtype does not appear underlying Caxias do Sul rocks in this region, it seems to have been the oldest magma erupted. Furthermore, this subtype underlies Caxias do Sul subtype rocks in the eastern part (columnar sections BM and RA, Fig. 3b), as in the Southern Etendeka, Namibia, where the Goboboseb ‘quartz latite’/Jacuí underlies the Springbok ‘quartz latite’/Caxias do Sul (MILNER et al., 1995; MARSH et al., 2001).

ATC outcrops liyng further north (Ourinhos subtype), which are not part of the scope of this study, were, hitherto, the only silicic units observed laying directly on the Botucatu sandstones (e.g. NARDY et al., 2002; JANASI et al., 2007). However, ATP units (Jacuí subtype) in the southern region, near the Sobradinho town, were found overlapping a 40 m thick Botucatu sandstone (columnar sections SO2 and SO3, Fig. 3c), which in turn was intruded at the base by an ATP body (Jacuí subtype?), forming peperite.

Peperites were also broadly found in the base and interlayered in the silicic volcanic succession in both areas (LUCHETTI et al., 2014), highlighting periods of quiescence between the basic and silicic volcanism and the silicic eruptions.

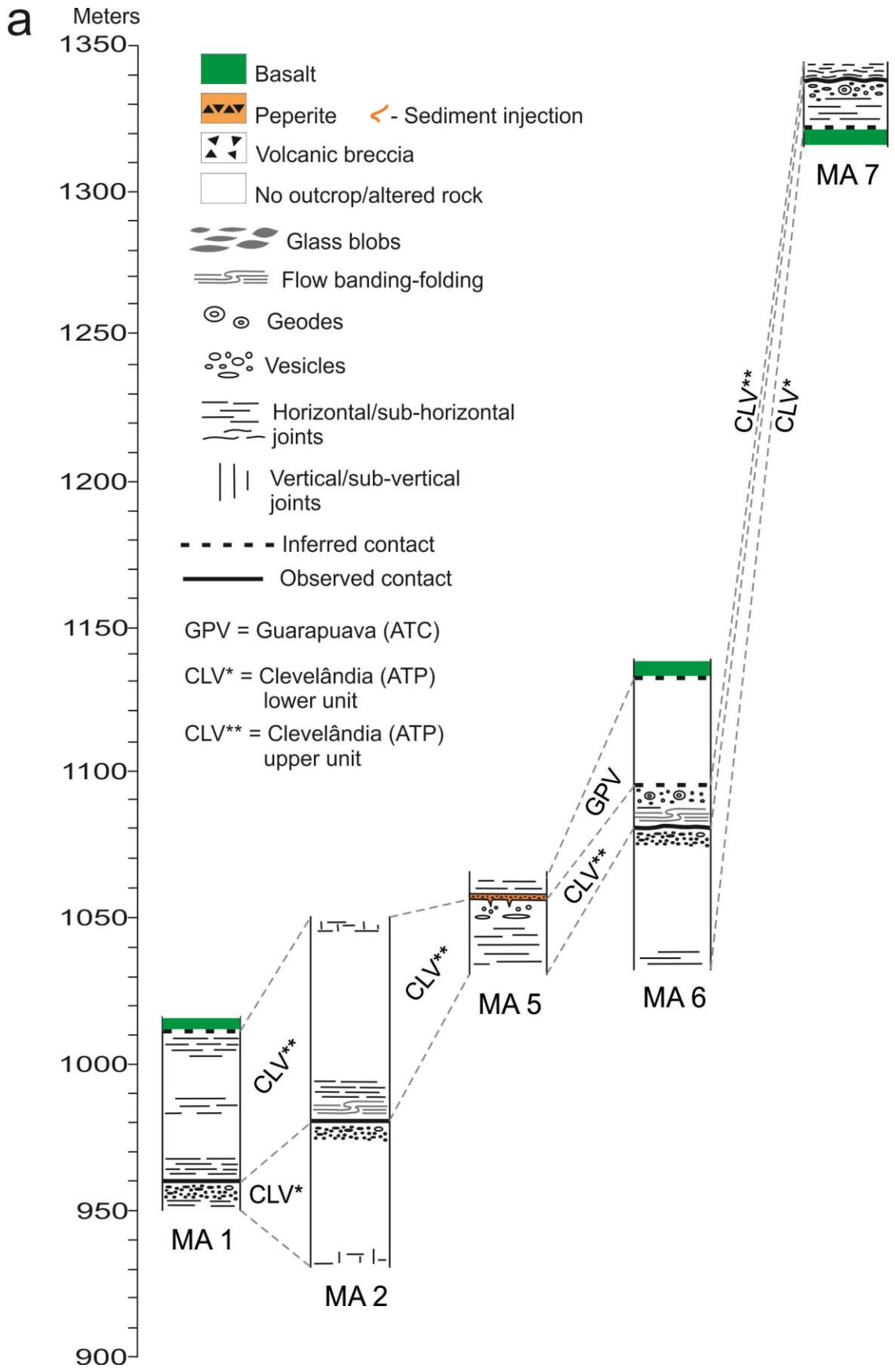
a
Meters
1350
1300
1250
1200
1150
1100
1050
1000
950
900
Basalt
Peperite
- Sediment injection
Volcanic breccia
No outcrop/altered rock
Glass blobs
Flow banding-folding
Geodes
Vesicles
Horizontal/sub-horizontal joints
Vertical/sub-vertical joints
Inferred contact
Observed contact
GPV = Guarapuava (ATC)
CLV* = Clevelândia (ATP) lower unit
CLV** = Clevelândia (ATP) upper unit
MA 1
MA 2
MA 5
MA 6
MA 7
CLV**
CLV*
GPV

Fig. 3 continued.

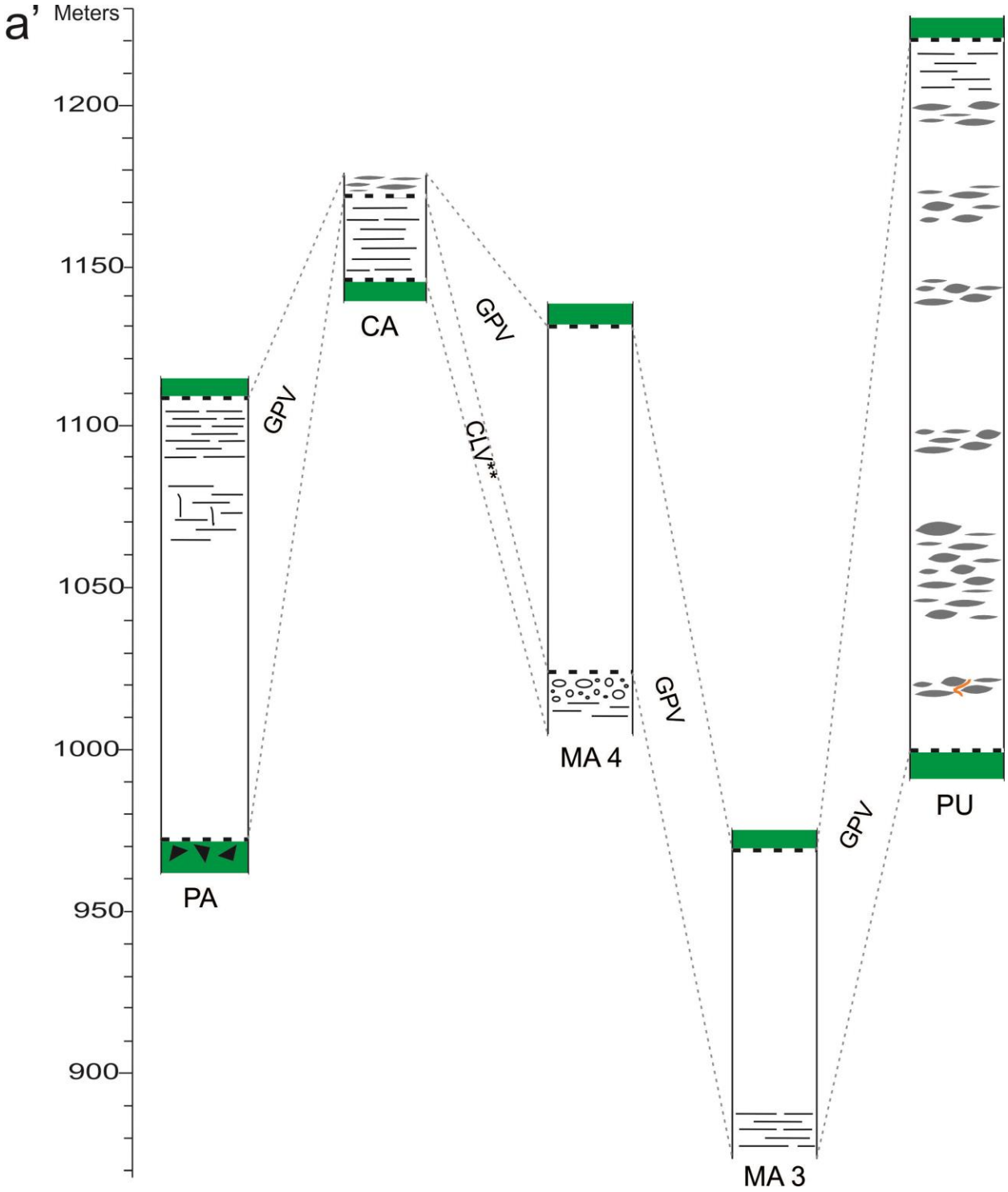

Fig. 3 continued.

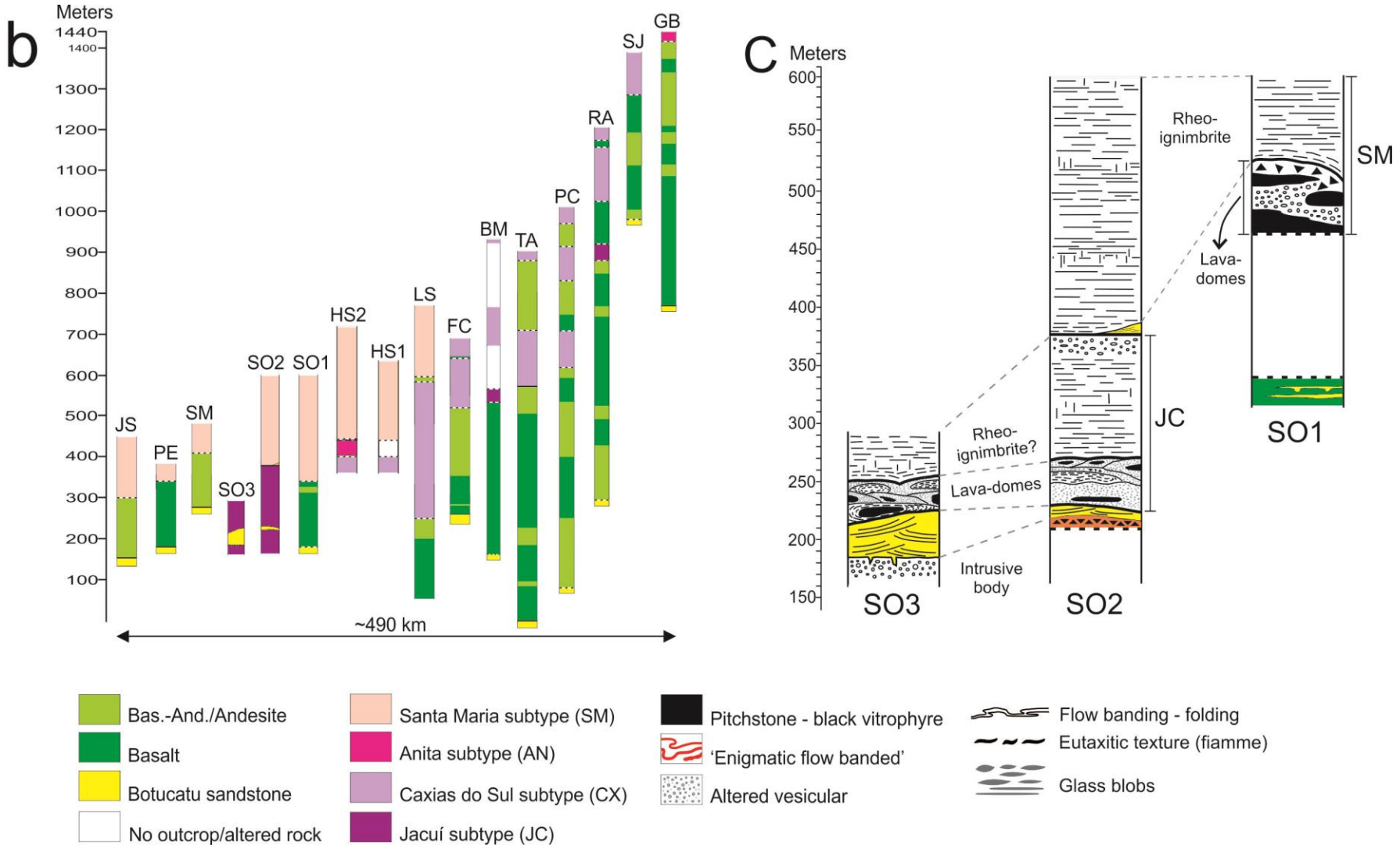

Fig. 3 continued.

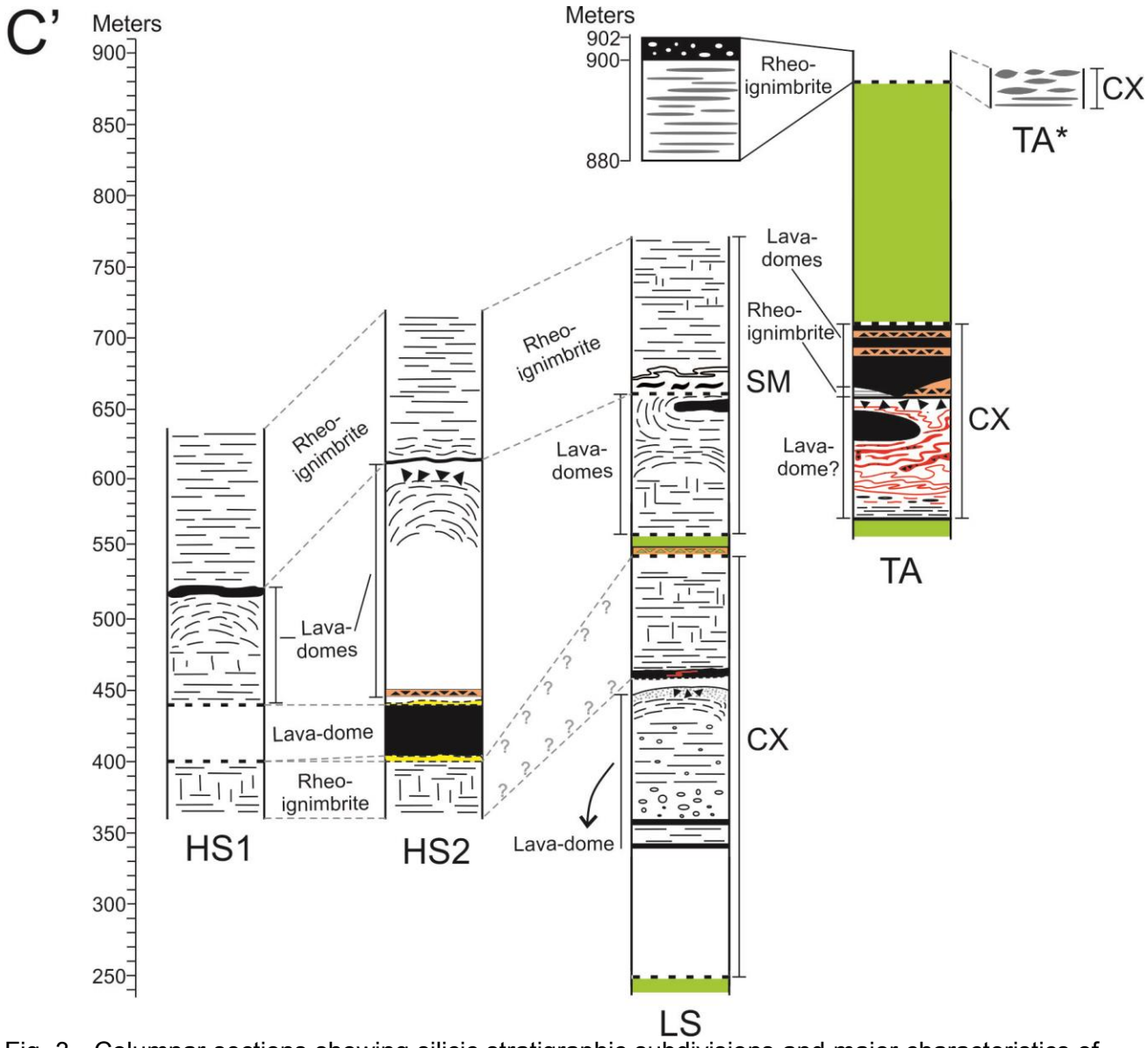

Fig. 3 - Columnar sections showing silicic stratigraphic subdivisions and major characteristics of the deposits. a-a' = columnar sections of rheoignimbrite deposits from northern region; b = chemical-stratigraphic sections from southern region, of which some 'key sections' were chosen to represent the major features of the deposits (c-c'). Dashed lines (in gray) are probable stratigraphic correlations. Location of sections in Fig. 1.

4.2 Silicic Lava Domes

Silicic lava domes are the early products of the Caxias do Sul, Jacuí and Santa Maria silicic sequences and the Anita Garibaldi unit in the southern region. (Fig. 3c-c'). They form clusters of staked outcrops with each thicknesses ranging from 90 to 10 m of pitchstones with vesicular outer layer and/or wrapped by matrix-supported autobreccias (Fig. 4a-b). Autobreccias comprise mainly angular to rounded, vesicular to dense clasts of the same composition with sizes ranging from large blocks (centimetric) to smaller clasts (millimetric). They are altered to beige and light-dark green colors and show perlitic fractures. Vesicles in clasts are spherical to elongated and stretched, many filled by quartz or silica minerals.

Basal breccias can also have matrix made up of unsorted fine-grained sediment in places representing peperites (LUCHETTI et al., 2014). Joints are poorly developed in the pitchstones which show a massive structure and conchoidal fracture. However, devitrified domains display conspicuous horizontal to platy joints, with spacing between them increasing inward (Fig. 4c). They can be tightly curved (concentric joints) in places, mainly in the outer parts of small lobes. Thicker units consist of massive pitchstone interior surrounded by horizontal-to-curved sheeting jointed devitrified rock with usually altered, brecciated in places, glassy external parts. Small lobate shapes are also common with massive/glassy interior and altered or oxidized, vesicular to devitrified exterior. At outcrops further west, near the Sobradinho town, lava domes directly overlap ~35 m thick aeolian sandstones (paleo-dune) of the Botucatu Formation, which in turn is intruded at its base by a silicic body forming peperite in places (Fig. 4d). The vesicles-amigdales in the volcanic clasts forming the peperite are upward oriented and the sandstone matrix contain vesicles, indicating it was wet. The coarser and thoroughly crystalline groundmass, compared to upper glassy lava domes, also point to a slower cooling due to shallow intrusion setting.

Fig. 4 – Lava dome features in ATP rocks. (a) Pitchstone (black interior) with brecciated base and external part in Caxias do Sul unit; (b) Santa Maria outcrop showing pitchstone with brecciated exterior (white dashed line) in contatct with overlying ignimbrite (yellow dashed line). (c) Curved sheeting to platy joints in a Jacuí lava dome; (d) peperite formed in the top of a Jacuí unit intruded in a sandstone from Botucatu Formation. Vesicles in the volcanic clasts (V) are upward oriented and the sandstone matrix also contain vesicles.

4.3 Extensive Sheets - Rheoignimbrites

Extensive sheets occur in the central region (Fig. 3a-a') and around and above lava domes and basalts in the southern region (Fig. 3c-c'). As previously mentioned, Santa Maria subtype sheets seems to be the youngest manifestations, overlying all other silicic units and basalts in the western region, with a package thickness of up to 220 m, whereas Caxias do Sul and Jacuí subtype sheets reach 160 m and 130 m thickness, respectively. In the central region, between Guarapuava and Palmas towns, Clevelândia subtype sheets totalling 120 m thick, underly Guarapuava subtype sheets (ATC), which in turn reach 220 m thickness. These extensive sheets form flat-topped terraces with a constructional architecture comprised of multiple sub-parallel, tabular packages. Total package thicknesses for ATP sheets range from ~30 to 160 m for Caxias do Sul subtype, 70 to 220 m for Santa Maria subtype and 130 m for Jacuí subtype in the southern region, and 120 m for Clevelândia subtype in the central region.

However these silicic units must have been much thicker, since the top was eroded and the base is not exposed in central region. They can be traced laterally for tens to hundreds of kilometers, thickening locally in small valleys and thinning to less than 2 m across topographic highs. These make estimation of eruption volumes difficult and, as the sources areas are unknown, thicknesses and extents estimation of proximal-distal ignimbrite is almost impossible.

A conspicuous feature in these sheets are the horizontal to subhorizontal jointing ranging in spacing from a few centimetres, in which the term ‘sheeting joints’ is appropriate, to a few metres and resulting in flaggy outcrops in the field (Fig. 5a). Vertical joints are also present in places with a few to several metres spacing. Sheets comprise largely massive, structureless rock or with a horizontally (to sub-horizontal) continuous diffuse layering marked by the alternation of microcrystalline quartz-feldspathic and spherulitic layers. Layer thicknesses ranges from millimeters to several centimeters with small-scale isoclinal folds in places (Fig. 5b), and parallel or sub-parallel jointing. Massive packets can occur interfingered with altered and/or weathered portions, indicating local variations in welding and multiple flow units (Fig. 5c).

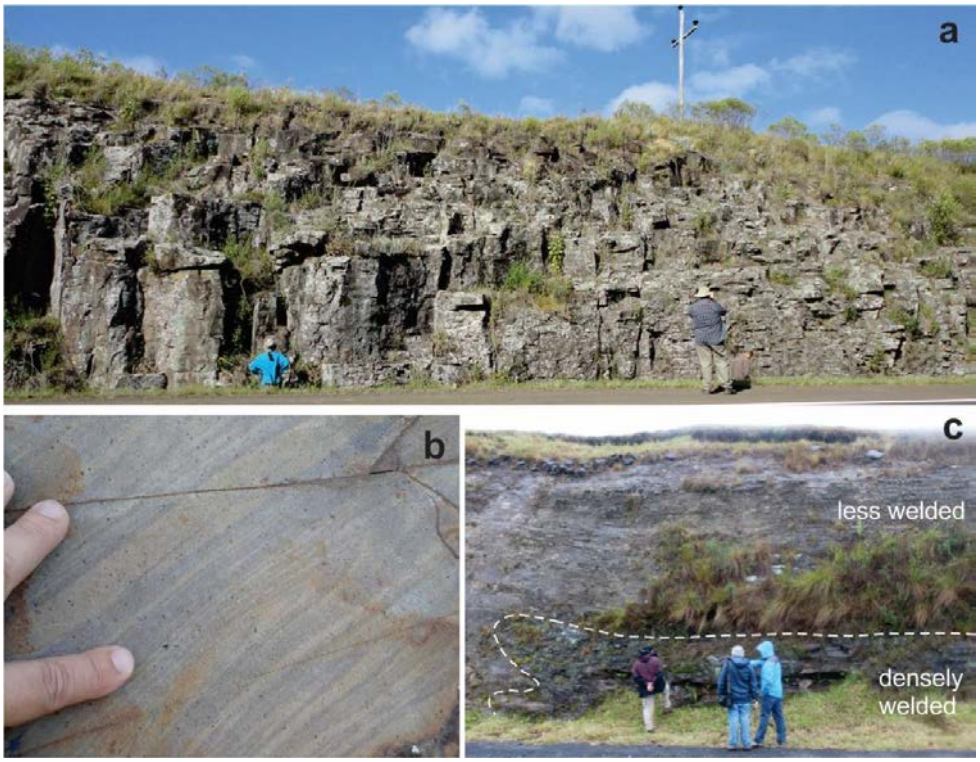

Fig. 5 – Common aspect of the extensive sheets, in especially Santa Maria unit, displaying massive horizontal jointed outcrops (a), flow banding-folding in places (b), and massive packets interfingered with altered and/or weathered portions, indicating local variations in welding (c); In (b) joints are sub-horizontal and the flow banding horizontal.

Basal autobreccias or lithic breccias are absent, with rare local breccias formed by the interaction with sediment, characterizing peperitic breccias or peperites. Localized black vitrophyre zones occur in the bottom and tops of Caxias do Sul and Santa Maria units, in most cases being completely homogeneous. An exception is an apparent vitrophyre in the bottom of Caxias do Sul sheet with a lamination marked by millimetre-scale vesicles filled by quartz and reddish lenses (Fig. 6a) which, in thin section, show a thoroughly devitrified-recrystallized groundmass. Glassy dark brown lenses-laminae show undulating margins and feathery terminations evidencing fiamme, however its outlines are diffuse and locally overprinted by the devitrification (Fig 7a-b). The sheets also show varying abundance of spherical to ellipsoidal vesicles and amigdales filled by silica minerals, with sizes ranging from millimeter to centimeter.

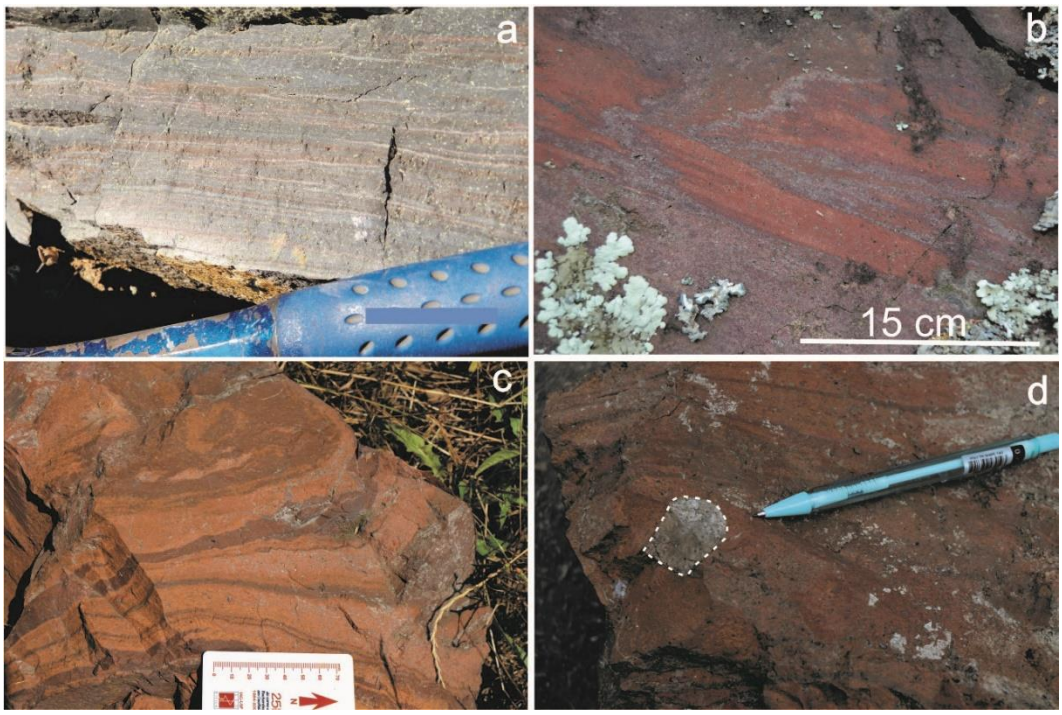

Fig. 6 – (a) Extremely flattened-stretched glassy reddish lenses and vesicles filled by quartz in apparent vitrophyre in the bottom of Caxias do Sul sheet; Estwing hammer cable as scale. (b-d) Oxidized Santa Maria outcrop with flattened-stretched juvenile clasts similar to fiamme (b); just above a lava-like lithofacies with flow banding and folding (c); and a granitic lithic clast (d) (dashed outline).

Vitroclastic texture was observed in a Santa Maria outcrop. The rock is reddened by oxidation, flat jointed in places and consists of flattened to extremely flattened juvenile clasts resembling collapsed pumices (fiamme) (Fig 6b). In thin section the matrix comprises plagioclase and Fe-Ti oxide phenocrysts, numerous small plagioclase-pyroxene laths and stretched to extremely stretched glass shards (Fig. 7c-e). The latter are deformed around the crystals and the Y-shape is still exhibited by some shards (Fig. 7d). The rock becomes strongly flow banding-laminated and folded in places (Fig. 6c), with millimeter-to-centimeter scale band thicknesses, glass shards are no longer recognizable and the crystals laths are orientend parallel to flow layering (Fig. 7f). A homogeneous vitrophyre, ~10 m thick, lies beneath this sheet and may represent the basal vitrophyre. For the rest, the sheet is flat jointed and massive. Joint spacing commonly coincide with the banding, but it can be sub-parallel in places.

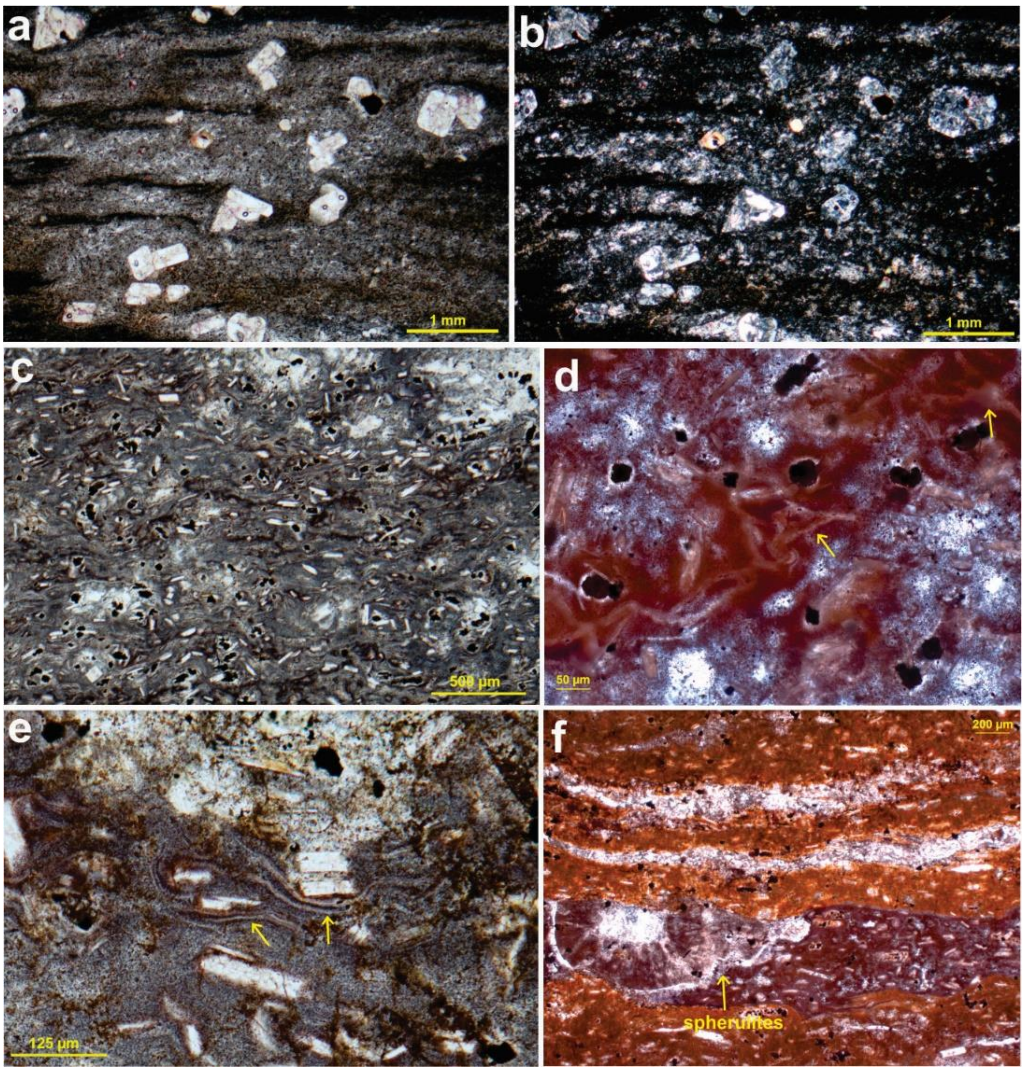

Fig. 7 – Photomicrographs of textures in the Caxias do Sul apparent vitrophyre (a-b) and Santa Maria outcrop (c-f) shown in Fig. 6. (a-b) extremely flattened, deformed by phenocrysts dark lenses in a quartz-feldspathic mosaic matrix. Lens outlines become quite diffuse in places overprinted by the devitrification; (a) = // pol. and (b) = X pol.; (c) oxidized groundmass overall aspect showing plagioclase-opaque microphenocrysts to microlites and vitroclastic texture with Y-shaped (d) (arrows) to extremely flattened-stretched, deflated by plagioclase laths glass shards (e) (arrows); (f) extremely flattened-stretched juvenile clasts ranging in devitrification (note the spherulite formed from the clast rim) in an entirely homogenized groundmass, with crystal laths oriented parallel to flow, characterizing a lava-like lithofacies; // pol.

Lithic fragments are rare, but where found they are mostly basalt-andesite or own silicic volcanics and more rarely granite (Fig. 6d), with angular to rounded shapes. The Santa Maria subtype seems to be composed of multiple flows and shows a remarkable vertical and lateral zoning of phenocryst abundance in the whole package. Lower parts

can consist of up to 3% of phenocrysts, with the top and westward being virtually phenocrysts-free. An upward decrease in phenocrysts abundance was also seen in a single outcrop. Although some phenocrysts show some breakage, it is not widespread, even in the ATC rocks bearing large plagioclase phenocrysts, and it can be said that broken phenocrysts are rare compared with typical ignimbrites. Groundmass is thoroughly devitrified to recrystallized showing spherulites into crypto-to-microcrystalline patches, giving a mottled or salt and pepper texture to the rock, to an entirely quartz-feldspathic microcrystalline texture.

ATC and Caxias do Sul sheets (ATP) show a characteristic eutaxitic texture marked by dark lens-shaped blobs set in a light matrix (Fig. 8). In basal sections of thick outcrops blobs are extremely flattened and/or stretched into the millimetre-scale laminations. Spherical to elongated vesicles are scattered throughout the sheet with some blobs deflated around them. Differential alteration can form 'blocky' outcrops highlighting lensoidal blocks and lumps (Fig. 8c). Where extremely flat, joint (sheeting) spacing can coincide with the layering. Some vertical fractures found in outcrops displaying this banding may indicate pipe-like gas escape structures.

Fig. 8 – Flattened and stretched glass blobs in Caxias do Sul (a-c) and Guarapuava (d-e) sheets. Note the large detached lens-shape block and lumps in (c).

Microscopically the contact between blobs and matrix is diffuse, almost indistinguishable, except for differences in groundmass textures, zonal alteration and crystal size distribution. In hand sample scale the matrix is made up of white dots (or spots) set in dark areas. Under optical microscope, dots are dark brown clouds and interstices comprise crypto-to-microcrystalline patches. SEM analysis show the dark clouds are minute fibres to aggregates forming a feldspathic composition mass and, in samples from outcrops showing less flattened, larger blobs, these dark brown clouds encompasses several small glass globules. White dots are mostly smaller and sparsely distributed in the blobs with a groundmass consisting mainly of crypto-to-microcrystalline patches of quartz-feldspathic composition. Furthermore, these two domains show different distribution patterns for plagioclase-pyroxene-magnetite microlites (≤ 100 μm), for which the blobs display a noticeably larger amount in SEM images. For phenocrysts, subtle differences in distribution pattern is better noted in the ATC porphyritic rocks in which blobs show larger amount of crystals, including larger crystal clusters.

The Jacuí unit is the least extensive, outcropping for ~25 km long from a likely source, where an intrusive body was found (columnar sections SO2 and 3). It comprises a massive and devitrified rock and the main feature is a ubiquitous horizontal to subhorizontal jointing.

4.4 ‘Enigmatic Flow Banded’ Rocks

In the eastern region, where Caxias do Sul subgroup rocks dominate, some pitchstones from the base of the lava domes sequence or underlying extensive silicic sheets show sudden flow banding-lamination. It is characterized by millimeter width and several centimeters long, flattened, stretched oxidized reddish lenses and vesicles filled by quartz in a dark fine-grained microcrystalline rock. Upward the banding is like that in lava flows, with alternation between reddish spherulitic flow bands, with varying thicknesses (Fig. 9a) and internally brecciated in places, and microcrystalline dark rock. It becomes steeply dipping with ramp structures, folding, magma mingling-like

structures (Fig. 9b) and red vesicular packets and/or clasts. In a quarry nearby Caxias do Sul town this steeply dipping and contorted banding is quite evident (Fig. 9e) and Lima et al. (2012) have proposed it being a feeder dike-like source area. Another interesting feature observed in the quarry is another type of flow banding-lamination comprising dark thin layers in a light matrix (Fig. 9c-d), including basalt-andesite clasts or enclaves with up to ~3.5 cm long, embayed outlines and rotated (Fig. 9d). SEM observations coupled to EDS analyzes show three different domains characterized by: light layers = (1) coarser plagioclase microlites; (2) fine-grained alkali-feldspar microlites; and dark layers = (3) quartz+alkali-feldspar microcrystalline intergowth, with all domains containing pyroxene and Fe-Ti oxides microlites. This may reflect a compositional layering between basic-intermediate and silicic magmas. Both flow banding-laminations comprise, folding, refolding, swirls, and magma mingling-like texture. The dark microcrystalline rock also occurs as massive and internally structureless domains or as centimeter size-scale welded lens-shaped clasts with tapered extremities interlayered or interfingered in the flow banded rock (Fig. 9c), and similar to the glass blobs previously described. Scattered spherulites and spherical vesicles filled by quartz of up to ~5 mm in diameter give a mottled appearance to the rock. Furthermore some giant vesicles of up to half a meter long also occur through the quarry and they can be elongated and/or deformed parallel to the flow in places (Fig. 9e).

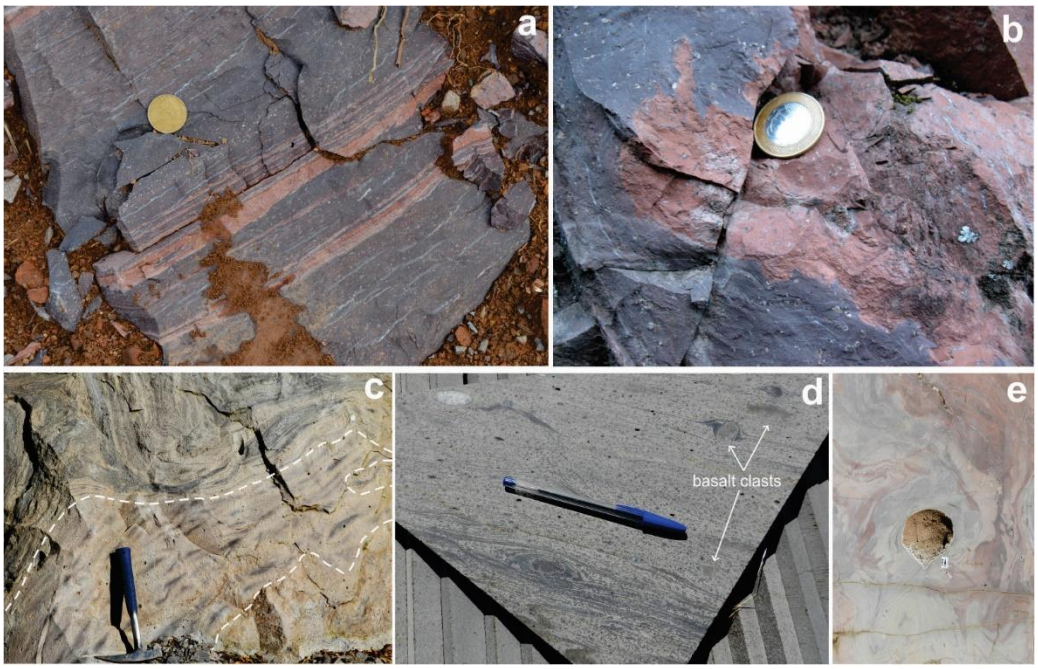

Fig. 9 – Aspects of the flow banded ‘fluidal’ unit, displaying oxidized red bands and stretched lenses filled by quartz (a) in dark devitrified rock; mingling-like structure (b); coins have 2.5 cm; portion formed by glass blobs (spatters?) (dashed outline) interlayerd in compositionally-granulometrically flow banded material (c); (d) polished slab showing flow lamination between dark crystalline material and light material comprising plagioclase and k-feldspar microlites domains, and (rotated) basalt clasts; (e) giant vesicle (ballon shape) in complex steeply dipping flow banded rock in the quarry wall; scale card is 8.5 cm long.

5 PETROGRAPHY

ATC type rocks from this study are porphyritic to sparsely porphyritic with up to ~20% of plagioclase (An_{30-49}), pyroxene (augite and pigeonite), Fe-Ti oxides (Ti-magnetite and ilmenite) and apatite phenocrysts (Figures 8 and 9). Euhedral to sub-rounded plagioclase crystals can reach up to 1 cm in length (major axis) and compose up to 15% of the rock. Augite and pigeonite crystals are subhedral to rounded and make up ~5%, rarely exceeding 2 mm long. Ti-magnetite and ilmenite comprise Fe-Ti oxides, not exceeding 2% of the rock. Apatite amounts to less than 1% and long crystals may reach 0.5 mm in length. The groundmass contains plagioclase, pyroxene and Fe-Ti oxide microlites with tabular habit to hollow, dendritic and swallowtail shapes and is thoroughly devitrified-recrystallized. It shows brown spherulitic patches are surrounded by microcrystalline material (quartz-feldspar intergrows) or entirely quartz-feldspar intergrown acquiring a microgranophyric texture.

ATP type rocks are sparsely porphyritic to aphyric with up to ~4% of plagioclase (An_{41-74}) (prevailing), pyroxene (orthopyroxene, augite and pigeonite) and Fe-Ti oxide pheno-microphenocrysts. Plagioclase crystals make up to 3% of the rock usually does not exceeding 1.5 mm of length, except some reaching 3 mm long. They are euhedral-subhedral to rounded and can show embayment, corroded edges and coarse sieve. Few crystals in a Caxias do Sul pitchstone are shattered and rotated, similar to “phenoclast” textures described by Best and Christiansen (1997) originated by bursting melt inclusions decompressed during explosive eruption. Pyroxene crystals represent up to ~1% of the rock, occurring only in the groundmass in the Santa Maria unit. They rarely exceed 1 mm in length, except for some long orthopyroxenes reaching more than 4 mm in length, and show subhedral to extremely rounded shapes, reacted or corroded edges and partial to complete alteration to brown or green material. Fe-Ti oxides make up less than 1% and are primarily Ti-magnetite with rare ilmenite thin lamellae. Apatite occurs as minute quantities in the groundmass. The Clevelândia and Anita units and some Santa Maria sheets are virtually phenocryst-free.

Groundmass is glassy to thoroughly devitrified groundmass with a broad range in microlite densities of plagioclase, pyroxene and Fe-Ti oxides. Devitrified samples groundmass show brown spherulitic patches surrounded by microcrystalline quartz-

feldspar intergrows to microgranophyric texture throughout. Microlite shapes comprise tabular (laths) to hollow, dendritic, acicular and swallowtail ends for plagioclase and irregular to acicular (up to 4 mm long) for pyroxene. Furthermore crystal clusters (or “glomerocrysts”) are a common feature in both ATC and ATP rocks consisting of plagioclase, pyroxene, plagioclase+pyroxene and plagioclase+pyroxene+Fe-Ti oxides assemblages.

6 DISCUSSION

In recent years it has been discussed more often the emplacement mode of the Paraná Magmatic Province silicic volcanics. Works by Whittingham (1989), in the South Brazil, and Milner et al. (1992) and Ewart et al. (1998), in the north-western Namibia, agree with a pyroclastic origin for the ATP rocks and related rocks in Namibia (Etendeka Formation) respectively. According to these authors, as such rocks show features typical of lava (e.g. flow banding, unbroken crystals, local breccias) and, at the same time, remaining glass shards and fiamme from a non welded unit, as well globular texture (fused shards) (MILNER et al., 1992), they have been emplaced as rheoignimbrites. Siviero et al. (2005) also interpreted some ATP units from South Brazil as ignimbrites, and for Arioli et al. (2008) ATC rocks from Guarapuava region are rheomorphic ignimbrites.

On the other hand other researchers argue for an effusive emplacement mode for the silicic volcanics. Despite Garland et al. (1995) report on pyroclastic textures preserved in a thin layer and crystal segregation in ATP flows, owing the lack of caldera structures and sparsity of pyroclastic textures, the authors did not rule out an effusive way for ATP rocks. For Chapecó type magma, they proposed a generation in mid-lower crustal depths (5-15 Km), rapid ascent via dykes and the spreading on the surface as lava flows. Umann et al. (2001), Waichel et al. (2012) and Lima et al. (2012) suggest the Caxias do Sul units from the eastern border of PMP comprise lava domes and tabular lavas with similar interpretation for the silicic units in the western region by Liza & Janasi (2014).

Extensive ATC and ATP units are interpreted here as high to extremely high grade ignimbrites originated from high mass-flux pyroclastic fountaining eruptions (BRANNEY & KOKELAAR, 1992, 2002), possibly via fissures.

The problem in distinguishing between lava and ignimbrite is the lack or non-preservation of primary pyroclastic textures such as pumice lapilli, fiamme, glass shards, broken phenocrysts and lithic fragments. According to Henry and Wolf (1992) base and/or top of units are the best parts for this recognition, since lavas contain thick upper and basal autobreccias (BONNICHSEN & KAUFFMAN, 1987) which are uncommon in ignimbrites. Likewise pyroclastic features would be preserved in these

parts due to quenching (HENRY WOLF, 1992). However these are often hidden, weathered or have been eroded. Furthermore pyroclastic deposits can be intensely welded from its bottom to top (ROSS & SMITH, 1961) or even have been undergone to rheomorphism, wherein explosive features can be totally destroyed and the terms ‘high to extremely high grade’ or ‘lava-like’ are applied (BRANNEY et al., 1992; BRANNEY AND KOKELAAR, 1992; 2002). Therefore, the lack of primary pyroclastic textures does not always means a lava flow origin. Many other works exist in the literature on the subtle differences and complexities between lavas and lava-like ignimbrites, in terms of their eruption, deposition, welding and rheomorphism, and field characteristics (e.g. SCHMINCKE & SWANSON, 1967; WOLFF AND WRIGHT, 1981; Walker 1983; HENRY et al., 1988; BRANNEY et al., 2008; FREUNDT & SCHMINCKE, 1995; FREUNDT, 1998; KOBBERGER & SCHMINCKE, 1999; SUMNER & BRANNEY, 2002). Unit extents are also a striking feature, with ignimbrites reaching hundreds of km in lenght and extensive silicic lavas little more than a few tens of km (BONNICHSEN & KAUFFMAN, 1987; BRANNEY et al., 2008).

The units show widespread sheet-like geometry, with lateral extents > 40 km, and problably ≥ 100 km for some sheets, areal extents up to ~16,000 km^2 (not considering individual units in the Etendeka reaching up to 8,800 km^2, Milner et al., 1992). In the southern region the topography where lava domes crop out is characterized by rounded-convex hills (Fig. 10a), whereas extensive plateaus dominate wide areas in the same region and in the central region (Fig. 10b), where extensive sheet deposits occur.

Fig. 10 - Different landscapes from areas where silicic lava domes crop out (a) vs flatten relief (b) of extensive sheet-like deposits. Surface irregularities (hillocks) in (b) would be due to differences in welding.

The absence of both basal and top autobreccias is also a strong indication for an emplacement by pyroclastic density currents rather than viscous lava flows. Main examples of extensive silicic lava flows described in the literature show widespread basal autobreccias (Snake River Plain – BONNICHSEN & KAUFFMAN, 1987; Bracks Rhyolite, Trans-Pecos Texas – HENRY et al., 1990; Gawler Range Province - ALLEN et al., 2008). Furthermore the vertical and/or horizontal zoning of phenocryst abundance in the Santa Maria sheets is an indication of transport and deposition regimes from granular fluid-based pyroclastic density currents (BRANNEY & KOKELAAR, 2002; BRANNEY et al., 2008).

Glass shards, fiamme, lithic fragments or broken phenocrysts are rare or not observed, except for some localized layers with fiamme texture and/or flattened to stretched shards described in this work and other pyroclastic features reported by Milner et al. (1992) and Garland et al. (1995). However all or nearly all remaining vestiges of shard and fiamme texture may have been pervasively transposed and obliterated by the welding, rheomorphism and subsequent devitrification-recrystallization. Less welded to non welded lithofacies are wheathered or have been eroded, since the exhumation is estimated in more than 1 km by apatite fission track (GALLAGHER et al., 1994). The lack of fiamme or pumice lapilli and lithic lapilli is a common characteristic of many rheoignimbrites from Snake River Plain, in which lava-like lithofacies comprise most part of the sheets (BONNICHSEN & CITRON, 1982; BRANNEY et al., 2008), revealing originally true tuffs (ANDREWS et al., 2008; BRANNEY et al., 2008). However, another feature shown by these rheoignimbrites is the presence of extensive, parallel-laminated, medium to coarse-grained ashfall deposits with large cuspate shards, reflecting high explosive eruptions (VEI 6-8) and therefore pointing to a peculiarity in the fragmentation process, not understood, with possible influence of meteoric water (BRANNEY et al., 2008). Unfortunately ashfall deposits have not been found or recognized as such in the PMP volcanism. Further the scarcity of lithic fragments and unbroken phenocrysts in extremely high-grade ignimbrites elsewhere indicate low explosivity eruptions from relatively hot, fluid and gas poor magmas (HENRY & WOLF, 1992).

The flow layering-lamination may have been established from healed fractures,

former vesicular zones and/or other textural heterogeneities originated in the surface in the coalesced flows after the end of primary flowage. Such structures developed parallel planes along which the ductile or ruptile shear can occur (BONNICHSEN & CITRON, 1982; PIOLI & ROSI, 2005; BRANNEY et al., 2008). Therefore these layers become planes of weakness along which the joints would form parallel during or after the devitrification. Low angle joints also occur sub-parallel to the flow banding probably developed during static devitrification after the anisotropy of the flow (BRANNEY et al., 2008). Completely homogeneous vitrophyres suggest extreme conditions of welding (ROSS & SMITH, 1961) or coalescence and ponding of glass particles to a viscous mass with nowhere to flow (BONNICHSEN & CITRON, 1982; BRANNEY & KOKELAAR, 1992), consistent with a likely flat surface at the time the sheets were emplaced, consisting of small valleys or basins set by previous basalt flows and silicic lava domes. Moreover the flat topography seems to have played a key role in the bulk deposition, since pervasive secondary flowage structures, commonly seen in many rheomorphic ignimbrites and near absent in the present rocks, are more easily originated in adownslope mass flowage moved downslope (BONNICHSEN & CITRON, 1982; PIOLI & ROSSI, 2005).

The eutaxitic texture defined by glass blobs in ATC and Caxias do Sul rocks also suggest these units are ‘hybrids’ and not exactly similar to conventional ignimbrites. As the fragmentation process is not as intense, the phenocrysts size distribution in blobs and matrix may indeed be similar to subtly different, as in ATP specimens. On the other hand a certain difference in the phenocryst size distribution in porphyritic ATC samples and a remarkable difference in the small crystals abundance in both ATC and ATP samples may be explained by the transport in a pyroclastic density current where they would be more easily transported, occurring in smaller quantities in the matrix. Numerous glass blobs are also described in the Pagosa Peak Dacite, interpreted as a voluminous lava-like ignimbrite which preceded a major ash-flow tuff, the Fish Canyon Tuff (BACHMANN et al., 2000). Moreover, despite the advanced devitrification coupled with alteration, the globule-shaped glass may express relict globular shards similar to those found in other rheomorphic ignimbrites (e.g. JOHNSON 1968; SUMNER & BRANNEY, 2002; BRANNEY et al., 2008) or glassy particles coalescence texture

reported for high grade Nuraxi Tuff by Gimeno et al., 2003, or even similar to those obtained from welding experiments for the rhyolitic Rattlesnake Tuff by Grunder et al., 2005. The final appearance of the sheet, with horizontally fairly continuous banding downward, resulted from an end-stage compaction followed by sheeting-joint formation, as the pattern typical of some is to outline dark lenses.

Temperatures estimated from phencrysts for these magmas are too high, ~ 950°C to > 1000°C (e.g. BELLIENI et al., 1986; GARLAND et al., 1995; NARDY et al., 2011; this study), even the primarily aphyric character of some units indicates liquidus temperature. Such a high temperature would be responsible for the decrease in viscosity and the resulting particle agglutination (BRANNEY et al., 1992; BRANNEY & KOKELAAR, 1992; 2002). The water content is also low, up to 2wt % maximum (e.g. NARDY et al., 2011; this study), consistent with the anhydrous mineralogy. Such combination of high T and low gas content and, therefore low gas velocity, led to low collapse heights and little heat loss during collapse, prerequisites for producing highly welded tuffs (e.g. SPARKS et al., 1978).

Nevertheless, some sheets are still ambiguous, such as the least extensive Jacuí unit. It may represent an extensive silicic lava flow, but more detailed studies in this unit are required in order to find pumiceous and/or brecciated carapaces. In the central region, the base of the lower Clevelândia sheet is buried and its top is extremely altered, but a vesicular-amigdaloidal carapace with several geodes in places is recognizable and it may indicate a lava flow origin for this sheet. However this pumiceous carapace crop outs along at least 30 km of a highway**.**

6.1 ‘Enigmatic Flow Banded’ Rocks

The flow banding observed in some Caxias do Sul outcrops and in a quarry are typical of lava flows. However such banding can also form in lava-like rheomorphic ignimbrites (e.g. SUMMER & BRANNEY, 2002) and fountain-fed lava flows (e.g. STEVENSON et a., 1993). Furthermore lensoidal glass fragments or blobs occurring above and interdigited in the flow banded rock may represent spatter-like structures. Spatter-rich deposits of non-basaltic composition are reported in the literature,

evidencing its transport in pyroclastic flow deposits (e.g. MELLORS & SPARKS, 1991; FURUKAWA & KAMATA, 2004), fallout deposits (e.g. SORIANO et al., 2002) and fountain-fed lava flows (e.g. STEVENSON et al., 1993; STEVENSON & WILSON, 97; FURUKAWA & KAMATA, 2004). Giant vesicles seem to be concentrated in the quarry area, since they were not observed elsewhere, and such structures to much larger ones are also described in a rheomorphic vent fill from Canary Islands (SORIANO et al., 2009). Nevertheless, distinguishing between lava-like rheomorphic ignimbrites and fountain-fed lava flows is almost impossible, since clasts (spatters) outlines can be completely erased resulting in a massive, homogenized rock (STEVENSON et a., 1993), and fountain-fed lava flows can be an end-member of ignimbrite-grade continuum (BRANNEY & KOKELAAR, 1992). Thus, an emplacement mode as lava-like rheomorphic or fountain-fed lava flows must be considered for these banded units, and therefore, more detailed studies are required in order to better define the contact relationships, reconstruct source areas and establish its emplacement mechanisms.

6.2 Tectonic Alignments and Source Areas

Another problematic factor in volcanological studies on the PMP silicic volcanics is its unknown sources locations. However silicic lava domes typically do not flow more than a few kilometers, and even coulées do not travel more than 10 km (CAS & WRIGHT, 1988; FINK AND ANDERSON, 2000; FRANCIS AND OPPENHEIMER, 2004). For this reason, lava domes are good indicators of feeder sources location or at least of its proximity and aligned outcrops can indicate fissure feeder. Therefore, in the southern region, lava dome outcrops can indicate the approximate location of source areas, and they seem to follow an alignment pattern parallel to the coastline, including ‘enigmatic flow banded’ outcrops (Fig. 11). This alignment is also similar to the northeast-trending linear feature defined by the Damaraland intrusive complexes in the South Etendeka, Namibia (e.g. MILNER & LE ROEX, 1996), of which the Messum Igneous Complex is regarded being the eruptive centre for the Goboboseb and Springbok quartz latites (MILNER et al., 1995; EWART et al., 1998). This reflects the extensional tectonic setting which resulted in the Gondwana continent breakup 10 Ma later.

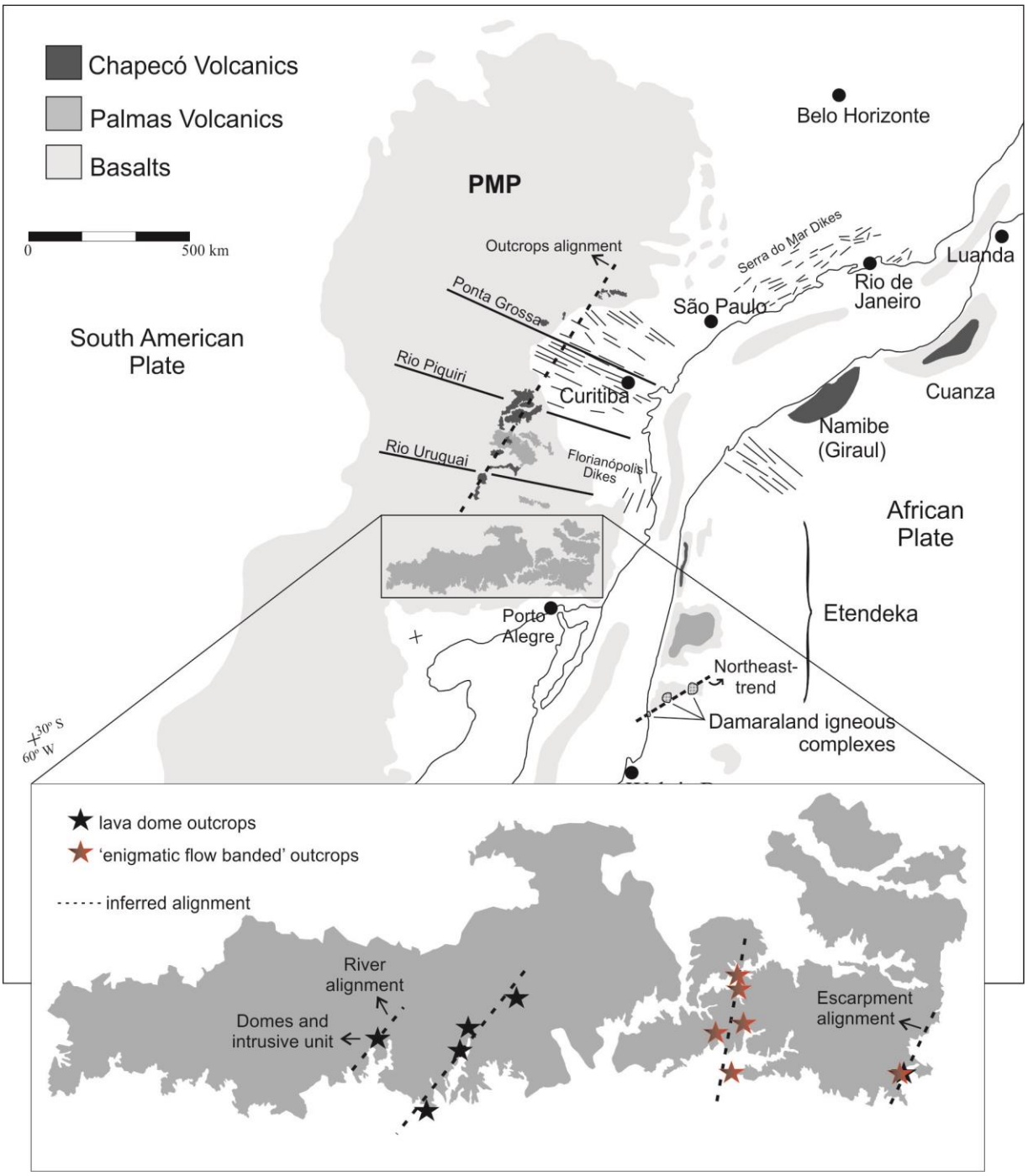

Fig. 11 –Pre-drift sketch of the Paraná Magmatic Province (PMP), modified from Milner el al. (1995b), Stewart el al. (1996), Peate (1997) e Nardy et al. (2002), showing ATP lava dome and 'flow banded-fluidal' outcrops in the southern region indicating possible sources areas. These lava domes also show a distribution parallel to the coastline, similar to the alignment of ATC outcrops.

9 CONCLUSIONS

Silicic volcanism in the Paraná Magmatic Province (PMP) is characterized by lava domes and high to extremely high grade ignimbrites. Lava domes are found in the southern region of PMP, where dacites, rhyodacites and rhyolites of Palmas type (ATP) crop out, and are characterized mainly by massive pitchstones with an usually altered, vesicular to brecciated carapace, or massive pichstone interior wrapped by concentrically jointed, devitrified rock. A silicic unit intruding in sandstone was also observed in the same area where lava domes appear. Its outcrops indicate nearby source areas and they form a trend parallel to the coast line, similar to those of ATC outcrops and the Damaraland intrusive complexes in the South Etendeka, reflecting the extensional tectonic setting which resulted in the Gondwana continent breakup 10 Ma later.

High to extremely high grade large volume ignimbrites comprise trachydacites to dacites of Chapecó (ATC) type and ATP rhyolites in the central region of PMP, where they occur interlayered in the basalt sequence with ATC sheets overlying ATP rocks in places; and ATP dacites to rhyolites overlying lava domes and basalts in the southern region. Such a scenario provides the silicic volcanism in the southern region evolved from effusive small volumes to explosive large volume flows.

The characteristic features of these high to extremely high grade large volume ignimbrites are:

(1) sheet-like geometry, with lateral extents > 40 km, and problably ≥ 100 km for some sheets, areal extents up to ~16,000 km^2. However if we consider sheets from Etendeka, Namibia, these areal extents are even much higher (individual units in the Etendeka reach up to 8,800 km^2, Milner et al., 1992);

(2) Landscapes dominated by extensive flat-topped terraces emphasizing the sheet-like geometry;

(3) Absence of both basal and top autobreccias, as well as basal pumiceous layers;

(4) Ubiquitous horizontal to subhorizontal joints ranging in thickness from a few centimetres, (sheeting joints) to a few metres, resulting in flaggy outcrops in the field. Vertical joints are also present;

(5) Massive to horizontally banded-laminated rock with flow folding in places;

(5) Completely homogeneous vitrophyres with some flow banding-lamination in places;
(6) Vertical and horizontal zoning of phenocryst abundance, with upward and lateral decrease in abundance;
(7) welded glass blobs characterizing eutaxitic texture;
(8) Phenocrysts breakage is not widespread; vitroclastic features such as fiamme texture and flattened to stretched shards are rare; scarcity of lithic fragments; globular groundmass characterizing globular shards (e.g. JOHNSON 1968; SUMNER & BRANNEY, 2002; BRANNEY et al., 2008), welding (GRUNDER et al., 2005) or glassy particles coalescence (GIMENO et al., 2003).

Nevertheless some ATP sheets remain ambiguous and its classification as ignimbrites or extensive lava flows requiring more detailed studies, such as the upper Jacuí unit, in the south-western region and the lower Clevelândia unit. In addition, the Caxias do Sul 'enigmatic flow banded' unit also shows both lava-like rheomorphic and fountain-fed lava flows features.

The high temperature estimated for these magmas would be responsible for the decrease in viscosity and the resulting particle agglutination (BRANNEY et al., 1992; BRANNEY & KOKELAAR, 1992; 2002) and, combined with low gas content (low gas velocity), lead to low collapse heights and little heat loss during collapse. Thus, the eruption mechanisms that gave rise to these extensive and voluminous sheets involved sustained, high mass-flux of very hot, and unusually low-viscosity, relatively anhydrous silicic magmas (Fig. 12a). The emplacement model (Fig. 12b) is similar to that developed for a deposit aggrading during the sustained passage of a pyroclastic density current (BRANNEY & KOKELAAR 1992, 2002). Hot particles agglutinate and/or coalesce just below a depositional boundary layer that migrates progressively upwards during deposition. Here, a transition from particulate flow (the overriding current) to non-particulate flow occurs. The non-particulate agglutinated or coalesced material, depending on the slope degree, may undergo complex syn-posdepositional welding and rheomorphism, and flow fabrics, flow folds and elongation lineations are produced (BRANNEY & KOKELAAR, 1992; BRANNEY et al., 2004; ANDREWS & BRANNEY, 2011).

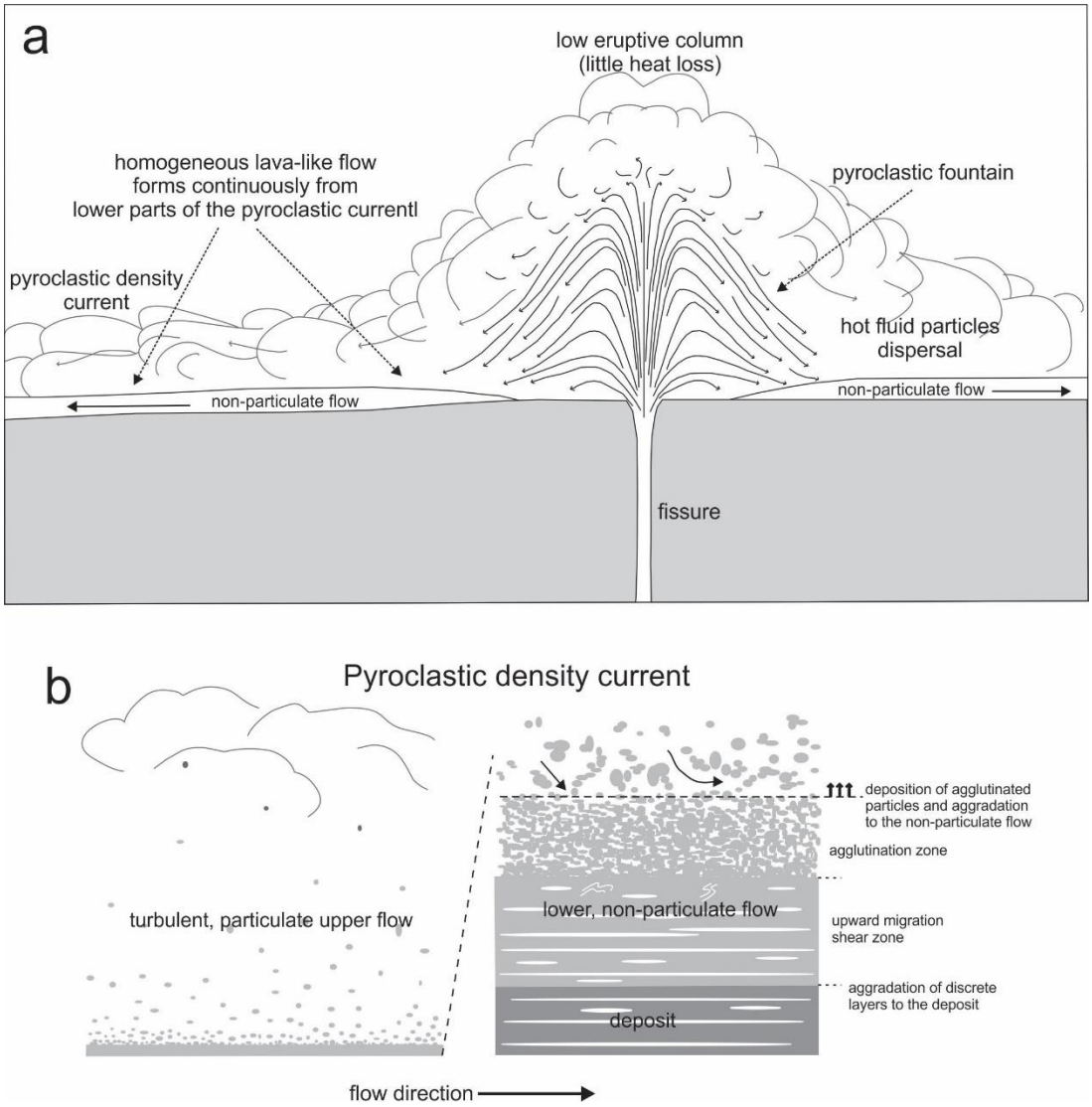

Fig. 12 – Eruptive dynamics (a) (modified of MOORE & KOKELAAR,1998) and deposition model (b) of a pyroclastic density current in flat areas for extensive silicic sheets (ATC and ATP) from the PMP (modified from PIOLI & ROSSI, 2005 and adapted from BRANNEY & KOKELAAR, 1992).

REFERENCES

ALBERTI, A.; PICCIRILLO, E.M.; BELLIENI, G.; CIVETTA, L.; COMIN-CHIARAMONTI, P.; MORAIS, E.A.A. 1992. Mesozoic acid volcanics from Southern Angola: petrology, Sr-Nd isotope characteristics, and correlation with the acid stratoid volcanic suítes of the Paraná Basin (south – eastern Brazil). Eur. J. Mineral, 4, 597-604.

ALLEN, S.R.; MCPHIE, J.; FERRIS, G.; SIMPSON, C. Evolution and architecture of a large felsic igneous province in western Laurentia: the 1.6 Ga Gawler Range Volcanics,

South Australia. J. Volcanol. Geoth. Res., 172, 132-147, 2008.

ANDREWS, G. D. M.; BRANNEY, M. J.; BONNICHSEN, B. Rhyolitic ignimbrites in the Rogerson Graben, southern Snake River Plain volcanic province: volcanic stratigraphy, eruption history and basin evolution. Bull. Volcanol., 70, 269-291, 2008.

ANDREWS, G.D. M., BRANNEY, M.J. Emplacement and rheomorphic deformation of a large rhyolitic ignimbrite: Grey's Landing, southern Idaho. Geol. Soc. Am. Bull. 123, 725-743, 2001. doi: 10.1130/B30167.1

ARIOLI, E. E. A.; LICHT, O. A. B.; VASCONCELOS, E. M. G.; BONNET, K. L.; dos SANTOS, E. M. Faciologia Vulcânica da Formação Serra Geral na Região De Guarapuava, Paraná. In: Simpósio de Vulcanismo e Ambientes Associados, 4, 2008. Foz do Iguaçu, PR. Anais

BACHMANN, O.; DUNGAN, M. A.; LIPMAN, P. W. Voluminous lava-like precursor to a major ash-flow tuff: low-column pyroclastic eruption of the Pagosa Peak Dacite, San Juan volcanic field, Colorado. J. Volcanol. Geoth. Res. 98, 153-171, 2000.

BELLIENI, G., BROTZU, P., COMIN-CHIARAMONTI, P., ERNESTO, M., ERNESTO, M., MELFI, A. J., PACCA, I. G., PICCIRILLO, E. M.: Flood basalt to rhyolites suites in the southern Paraná plateau (Brazil): paleomagnetism, petrogenis and geodynamic implications. J. Petrol., 25, 579-618, 1984.

BELLIENI, G., COMIN-CHIARAMONTI, P., MARQUES, L. S., MELFI, A. J., NARDY, A. J. R., PAPATRECHAS, C., PICCIRILLO, E. M., ROISENBERG, A.: Petrogenetic aspects of acid and basaltic lavas from the Paraná plateau (Brazil): geological, mineralogical and petrochemical relationships. J. Petrol., 27, 915-944, 1986.

BONNICHSEN, B. & CITRON, G. P. The Cougar Point Tuff, southwestern Idaho. In: Bonnichsen B, Breckenridge RM (eds) Cenozoic Geology of Idaho. Idaho Bur. Mines. Geol. Bull., 26, 255-281, 1982.

BONNICHSEN, B. & KAUFFMAN, D. F. Physical features of rhyolite lava flows in the Snake River Plain volcanic province, Southwestern Idaho. Geol. Soc. Am., 212, 119-145, 1987. (Special Paper)

BRANNEY, M. J.; KOKELAAR, B. P.; MCCONNELL, B. J. The Bad Step Tuff: a lava-like ignimbrite in a calc-alkaline piecemeal caldera, English Lake District. Bull. Volcanol., 54, 187-199, 1992.

BRANNEY, M. J. & KOKELAAR, B. P. A reappraisal of ignimbrite emplacement: changes from particulate to non-particulate flow during progressive aggradation of high-grade ignimbrite. Bull. Volcanol., 54, 504-520, 1992.

BRANNEY, M. J. & KOKELAAR, B. P. Pyroclastic density currents and the sedimentation of ignimbrites. Geol Soc Lond, Memoirs, 27, 1-152, 2002.

BRANNEY, M.J.; BONNICHSEN, B.; ANDREWS, G. D. M., ELLIS, B.; BARRY, T. L.; McCURRY, M. 'Snake River (SR)-type' volcanism at the Yellowstone hotspot track: distinctive products from unusual, high-temperature silicic super-eruptions. Bull. Volcanol., 70, 293-314, 2008.

BRYAN, S. E., UKSTINS-PEATE, I., PEATE, D. W., SELF, S., JERRAM, D. A., MAWBY, M. R., MARSH, J. S., MILLER, J. A.: The largest volcanic eruptions on Earth. Earth-Sci. Rev., 102, 207-229, 2010.

CAS, R. A. F. & WRIGHT, J. V. Volcanic successions: modern and ancient. London: Alan & Unwin, 1987.

ERNESTO, M., RAPOSO, M. I. B., MARQUES, L. S., RENNE, P. R., DIOGO, L. A., DE MIN, A.: Paleomagnetism, geochemistry and $^{40}Ar/^{39}Ar$ dating of the north-eastern Paraná Magmatic Province. Tectonic implications. J. Geodyn., 28, 321-340, 1999.

EWART, A., MILNER, S. C., ARMSTRONG, R. A. & DUNCAN, A. R. Etendeka volcanism of the Goboboseb Mountains and Messum Igneous Complex, Namibia. Part II: Voluminous quartz latite volcanism of the Awahab magma system. J. Petrol., 39, 227-253, 1998.

FINK, J. H. & ANDERSON, S.,W. 2000. Lava domes and Coulees, In: SIGURDSSON, H.; HOUGHTON, B.; MCNUTT, S.; RYMER, H.; STIX, J. (eds). Encyclopedia of Volcanoes, Academic Press, 2000. 307-319.

FRANCIS, P. & OPPENHEIMER, C. Volcanoes. Second Edition. New York: Oxford University Press, 2003.

FRANK, H. T., GOMES, M. E. B., FORMOSO, M. L. L.: Review of the areal extent and the volume of the Serra Geral Formation, Paraná Basin, South America. Pesquisas em Geociências, 36 (1), 49-57, 2009.

FREUNDT , A. 1998. The formation of high-grade ignimbrites, I: experiments on high- and low-concentration transport systems containing sticky particles. Bull. Volcanol., 59, 414-435, 1988.

FREUNDT, A. & SCHMINCKE, H. U. Eruption and emplacement of a basaltic welded ignimbrite during caldera formation on Gran Canaria. Bull. Volcanol., 56, 640-659, 1995.

FURUKAWA, K. & KAMATA, H., 2004. Eruption and emplacement of the Yamakogawa Rhyolite in central Kyushu, Japan: a model for emplacement of rhyolitic spatter. Earth, Planets and Space 56, 517–524, 2004.

GALLAGHER, K.; HAWKESWORTH, C. J.; MANTOVANI, M. S. M. The denudation history of the onshore continental margin of SE Brazil inferred from apatite fission track data. J. Geophys. Res., 99, 18177-18145, 1994.

GARLAND, F., HAWKESWORTH, C. J., MANTOVANI, M. S. M.: Description and

Petrogenesis of the Paraná Rhyolites, Southern Brazil. J. Petrol., 36 (5), 1193-1227, 1995.

GIMENO, D.; DIAZ, N.; VALLÉS, M.G.; MANENT, S. M. Genesis of bottom vitrophyre facies in rhyolitic pyroclastic flows: a case study of syneruptive glass welding (Nuraxi unit, Sulcis, SW Sardinia, Italy). J. Non-Crystall. Solids, 323, 91-96, 2003.

GRUNDER, A. L.; LAPORTE, D.; DRUITT, T. H. Experimental and textural investigation of welding: effects of compaction, sintering, and vapor-phase crystallization in the rhyolitic Rattlesnake Tuff. J. Volcanol. Geoth. Res., 142, 89-104, 2005.

HENRY, C. D.; PRICE, J. G.; RUBIN, J. N.; PARKER, D. F.; WOLFF, J. A.; SELF, S.; FRANKLIN, R.; BARKER, D. S. Widespread, lava-like silicic volcanic rocks of Trans-Pecos Texas. Geology, 16, 509-512, 1988.

HENRY, C. D.; PRICE, J. G.; RUBIN, J. N.; LAUBACH, S. E. Case study of an extensive silicic lava: the Bracks Rhyolite, Trans-Pecos Texas. J. Volcanol. Geoth. Res. 43, 113-132, 1990.

HENRY, C. D. & WOLFF, J. A. Distinguishing strongly rheomorphic tuffs from extensive silicic lavas. Bull. Volcanol., 54, 171-186, 1992.

JANASI, V. A., FREITAS, V. A., HEAMAN, L. H.: The onset of flood basalt volcanism, Northern Paraná Basin, Brazil: A precise U–Pb baddeleyite/zircon age for a Chapecó-type dacite. Earth. Planet. Sc. Lett., 302, 147–153, 2011.

JOHNSON, R. W. Volcanic globule rock from Mount Suswa, Kenya. Geol. Soc. Amer. Bull. 79, 647-651, 1968.

KOBBERGER, G. & SCHMINCKE, H. U. Deposition of rheomorphic ignimbrite D (Mogán Formation), Gran Canaria, Canary Islands, Spain. Bulletin of Volcanology, 60, 455–485, 1999.

LE BAS, M. J.; LE MAITRE, R. W., STRECKEISEN, A.; ZANETTIN, B. A chemical classification of volcanic rocks based on the total lkali-silica diagram. J. Petrol., 27, 745-750, 1986.

LIMA E. F.; PHILIPP R. P.; RIZZON G.C.; WAICHEL B.L.; ROSSETTI L. M. M. Sucessões Vulcânicas e Modelo de Alimentação e Geração de Domos de Lava Ácidos da Formação Serra Geral na Região de São MarcosAntonio Prado (RS). Geologia USP Série Científica, 12, 49-64, 2012.

LUCHETTI, A. C. F.; NARDY, A. J. R.; MACHADO, F. B.; MADEIRA, J. E. O.; ARNOSIO, J. M. New insights on the occurrence of peperites and sedimentary deposits within the silicic volcanic sequences of the Paraná Magmatic Province, Brazil. Solid Earth, 5, 121-130, 2014.

MARSH, J. S.; EWART, A.; MILNER, S. C.; DUNCAN, A. R.; McG. MILLER, R. The Etendeka Igneous Province: magma types and their stratigraphic distribution with implications for the evolution of the Parana-Etendeka flood basalt province. Bull. Volcanol. 62, 464-486, 2001.

MARQUES, L. S. AND ERNESTO, M.: O magmatismo toleítico da Bacia do Paraná. In: Geologia do Continente Sul-Americano, Mantesso-Neto, V.; Bartorelli, A.; Carneiro, C.D.R.; Brito-Neves, B.B. Beca Produções Culturais Ltda, 2004.

MELLORS, R. A. & SPARKS, R. S. J. Spatter-rich pyroclastic flow deposits on Santorini, Greece, Bull. Volcanol., 53, 327–342, 1991.

MILNER, S. C., DUNCAN, A. R., EWART, A. Quartz latite rheoignimbrite flows of the Etendeka Formation, north western Namibia. B. Volcanol., 54, 200- 219, 1992.

MILNER, S. C.; DUNCAN, A. R.; WHITTINGHAM, A. M.; EWART, A., 1995b. Trans-Atlantic correlation of eruptive sequences and individual silicic volcanic units within the Parana-Etendeka igneous province. J. Volcanol. Geotherm. Res. 69, 137-157, 1995.

MINCATO, R. L., ENZWEILER, J., SCHRANK, A.: Novas idades 39Ar/40Ar e implicações na metalogênese dos depósitos de sulfetos magmáticos de Ni-Cu-EPG na Província Ígnea Continental do Paraná. in: 9th Brazilian Congress of Geochemistry, Belém (Pará), Brazil, 2 – 9 November 2003, 67-92, 2003.

MOORE, I. & KOKELAAR, P. Tectonically controlled piecemeal caldera collapse: A case study of Glencoe volcano, Scotland. Geol. Soc. Am. Bull., 11, 1448-1466, 1998.

NARDY, A. J. R. Geologia e Petrologia do Vulcanismo Mesozóico da Região Central da bacia do Paraná. Rio Claro, 1995. 316 p. Tese (Doutorado em Geociências) – Instituto de Geociências e Ciências Exatas, Universidade Estadual Paulista.

NARDY, A. J. R., ENZWEILER, J., BAHIA F, O., OLIVEIRA, M. A. F., PENEIRO, M. A. V.: Determinação de elementos maiores e menores em rochas silicáticas por espectometria de fluorescência de raios-x: resultados preliminares. In: 6th Brazilian Congress of Geochemistry, Salvador (Bahia), Brazil, 346-348, 1997.

NARDY, A. J. R., OLIVEIRA, M. A. F., BETANCOURT, R. H. S., VERDUGO, D. R. H., MACHADO, F. B.: Geologia e estratigrafia da Formação Serra Geral. Revista Geociências, 21, 15-32, 2002.

NARDY, A. J. R., MACHADO, F. B., OLIVEIRA, M. A. F.: As rochas vulcânicas mesozóicas ácidas da Bacia do Paraná: litoestratigrafia e considerações geoquímico-estratigráficas. Brazilian Journal of Geosciences, 38 (1), 178-195, 2008.

PEATE, D.; HAWKESWORTH, C. J.; MANTOVANI, M. S. M. Chemical Stratigraphy of the Paraná Lavas (South America): Classification of Magma Types and their Spatial

Distribution. Bulletin of Volcanology, 55, 119-139, 1992.

PEATE, D. W. The Paraná-Etendeka Province. In: Mahoney J.J., Coffin M.F. (eds.) Large igneous provinces: continental, oceanic and planetary flood volcanism. Geophysics Monography Series, 1997. 100, 217-245.
PICCIRILLO, E. M. & MELFI, A. J. (eds.): The Mesozoic Flood Volcanism of the Paraná Basin: Petrogenetic and Geophysical Aspects. Instituto Geofísico, Astronômico e Ciências Atmosféricas, Universidade de São Paulo, São Paulo, Brazil, 1988.

PINTO, V. M.; HARTMANN, L. S.; SANTOS, J. O. S.; McNAUGHTON, N. J.; WILDNER, W. Zircon U-Pb geochronology from the Paraná bimodal volcanic province support a brief eruptive cycle at ~135 Ma. Chem. Geol., 28 (2), 93-102, 2010.

PIOLI, L. & ROSSI, M. Rheomorphic structures in a high-grade ignimbrite: The Nuraxi Tuff, Sulcis volcanic district (SW Sardinia, Italy). J. Volcanol. Geoth. Res., 142, 11-28, 2005.

POLO, L. A. & JANASI, V. A. Volcanic Stratigraphy of Intermediate to Acidic Rocks in Southern Paraná Magmatic Province, Brazil. Geologia Usp Série Científica, 14, 83-100, 2014.

RENNE, P. R., ERNESTO, M., PACCA, I. G., COE, R. S., GLEN, J. M., PRÉVOT, M., PERRIN, M.: The age of Parana flood volcanism, rifting of Gondwanaland, and the Jurassic–Cretaceous boundary. Science 258, 975–979, 1992.

RENNE, P. R., DECKART, K., ERNESTO, M., FÉRAUD, G., PICCIRILLO, E. M.: Age of the Ponta Grossa dyke swarm (Brazil), and implications to Paraná flood volcanism. Earth. Planet. Sc. Lett. 144, 199–211, 1996a.

RENNE, P. R., GLEN, J. M., MILNER, S. C., DUNCAN, A. R.: Age of Etendeka flood volcanism and associated intrusions in southwestern Africa. Geology 24, 659–662, 1996b.

ROSS, C. S. & SMITH, R. L. Ash-flow tuffs, their origin, geological relations and identification. US Geol. Surv. Prof. Pap., 366, 1-77, 1961.

SCHMINCKE, H. U. & SWANSON, D. A. Laminar viscous flowage structures in ash-flow tuffs from Gran Canaria, Canary Islands. J. Geol., 75, 641–664, 1967.

SIVIERO, R.S.; RAMAGE, L.; MENEGAT, R.; MIZUSAKI, A.M.P. Caracterização dos ignimbritos da Formação Serra Geral na região de Sananduva, terra indígena de Ligeiro, RS. In: Simpósio de Vulcanismo e Ambientes Associados, 3, 2005. Cabo Frio, RJ. Anais

SORIANO, C.; ZAFRILLA, S.; MARTI, J.; BRYAN, S.; CAS, R. A. F.; Ablay, G. Welding and rheomorphism of phonolitic fallout deposits from the Las Canadas Caldera, Tenerife, Canary Islands. Geol. Soc. Am. Bull., 114, 883-895, 2002.

SORIANO, C; GIRODANO, D.; GALINDO, I.; HURLIMANN, M.; ARDIA, P. Giant gas bubbles in a rheomorphic vent fill at the Las Cañadas caldera, Tenerife (Canary Islands). Bull. Volcanol. 71, 919-932, 2009.

SPARKS, R.S.J.; WILSON, L.; HULME, G. Theoretical modeling of the generation movement and emplacement of pyroclastic flows by column collapse. J. Geophys. Res. 83, 1727-1739, 1978.

STEVENSON, R. J.; BRIGGS, R. M.; HODDER, A. P. W. Emplacement history of a low-viscosity, fountain-fed pantelleritic lava flow, J. Volcanol. Geoth. Res., 57, 39-56, 1993.

STEVENSON, R. J., WILSON, L., 1997. Physical volcanology and eruption dynamics of peralkaline agglutinates from Pantelleria. Journal of Volcanology and Geothermal Research 79, 97–122.

STEWART, K.; TURNER, S.; KELLEY, S.; HAWKESWORTH, C. I.; KIRSTEIN, L.; MANTOVANI, M. S. M. 3-D ^{40}Ar-^{39}Ar geochronology in the Paraná flood basalt province, Earth Planet. Sci. Lett., 143, 95-1 10, 1996.

SUMNER, J. M. & BRANNEY, M. J. The emplacement history of a remarkable heterogeneous, chemically zoned, rheomorphic and locally lava-like ignimbrite: 'TL' on Gran Canaria. J. Volcanol. Geoth. Res., 115, 109-138, 2002.

THIEDE, D.S., VASCONCELOS, P.M. Paraná flood basalts: rapid extrusion hypothesis confirmed by new $^{40}Ar/^{39}Ar$ results. Geology, 38 (8), 747-750, 2010.

TURNER, S., REGELOUS, M., KELLEY, S., HAWKSWORTH, C., MANTOVANI, M. M. S.: Magmatism and continental break-up in the South Atlantic: high precision $^{40}Ar/^{39}Ar$ geochronology. Earth Plan. Sci. Lett., 121, 333-348, 1994.

UMANN L. V.; LIMA E. F.; SOMMER C. A.; DE LIZ J. D. Vulcanismo ácido da região de Cambará do Sul-RS: litoquímica e discussão sobre a origem dos depósitos. Rev. Bras. Geoci., 31(3), 357-364, 2001.

WALKER, G. P. L. Ignimbrite types and ignimbrite problems. J. Volcanol. Geoth. Res., 17, 65-88, 1983.

WHITE, J. D. L.; BRYAN, S. E.; ROSS, P. R.; SELF, S.; THORDARSON, T. Physical volcanology of continental Large Igneous Province: update and review. In: THORDARSON, T.; SELF, S; LARSEN, G.; ROWLAND, S. K.; HOSKULDSSON, A. Studies in Volcanology: The Legacy of George Walker. London: Geological Society of London, 2009. p. 291-321.

WHITTINGHAM, A. M. Geological features and geochemistry of the acid units of the Serra Geral Formation, south Brazil. In: Continental Magmatism, Santa Fé IAVCEI

Abstracts: Santa Fé, New Mexico, p. 293, 1989.

WOLFF, J. A. & WRIGHT, J. V. 1981. Rheomorphism of welded tuffs. J. Volcanol. Geoth. Res., 10, 13-34, 1981.

Chapter 3: Physical Parameters and Crystal Size Distribution of Silicic Volcanism of the Paraná Magmatic Province

1 INTRODUCTION

Chapecó and Palmas silicic volcanic rocks are part of the Serra Geral Formation, in the Paraná Basin, and make up part of the Lower Cretaceous age Paraná Magmatic Province (PMP), a giant bimodal tholeiitic volcanism (~1 million km^3), which preceded the Gondwana breakup and the subsequent opening of the Atlantic Ocean.

Geochronological dating by $^{40}Ar/^{39}Ar$ shows that the age of volcanic rocks of the Serra Geral Formation ranges from 133.6 to 131.5 Ma in its northern sector, and from 134.6 to 134.1 Ma in the south (RENNE et al., 1992, 1996a, b; TURNER et al., 1994; ERNESTO et al., 1999; MINCATO et al., 2003; THIEDE & VASCONCELOS, 2010; PINTO et al., 2010). More recently, Janasi et al. (2011), using U/Pb ratios from baddeleyite/zircon crystals determined by ID-TIMS from rocks of the Chapecó Member, obtained an age of 134.3 ± 0.8 Ma, compatible with the previous age determinations. These ages obtained in the dominant basaltic flows indicate a duration of the volcanism of around 3 Ma, also consistent with paleomagnetic data presented by Marques & Ernesto (2004).

Chapecó type rocks (ATC) appears more northerly and includes porphyritic, crystal-rich, high-Ti dacites and trachydacites, whereas Palmas type (ATP) includes fine-grained, crystal-poor, low-Ti dacites and rhyolites. Even comprising a small proportion of the total erupted volume (2.5%), these rocks correspond to an extensive and voluminous (~14,500 km^3) (NARDY et al.,2008), significant flare-up of silicic volcanism over a short period of time.

The silicic volcanism evolved from lava domes to extensive high to extremely high grade ignimbrites and the extremely high T of these magmas seems to play a key role in its emplacement mode. This study aimed to investigate the depths and temperatures at which magmas were stored, as well as water contents in order to constrain its conditions prior to eruption and improving our understanding regarding the feeder magma plumbing system. Therefore mineral-melt thermobarometers-hygrometer were applied, since they can play a crucial role in such studies because by determining crystallization depths we can establish where magmas are stored prior to eruption. In

addition first crystal size distribution (CSD) studies were performed in order to try to understand the history and evolution of these large magma bodies.

2 GEOLOGICAL SETTING

The Paraná Magmatic Province (PMP) comprises volcanic rocks of the Serra Geral Formation covering 917,000 km^2, with 650 m thick average sequences, resulting in ~450,000 km^3 of volcanic products (FRANK et al., 2009). Basalt flows make up about 90%, whereas intermediate (basaltic-andesites and andesites) and silicic compositions make up 7 and 2.5% respectively (BELLIENI et al., 1984; PICCIRILLO & MELFI, 1988). However much larger volumes must be considered, since significant erosion affected the South American Platform (GALLAGHER et al., 1994). Also, part of this volcanism is preserved in the African Continent, in the Etendeka (Namibia), Kwanza and Namibe (Angola) basins (ALBERTI et al., 1992), giving rise the Paraná-Etendeka LIP. In Brazil the PMP volcanics were emplaced on aeolian sandstones of the Botucatu Formation in the Paraná Basin.

Based on volcanics chemistry and spacial distribution data Bellieni et al. (1984) proposed the Paraná basin to be schematically subdivided into three main regions: (1) southern, encompassing tholeiitic suite lying south of the Uruguay River alignment; (2) northern, with tholeiitic-transitional rocks lying north of the Piquiri River alignment; and (3) central, between Piquiri River and Uruguay River alignments (Fig. 1).

Despite the silicic volcanics represent a small part of the PMP total volume, by no means they are negligible. The main outcrop remnants of Chapecó type silicic volcanic rocks (ATC) occur mainly north of the Uruguay River alignment, with some outcrops south of the Uruguay River alignment. They currently cover an area of ~6,000 km^2 with a total volume of ~1,000 km^3 following a NE-SW trending parallel to the coastline. Palmas type silicic volcanic rocks (ATP) are spatially and volumetrically more significant than ATC rocks. They lie mainly in the southern region covering a current area of ~35,000 km^2 with a total volume of ~12,000 km^3, whereas smaller units (~5,000 km^2 and ~700 km^3 total) crop out in the central region (Fig. 1).

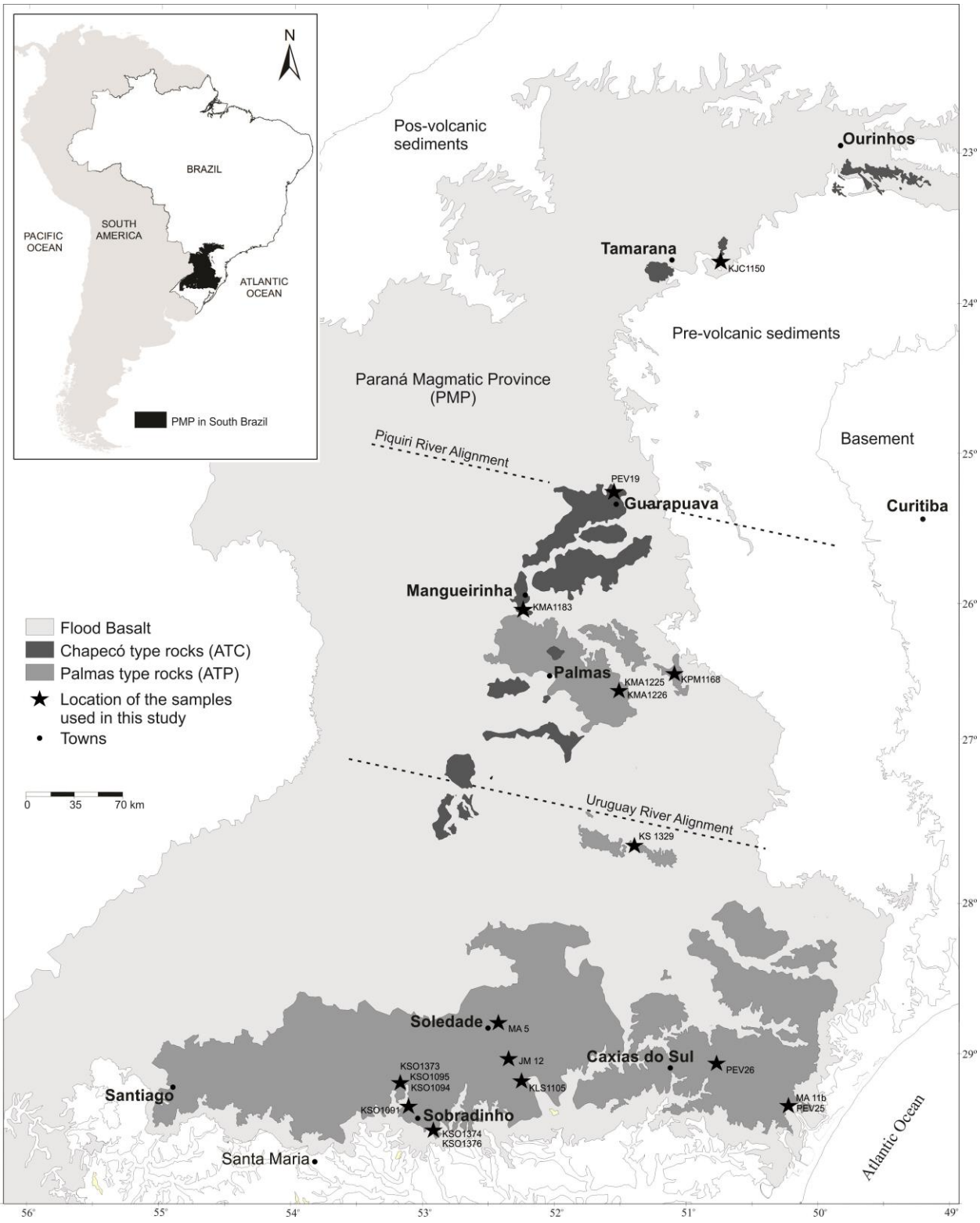

Fig. 1 – Geological and location map for the ATC and ATP units in the PMP, modified from Nardy et al. (2002), with sample locations used in this study (stars). Dashed lines mark the Piquiri-Uruguay rivers lineaments which divide the Paraná Basin in northern, central and southern regions (Bellieni et al.,1984).

3 ANALYTICAL METHODS

Geochemical data for bulk rock compositions were obtained from a set of 250 samples of fresh basaltic-to-silicic rocks. Major and trace elements were carried out at Department of Petrology and Metallogeny laboratories of the São Paulo State University (Unesp), using X-ray fluorescence spectrometry. Major elements were analysed using fusion beads (1:10 lithium tetraborate) while trace elements were obtained using pressed (30 ton/cm^2) powder discs (mixed with 25 wt% of micropowder wax). All methodology (including errors) is described in Nardy et al. (1997).

The main mineral assemblage phases (plagioclase, pyroxene and Fe-Ti oxides) of representative samples of the different silicic subgroups were analysed in the Electron Microprobe Laboratory in the same department. Chemical analysis were performed in a JEOL-JXA 8230 Superprobe by WDS (Wavelength-Dispersive X-Ray Spectroscopy) with 15kv of acceleration voltage, beam current of 20nA and spot of 10μm.

X-ray compositional maps were also generated for CSD purposes, by both EDS (Energy Dispersive X-Ray Spectroscopy) and WDS with accelerating voltage of 15 kV and dwell times of 8-10 ms. Largest areas possible (averaging 38 x 21 mm) of thin sections were covered in order to ensure enough crystals amount. Main elements, such as Al (aluminum), Mg (magnesium) and Ti (titanium) were chosen for plagioclase, pyroxene and Fe-Ti oxides recognition respectively. X-ray maps were processed by using ImageJ free software (Fig. 2) to obtain intersection data of each grain/crystal (major-minor axis, area, angle, x and y). Touching crystals were manually separated with the aid of an optical microscope under which crystals were identified by differences in extinction angles and/or interference color.

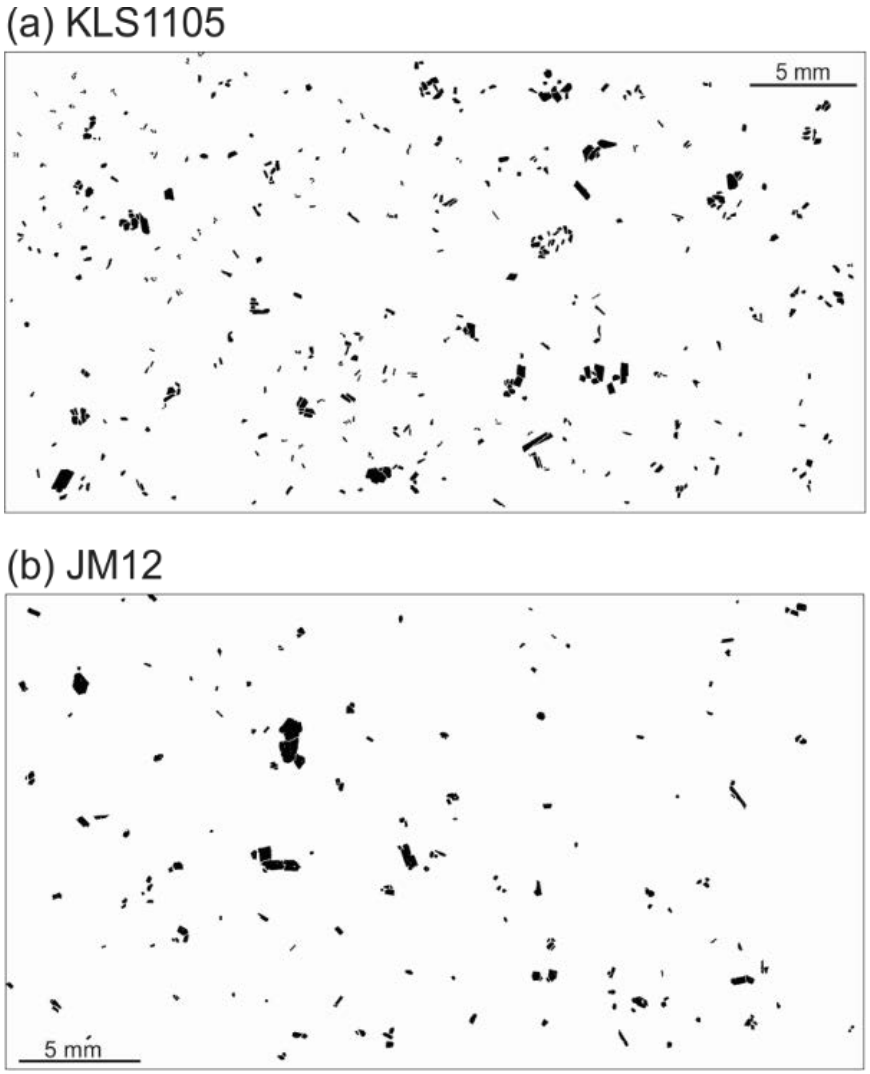

Fig. 2 – Processed (thresholding and crystals touching separation) Al x-ray maps for plagioclase phase of a Caxias do Sul thin section (a) and Santa Maria thin section (b).

3.1 EBSD (Electron Backscatter Diffraction)

EBSD is an analytical technique (see explanatory scheme in Fig. 3) coupled to the SEM detecting Electron Back-Scattering Patterns (EBSPs). It provides quantitative microstructural information regarding crystallographic nature of minerals such as size, boundary character, orientation (twins), texture and, as well as phases identity in a specimen (MAITLAND & SITZMAN, 2007). Thus, in CSD studies this technique would solve the problem related to clusters-bearing samples whose crystals touching boundaries are difficult or impossible to define using only optical microscopy. This is

precisely the case of the rocks in question.

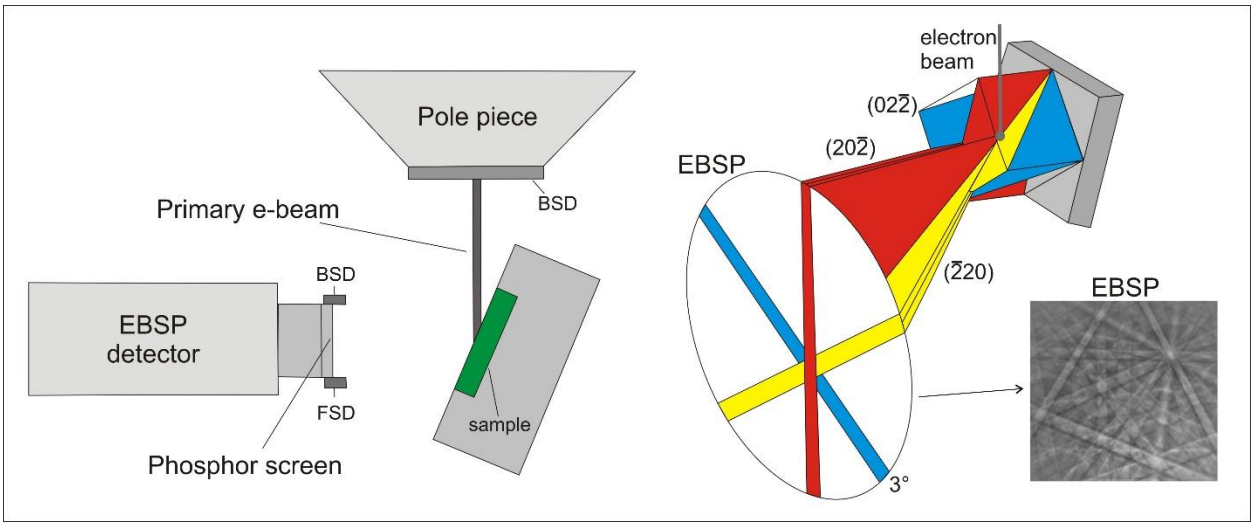

Fig. 3 – Scheme showing the arrangement of the sample in SEM for EBSD data acquisition. Interaction between primary beam and crystal lattice causes the backscattered electrons (low energy loss) channeled to different paths leading to constructive and destructive interferences. The diffraction pattern (EBSP) is 'captured' by a phosphor screen placed a short distance from the sample. (illustrations modified from DAY et al., 1999); FSD - Forward-scattered Electron Detector; BSD - Backscattered Electron Detector.

A flat, highly polished sample placed in a shallow angle (~20° - SEM stage tilt usually 70°) is crucial for the success obtaining EBSD data. Therefore thin sections, properly polished for microprobe analysis, were subjected to at least three-hour final polishing stage with a non-crystallizing colloidal silica polishing suspension on a Buehler VibroMet 2 Vibratory Polisher. No coating was applied on the samples, since it interferes in the EBSPs acquisition, as well as the operation was conducted in low vacuum to prevent electrical charging.

EBSD data were collected with Oxford EBSD detectors coupled in a Tescan Vega 3 LM Variable Pressure Scanning Electron Microscope at Vanderbilt University. Working distance of 10 mm, 70° sample tilt and beam settings were at 20 kV accelerating voltage and 4 nA beam current. Images were processed using the HKL CHANNEL5 module Tango software from Oxford Instruments (Fig.4).

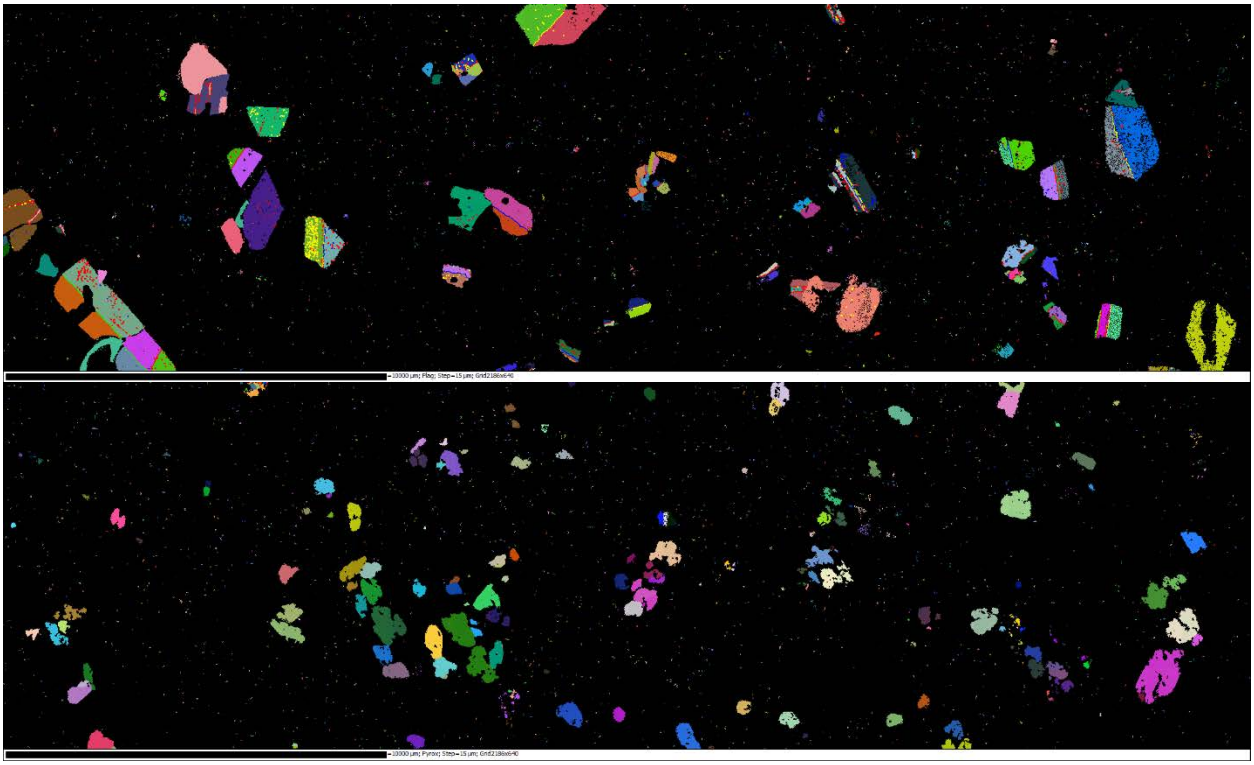

Fig. 4 – Euler maps from EBSD for ATC sample, after processing in HKL CHANNEL5 module Tango software. Above is plagioclase and below is pyroxene. Colors represent different crystal orientations. The black bar at the bottom of each image is 10 mm long.

The two methods described above used for crystal measurements provided 2D data rather than 3D crystal shapes. Thus, the CSDSlice program (MORGAN & JERRAM, 2006) was used to determine 3D crystal shapes (aspect ratios). It compares 2D measurements (major-minor axis) to a crystal shapes database yielding a best fit 3D crystal habit by regression calculations. Then, 3D crystal size distributions were created in the CSDCorrections 1.50 (HIGGINS, 2000) which convert 2D dimensional data through intersection probability effect and cut-section effect corrections.

4 GEOCHEMISTRY

The silicic volcanics of the PMP are chemically quite different. The Chapecó type silicic volcanic rocks (ATC) are trachytes-dacites (Fig. 5), enriched in TiO_2, P_2O_5, Al_2O_5 and impoverished in Fe_2O_3, CaO and MgO when compared to Palmas dacites-rhyolites (ATP). ATC rocks are also enriched in some incompatible elements such as Ba, Nb, La, Ce, Zr, P, Nd, Y, Yb, Lu and K, and impoverished in Rb, Th and U relative to ATP rocks.

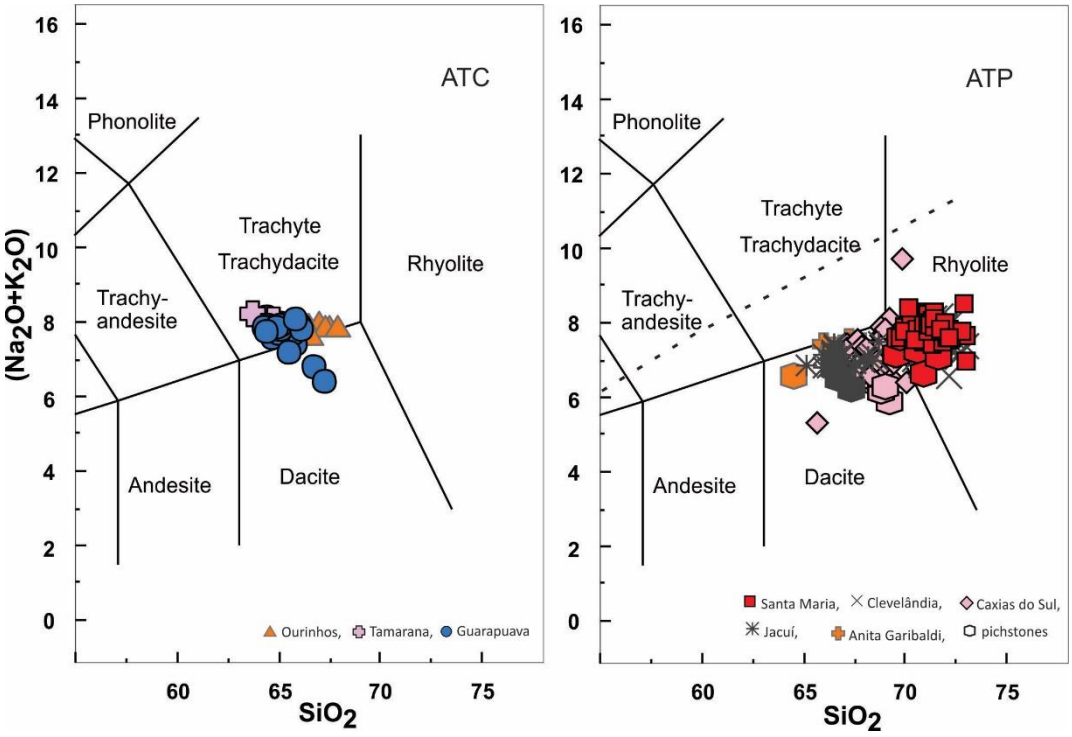

Fig. 5 – TAS diagram (LE BAS et al., 1986) for classification and nomenclature of ATC and ATP silicic volcanic rocks.

These two main silicic groups have been divided in subgroups or magma subtypes based on TiO_2 and P_2O_5 contents (Fig. 6; PEATE et al., 1992; GARLAND et al., 1995; NARDY et al., 2008). Thus the Guarapuava ($TiO_2 \geq 1,47\%$), Ourinhos ($TiO_2 \leq 1,29\%$) and Tamarana ($1.38 \leq TiO_2 \leq 1.5\%$) subgroups comprise the ATC rocks. ATP rocks are formed by two subgroups: Low-Ti ($TiO_2 \leq 0,87\%$), composed by the Santa Maria ($P_2O_5 \leq 0,21\%$) and Clevelândia ($0,21\% < P_2O_5 \leq 0,23\%$) subtypes; and High-Ti ($TiO_2 \geq 0,90\%$), composed by the Caxias do Sul ($0,91\% < TiO_2 < 1,03\%$ and $0,25\% < P_2O_5 < 0,28\%$), Jacuí ($1,05\% < TiO_2 < 1,16\%$ and $0,28\% < P_2O_5 < 0,31\%$) and Anita Garibaldi ($1,06\% < TiO_2 < 1,25\%$ and $0,32\% < P_2O_5 < 0,36\%$) magma subtypes.

Furthermore, it can be noted from the TAS diagram (Fig. 5) that Jacuí and Anita samples fall in the dacites field, Caxias do Sul in the dacites-rhyolites fields, and Santa Maria and Clevelândia in the rhyolites field.

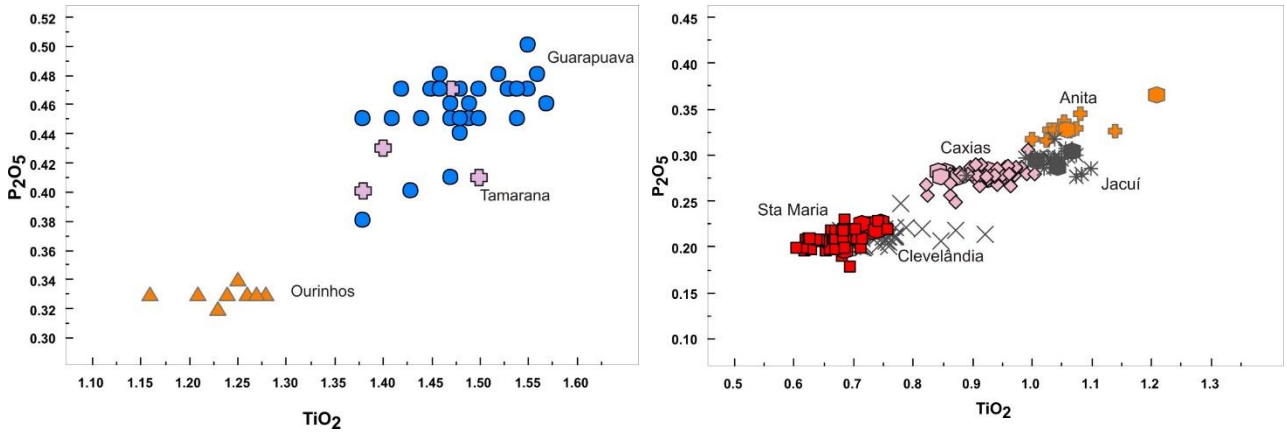

Fig. 6 - TiO_2 x P_2O_5 variation diagrams for ATC (left) and ATP (right) rocks showing divisions of magma subtypes.

Unpublished data of Sr and Nd isotopic analysis, shown in Fig. 7, confirm results reported in the literature (e.g. MANTOVANI et al., 1985, PICCIRILLO et al., 1987, CORDANI et al., 1988; GARLAND et al., 1995). These show very different characteristics between ATC and ATP volcanic rocks and that the ATP rocks were significantly affected by crustal contamination processes. Also the ATP magma subtypes were affected by varying degrees of contamination, wherein the Clevelândia subtype shows higher $^{87}Sr/^{86}Sr$ ratios. Analysis of Tamarana (KJC-1150) and Santa Maria (KSO-1374) subtypes showed inconsistencies in the Sr initial isotopic ratio ($^{87}Sr/^{86}Sr_{(133)}$: KJC-1150 = 0.70421 and KJC-1150 = 0, 73 545) and therefore, they will be repeated.

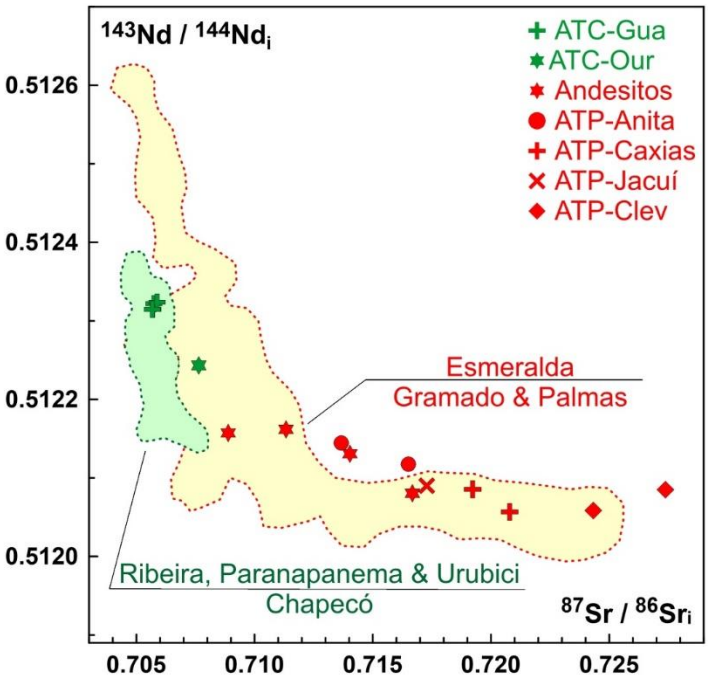

Fig. 7 - $^{87}Sr/^{86}Sr$ vs. $^{143}Nd/^{144}Nd$ diagram for ATC and ATP rocks recalculated to the 133Ma age. Fields defining the high-Ti (Ribeira, Paranapanema and Urubici) and low-Ti basalts (Esmeralda and Gramado) are part of Marques, LS' collection (personal communication).

Table 1 - Chemical compositions of samples used in this study.

Sample	KJC1150	KMA1183	PEV19	KMA1225	KMA1226	MA5	JM12*	KSO1374*	KSO1376	KLS1105*	MA11B*	PEV26	PEV25*	KPM1168	KS1329	KSO1091	KSO1095*	KSO1373*
Type	ATC	ATC	ATC	ATP	ATP	ATP	ATP	ATP	ATP	ATP	ATP	ATP	ATP	ATP	ATP	ATP	ATP	ATP
Subtype	Tamarana	Guarapuava	Guarapuava	Clevelândia	Clevelândia	Santa Maria	Santa Maria	Santa Maria	Santa Maria	Caxias do Sul	Caxias do Sul	Caxias do Sul	Caxias do Sul	Anita Garibaldi	Anita Garibaldi	Jacuí	Jacuí	Jacuí
SiO_2	65.37	64.82	63.69	72.51	72.31	71.91	69.85	68.43	69.61	68.27	66.51	66.96	68.20	67.37	66.91	67.73	66.33	64.86
TiO_2	1.40	1.41	1.46	0.71	0.70	0.69	0.68	0.75	0.74	0.88	0.85	0.93	0.83	1.05	1.04	0.99	1.01	1.06
Al_2O_3	13.32	12.67	12.51	12.01	11.85	11.87	12.26	12.23	12.15	12.44	12.36	12.55	11.67	12.97	12.31	12.55	12.76	12.49
Fe_2O_3	7.41	7.31	8.02	5.26	5.17	5.15	5.40	5.53	5.60	6.15	6.11	6.49	5.94	6.79	6.23	6.68	6.92	7.11
MnO	0.18	0.15	0.16	0.08	0.08	0.09	0.10	0.10	0.10	0.11	0.10	0.11	0.10	0.11	0.11	0.11	0.12	0.13
MgO	1.04	1.35	1.15	0.63	0.41	0.59	0.74	0.80	0.68	1.22	0.96	1.23	0.67	1.26	1.42	1.00	1.30	1.52
CaO	2.44	2.87	3.42	1.77	1.68	1.80	2.44	2.53	1.55	3.31	3.01	3.36	2.18	3.45	3.15	2.86	3.58	3.73
Na_2O	3.48	3.07	3.76	2.36	2.38	2.61	2.82	3.26	2.67	2.90	3.67	3.27	2.47	3.31	3.37	2.92	3.32	3.22
K_2O	4.12	4.30	4.11	5.24	5.25	5.22	4.31	4.14	5.32	3.31	2.85	3.90	4.70	3.62	3.93	4.08	2.78	3.43
P_2O_5	0.43	0.45	0.47	0.21	0.21	0.20	0.20	0.23	0.22	0.28	0.28	0.28	0.26	0.33	0.33	0.30	0.29	0.30
LOI	1.03	1.33	0.65	0.72	0.67	0.56	2.20	1.74	1.42	1.48	3.42	0.73	1.69	0.66	1.15	1.11	2.12	2.05
SUM	100.22	99.73	99.39	101.50	100.72	100.69	101.00	99.72	100.05	100.33	100.12	99.80	98.69	100.92	99.95	100.32	100.54	99.90

* Pitchstone samples

5 MINERALOGY – PETROGRAPHY

ATC type rocks of this study are porphyritic to sparsely porphyritic with up to ~15% of plagioclase (An_{30-49}), pyroxene (augite and pigeonite), Fe-Ti oxides (Ti-magnetite and ilmenite) and apatite phenocrysts (Figures 8 and 9). Plagioclase crystals can reach up to 1 cm in length (major axis) and compose up to 10% of the rock (Fig. 10). They are euhedral to sub-rounded with normal, inverse or oscillatory zoning (Fig. 10c) and displaying embayment, corroded edges and pyroxene and Fe-Ti oxides inclusions. Augite ($En_{35-39}Wo_{32-37}$) and pigeonite ($En_{44-49}Wo_{9-10}$) crystals make up ~5% and rarely exceed 2 mm long. They are subhedral, rounded to irregular outlines, fractured, with corroded-reacted edges indicating resorption, and Fe-Ti oxide and apatite inclusions (Fig. 10d). Ti-magnetite (37-96% ulv) and ilmenite (74-97% ilm) comprise Fe-Ti oxides with euhedral to irregular shapes and embayment, also recording resorption (Fig. 10d). They do not exceed 2% of the rock with up to 0.5 mm long with llmenite also occurring as lamellae in the Ti-magnetite. Apatite amounts to less than 1% and long crystals may reach 0.5 mm in length. Groundmass microlites (<100 μm) are the same as phenocrysts except for more evolved plagioclase compositions ($An_{0.02-35}$) and the appearing of alkali feldspar (Or_{55-64}). They show tabular habit to hollow, dendritic and swallowtail shapes. The groundmass is through devitrified, ranging from brown spherulitic patches surrounded by microcrystalline material (quartz-feldspar intergrows) to microgranophyric with quartz-feldspar intergrowths. Crystal clusters (or “glomerocrysts”) are also a common feature in these rocks consisting of plagioclase, pyroxene, plagioclase+pyroxene and plagioclase+pyroxene+Fe-Ti oxides assemblages.

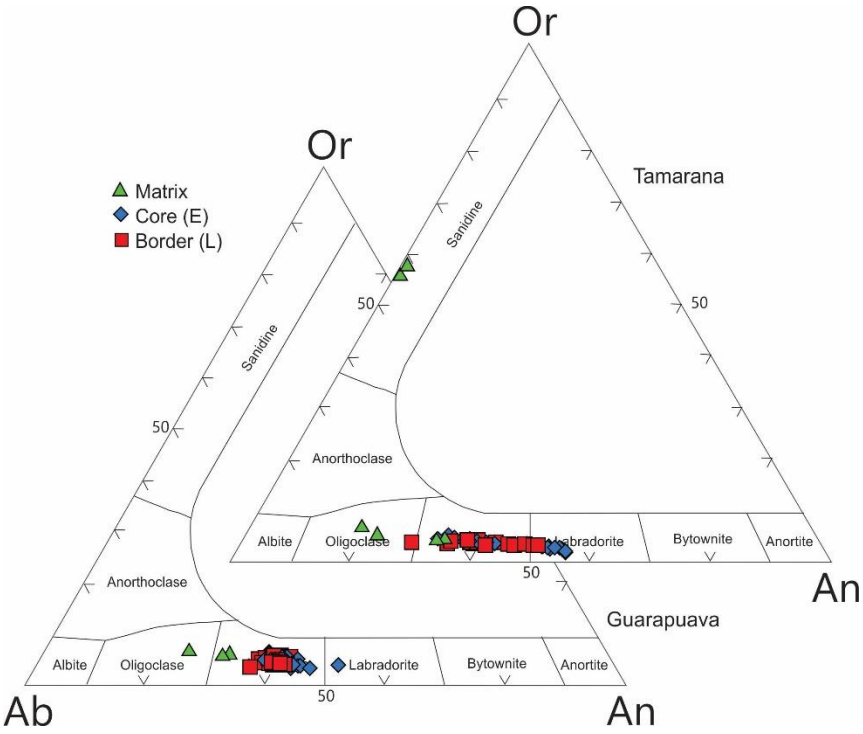

Fig. 8 – Ab-An-Or diagrams for classification of ATC plagioclase crystals.

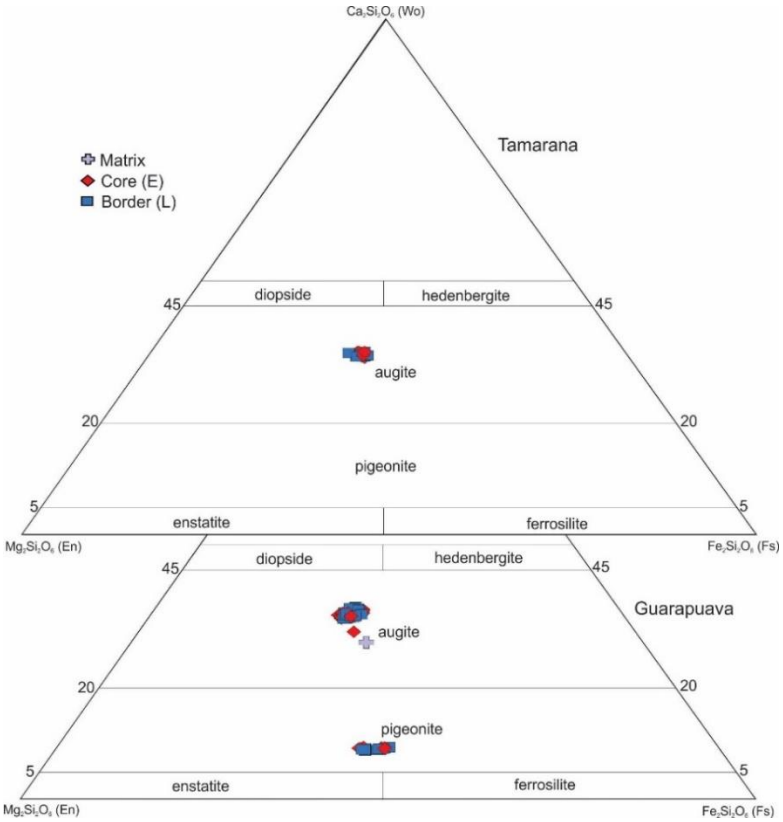

Fig. 9 - En-Fs-Wo diagrams for pyroxene classification for ATC rocks.

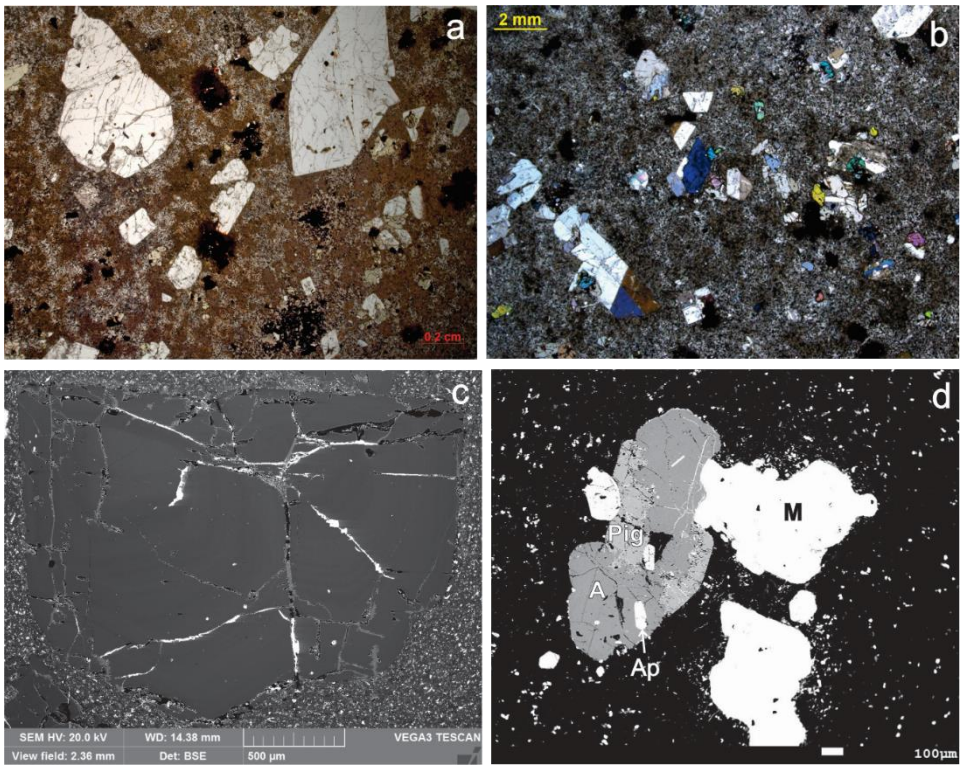

Fig.10 – Photomicrographs (a-b) and BSE images (c-d) of ATC rocks. (a-b) porphyritic aspect marked by plagioclase, pyroxene, Fe-Ti oxides and apatite phenocrysts and clusters-glomerocrysts in brown spherulitic patches surrounded by quartz-alkali feldspar microgranophyric intergrowths; // and X pol. respectively; (c) plagioclase phenocryst showing quite developed zoning; (d) augite phenocryst (A) with pigeonite exsolution (Pig) and apatite inclusions (Ap) and Ti-magnetite (M) phenocrysts with irregular outlines indicating resorption as well as the pyroxene.

ATP type rocks are sparsely porphyritic to aphyric with up to ~4% of plagioclase (prevailing), pyroxene and Fe-Ti oxide pheno-microphenocrysts. Mineralogical assemblages (Table 2; Figures 11 and 12) in each subgroup are plag + orthopx +Ti-mag, plag + orthopx + aug + pig +Ti-mag, plag + orthopx + aug +Ti-mag and plag + orthopx + pig +Ti-mag (Caxias do Sul); plag + aug + Ti-mag and plag + pig + aug + Ti-mag (Jacuí); plag + Ti-mag (Santa Maria); and Ti-mag (Clevelândia). Anita specimens do not contain phenocrysts (intratelluric) as the other subgroups. Its groundmass show high densities of plag + aug (+pig) + Ti-mag microcrysts-to-microlites. These 'microcrysts'-microlites may comprise up to 20% of rock volume and reach 0.45 (plagioclase) and 0.6 mm in length (pyroxene). Thus, these crystals can be considered as groundmass crystals. In the Clevelândia subgroup plagioclase and pyroxene (aug + pig) only occur as groundmass microphenocrysts-to-microlites in lower densities and

sizes (up to 250 μm long) than in Anita type samples. Pigeonite occurs mainly as rim in orthopyroxene (Fig. 13c-d) and augite crystals. However, some pigeonite crystals and pigeonite cores with augite borders were observed in a Jacuí sample (Fig. 13e). Groundmass assemblages are plag + aug + pig + Ti-mag and plag + aug + Ti-mag (Caxias do Sul, Jacuí and Anita) and plag + pig + Ti-mag (Santa Maria, Caxias do Sul and Clevelândia) with lower An content plagioclase and lower CaO and MgO and higher FeO w% pyroxene relative to the phenocrysts.

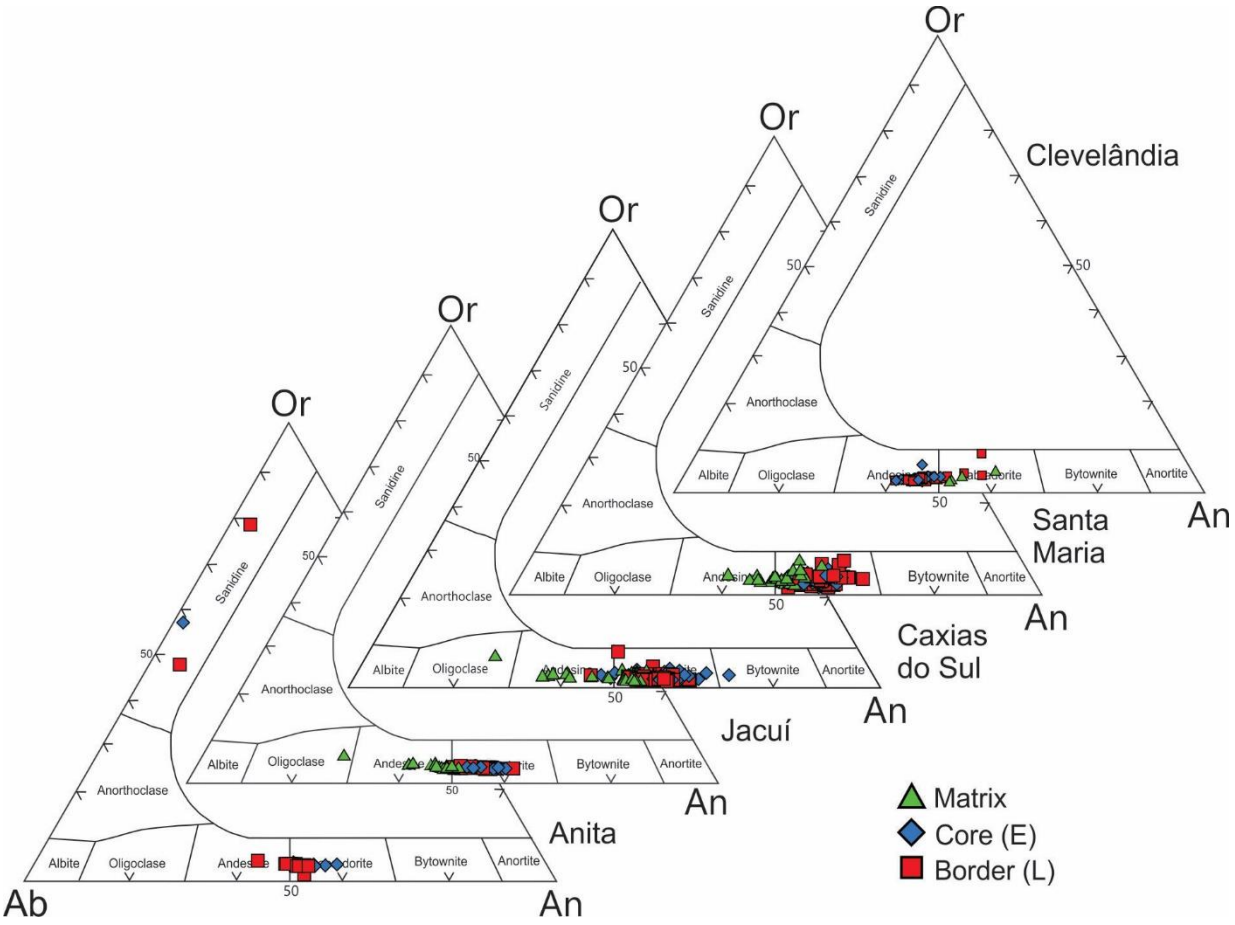

Fig. 11 - Ab-An-Or diagrams for classification of ATP plagioclase crystals.

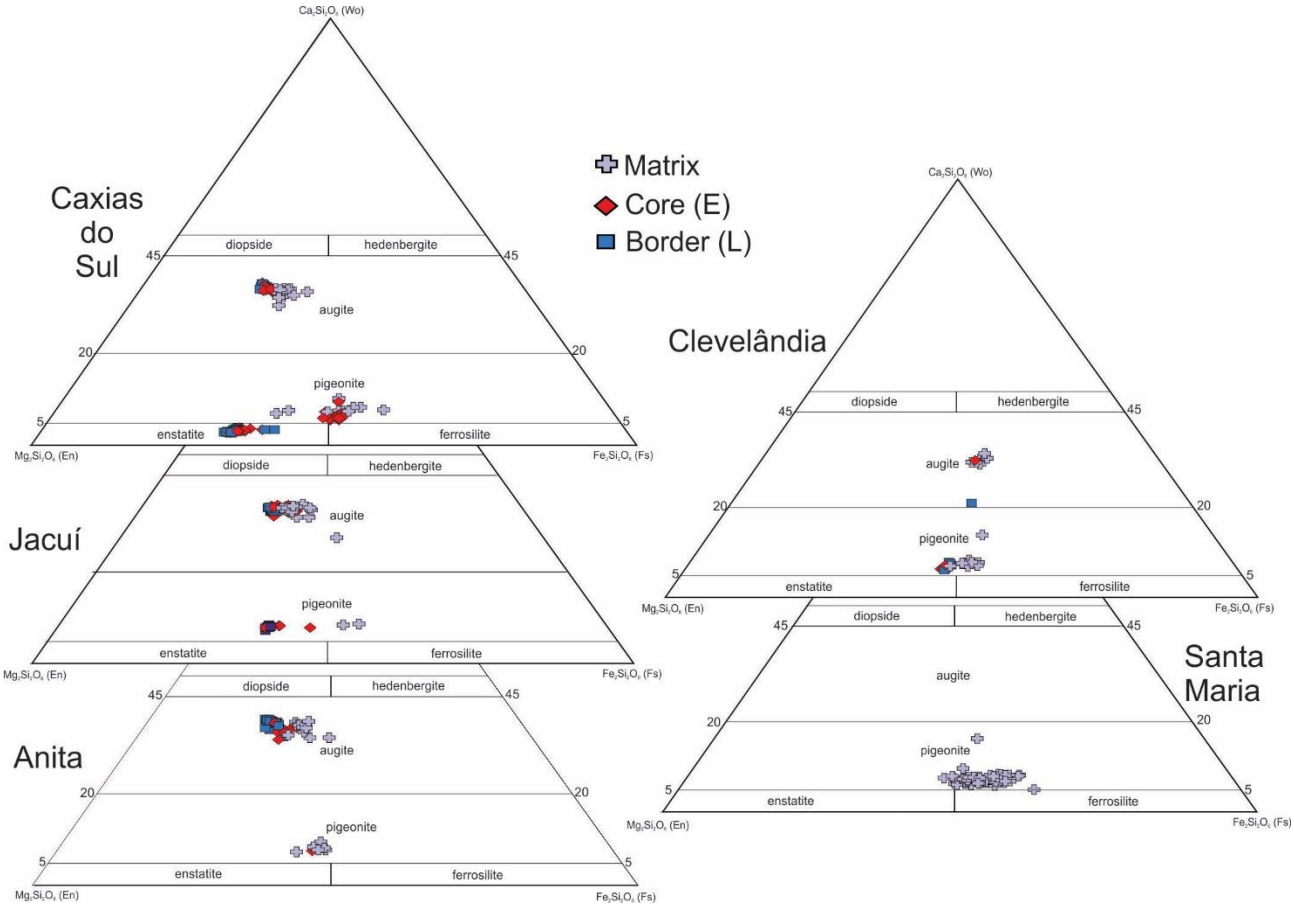

Fig. 12 - En-Fs-Wo diagrams for pyroxene classification for ATP rocks.

Plagioclase crystals make up to 3% of the rock and usually does not exceed 1.5 mm in length (Fig. 13a). An exception is a sample from Caxias do Sul subgroup containing some 3 mm long crystals. These also appear in Caxias do Sul lowermost units and more rarely in the Santa Maria subgroup. Overall crystals are euhedral-subhedral to rounded with embayment, corroded edges and normal, inverse and oscillatory zoning (Fig. 13f). The larger ones show coarse sieve (Fig. 13d) or even can be shattered and rotated, similar to “phenoclast” textures described by Best and Christiansen (1997) as evidence of disruption by bursting melt inclusions decompressed during explosive eruption. Pyroxene crystals represent up to ~1% of the rock rarely exceeding 1 mm in length, except for some long orthopyroxenes reaching more than 4 mm in length (Fig. 13b). They are subhedral to extremely rounded, especially orthopyroxenes show reacted or corroded edges and partial to complete alteration to brown or green material (Fig. 13b-d). Fe-Ti oxides make up less than 1% and are

primarilly Ti-magnetite with rare ilmenite thin lamellae. Apatite occurs as minute quantities in the groundmass. Crystals are distributed mainly as clusters or glomerocrysts (Fig. 13), as in the ATC rocks, in a glassy to thoroughly devitrified groundmass with a broad range in microlite densities. Devitrified samples groundmass show brown spherulitic patches surrounded by microcrystalline quartz-feldspar intergrows to microgranophyric texture throughout. Microlite shapes comprise tabular (laths) to hollow, dendritic, acicular and swallowtail ends for plagioclase and irregular to acicular (up to 4 mm long) for pyroxene.

Table 2 – Pheno-microphenocrysts and microlites compositions of plagioclase and pyroxene from ATP rocks.

Subgroups	Pheno-Microphenocrysts				Groundmass microlites		
	Plag.	**Aug.**	**Pig.**	**Ortho.**	**Plag.**	**Aug.**	**Pig.**
Caxias do Sul	An_{49-74}	En_{41-43} Wo_{36-38}	En_{45-48} Wo_{6-8}	En_{57-66} Wo_{3-4}	An_{25-56}	En_{36-42} Wo_{33-37}	En_{37-55} Wo_{8-11}
Santa Maria	An_{48-65}				An_{45-54}		En_{35-48} Wo_{5-15}
Jacuí	An_{48-61}	En_{38-42} Wo_{35-37}	En_{49-57} Wo_{8-9}		An_{27-51}	En_{34-40} Wo_{30-38}	En_{41-43} Wo_{9-10}
Anita	An_{41-54}	En_{36-42} Wo_{35-40}			An_{25-48}	En_{33-40} Wo_{35-39}	En_{47-52} Wo_{8-10}
Clevelândia	An_{38-57}				An_{37-52}	En_{28-36} Wo_{23-35}	En_{38-49} Wo_{7-15}

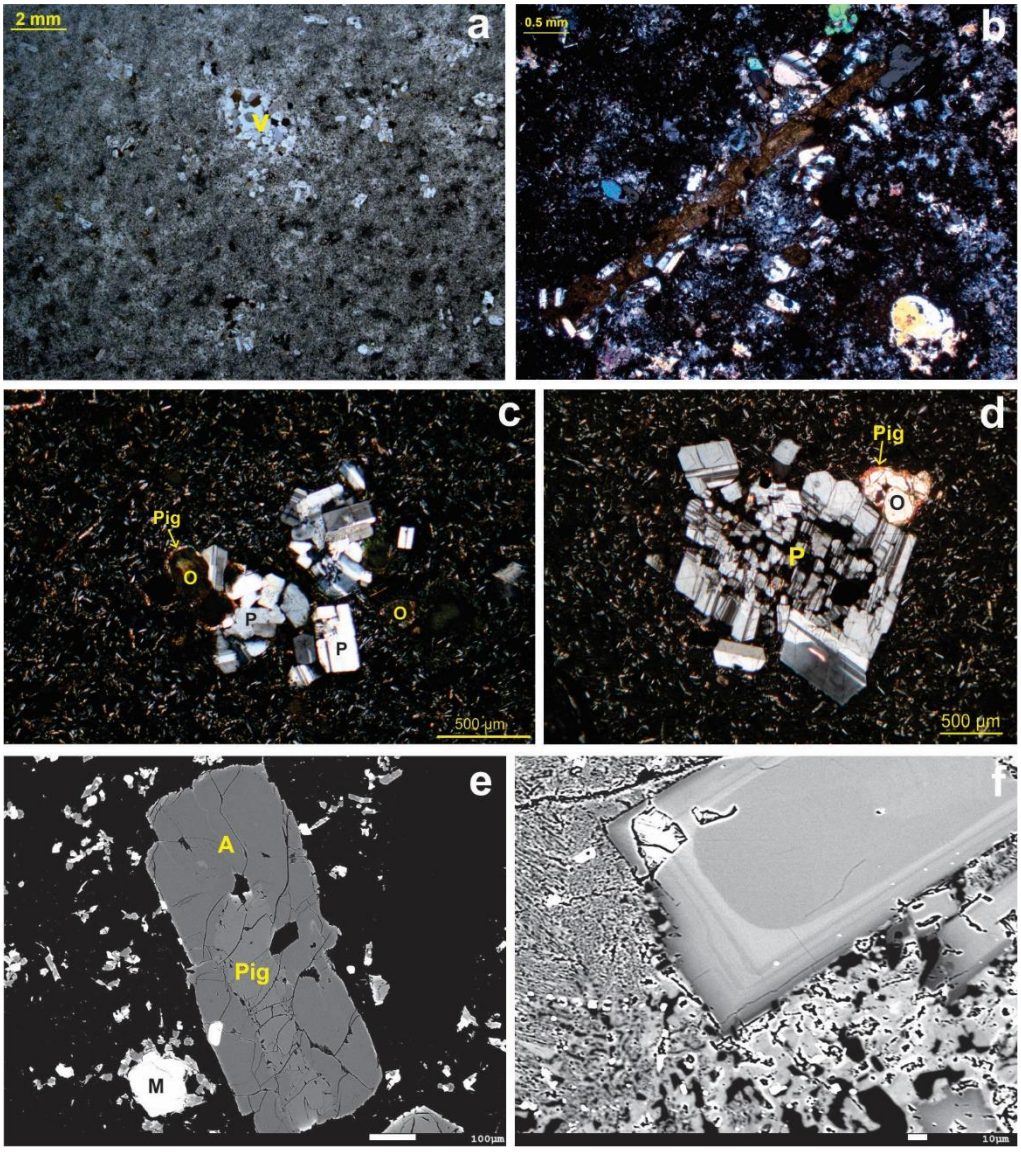

Fig. 13 – Photomicrographs (a-d) and BSE images (e-f) of ATP rocks. (a) Microporphyritic general aspect of a PEV26 sample thin section with plagioclase, pyroxene and Fe-Ti oxide crystals and clusters distributed in a fine groundmass composed of glassy-spherulitic portions surrounded by quartz-alkali feldspar microgranophyric intergowths; // pol.; (b) long altered orthopyroxene crystal (brown) surrounded by plagioclase, augite and smaller orthopx crystals in PEV26 sample; (c) plagioclase crystal with coarse sieve and orthopyroxene crystal with pigeonite corona in vitrophyre (MA11b); (d) same vitrophyre displaying clusters of plagioclase and altered orthopyroxene with pigeonite corona; X pol.; (e) zoned pyroxene crystal in vitrophyre (KSO1095) with pigeonite core and augite border; (f) plagioclase crystal with zoning in microcrystalline groundmass, dark gray areas are more sodic than lighter gray ones; V – vesicle, P – plagioclase, O – orthopx, Pig – pigeonite, A – augite, M – magnetite.

6 THERMOBAROMETRY

Constraints on pre-eruptive conditions under which these magmas evolved is primordial in understanding volcanic processes involved in its eruption. Parameters such as temperature, depth, and volatile content play a major role, if not primary, on the storage conditions and magma rheological properties control. Mean temperature estimates from 930 to 1130°C for ATC rocks and 975 to 1150°C for ATP rocks have been reported by Bellieni et al., 1986, Whittingham, 1991 and Garland et al., 1995. These temperatures were calculated based on plagioclase, pyroxene and magnetite phenocrysts compositions through models developed by Kudo and Weill (1970), Mathez (1973), Kretz (1982), Ishii (1975), Lindsley (1983) and Nathan & Van Kirk (1978). Recent works by Nardy et al. (2011) and Polo (2014) provide average T-P-H_2O estimates (table 3) calculated using Putirka' (2005; 2008) models for plagioclase and Putirka et al. (2003) and Putirka (2008) for clinopyroxene and orthopyroxene.

Table 3 – P-T-H_2O estimates from Nardy et al. (2011) and Polo (2014) for ATC and ATP rocks.

	Type	Subgroup	T (°C)	P (kbar)	H_2O (%)
Nardy et al. (2011)	ATC (clino)		995 ±26	1.8 ±0,9	1 ±0.3
	ATC (plag)		1033 ±12	3.2 ±1	
	ATP (clino)		1028 ±38	3.2 ±1.2	
	ATP (plag)		1043 ±5	1.9 ±1	
Polo (2014)	ATP (px)	Caxias do Sul	976 (clino) 1027 (orthopx)	1.6	
		Barros Cassal (Anita)	986	0.46	
		Santa Maria	953		0.8
	ATP (plag)	Caxias do Sul	977		1.8
		Barros Cassal	1005		1.8

Because these rocks bear plagioclase, clinopyroxene and/or orthopyroxene phenocrysts, Putirka et al. and Putirka' models were also chosen in the present study to evaluate temperature, pressure and H_2O content for the PMP silicic volcanic rocks. Furthermore Putirka et al. (2003) have been widely used and (e.g. SCHWARZ et al.,

2004; CAPRARELLI & RIEDEL, 2005; KLÜGEL et al., 2005; GALIPP et al., 2006; MORDICK & GLAZNER, 2006; LONGPRÉ et al., 2008; BERGER et al., 2008; BARKER et al., 2009; PUTIRKA et al. 2009) and able to recover P-T conditions in which crystals formed with a reasonable error margin (PUTIRKA, 2008; PUTIRKA et al., 2009).

Putirka et al. (2003) thermobarometer was applied for clinopyroxene and it is based on the Di/Hd-Jd (thermometer) and Jd (barometer) exchange equilibria between clinopyroxene and co-existing melt with standard errors of estimate (SEE) of ±33°C and ±1.7 kbar. For orthopyroxene the equations (eqn) 28a and 29a of Putirka (2008) were chosen as thermometer and barometer respectively. Eqn 28a (SEE = ±39°C) result from Beattie (1993)' orthopx-liquid thermometer improvement employing the mole fraction of $Fm_2Si_2O_6$ (or enstatite + ferrosilite, EnFs), where Fm = Fe + Mn + Mg, while eqn 29a (SEE = ±2.6 kbar) is based on the $NaAlSi_2O_6$ component (or Jd).

Putirka' (2005, 2008) thermometers, barometer and hygrometers were applied for plagioclase. They are based on the plagioclase–liquid exchange reaction between albite and anorthite with SEE = ±36°C, ±2.47 kbar and ±1.5% H_2O. P values required as input in the plagioclase-liquid and orthopx-liquid thermometers were based on Putirka et al. (2003) clinopyroxene-liquid barometer estimates. These thermometers also require H_2O values as input. Based on the following assumptions: the mineralogical assemblages of ATC-ATP rocks are composed of anhydrous minerals; amphibole is stable in melts containing at least 4wt % H_2O (RUTHERFORD & HILL, 1993); and Barclay & Carmichael (2004) experiments showed that amphibole can crystallize at relatively low water contents (c. 2wt % at P < 50 to 300 MPa), and at 1000-1050°C, amphibole is stable down to at least 2.5wt % H_2O, we can assume that the maximum water content is up to 2wt %. Thus, the maximum water value considered as input in the models was 1.5wt %.

6.1 Crystal-liquid equilibrium tests

All these thermobaromemters and hygrometers require mineral and liquid compositions input. Since the mineral-liquid pairs must be in equilibrium, exchange coefficients between mineral and liquid were used to verify this condition. K_D(Fe-Mg) is

expected to be 0.27 ±0.03 for clinopyroxene-liquid (PUTIRKA, 1999; PUTIRKA, et al., 2003) and 0.29 ±0.06 for orthopx-liquid (PUTIRKA, 2008). The plagioclase-liquid equilibrium constant for An-Ab exchange are divided in two temperature intervals yielding K_D(An-Ab) = 0.10 ±0.05 for T <1050°C and K_D(An-Ab) = 0.27 ±0.11 for T ≥1050°C (Putirka, 2008). Other useful tests were also applied comparing the clinopyroxene predicted DiHd-EnFs-CaTs components versus observed components (PUTIRKA, 1999) and the Mg number (100*Mg#) between orthopx and liquid (RHODES et al., 1979). For plagioclase, calculated T from equations 23 (PUTIRKA, 2005) or 24a (PUTIRKA, 2008) could be compared to saturation T from equation 26 (PUTIRKA, 2008). If these values closely match, it indicates equilibrium between mineral and liquid likewise those have not obeyed all these conditions were discarded.

7 RESULTS

7.1 Temperature, pressure and H_2O estimates

Appropriate liquids in thermobarometric studies can be the host whole rock, groundmass composition (glass), whole rock compositions after chemical adjustments for phenocryst contents and other compositions in the geological context (PUTIRKA 1997; PUTIRKA & CONDIT 2003; PUTIRKA, 2008). For the present work, as there is no available groundmass composition analysis, host whole rocks were taken as starting compositions.

Final liquids for ATC rocks resulted from a subtraction of 10% plagioclase for clinopyroxene and 5% clinopyroxene for plagioclase. A Caxias do Sul subtype whole rock composition of 66.97wt % SiO_2 resulted the best equilibrium conditions for PEV25, MA11b and KLS1105 samples plagioclase. For Santa Maria samples, as the host whole rocks did not satisfy all the requirements for equilibrium and this subgroup has no compositions with less than 69wt % SiO_2, an Anita subtype whole rock composition (66.90wt % SiO_2) was tested resulting in an appropriate liquid.

On the other hand, ATP pyroxene crystals have not shown to be in equilibrium with acid liquids. Therefore, three other whole rock compositions were also considered: Gramado type basalt (50.35% SiO_2), basaltic andesite (55.61% SiO_2) and andesite (60.85% SiO_2). Since there is a genetic link consensus between these silicic rocks and the associated basalts-to-andesites (BELLIENI et al., 1984, 1986; PICCIRILLO et al., 1987; GARLAND et al., 1995) and also fractional crystallisation from these liquids have shown to be feasible for the ATP magmas generation in petrogenetic studies by Prado (2015, unpublished data). Equilibrium tests have shown a strong correlation between these three liquids, with best fits achieved between the Gramado basalt and clinopyroxene for Jacuí subgroup (Fig. 14b) and between the andesite whole rock and orthopx (Fig. 14a) and clinopx (Fig. 14c) for Caxias do Sul subgroup. A basaltic andesite whole rock (53.13% SiO_2) of Urubici type yielded good fits for Anita clinopyroxene and so, it was used as liquid input.

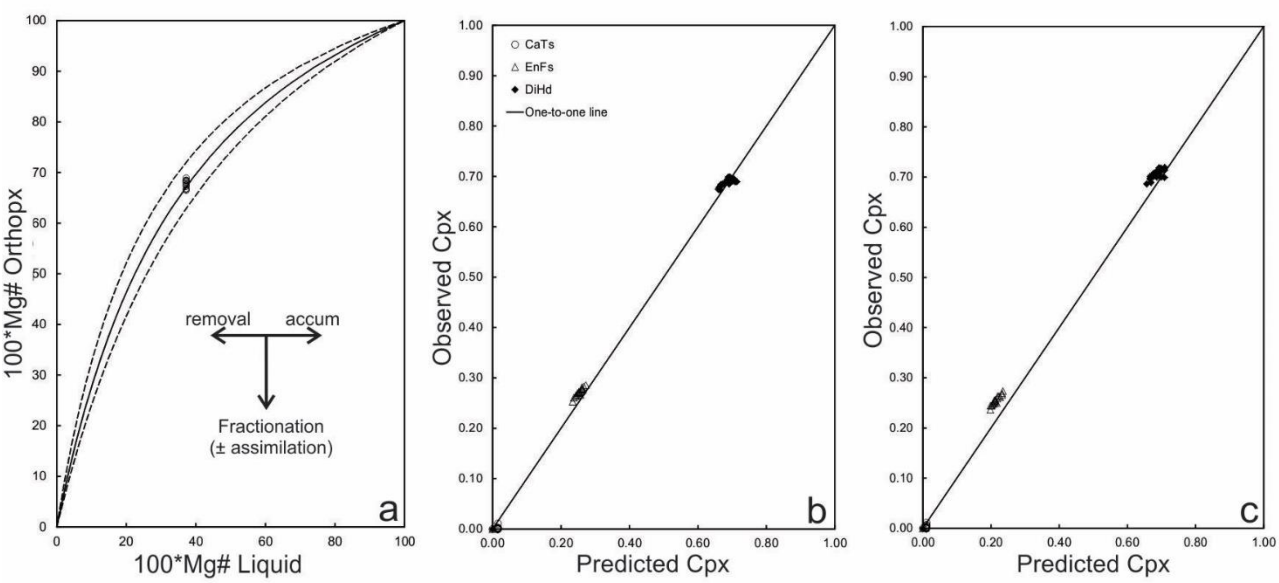

Fig. 14 – Equilibrium test diagrams for ATP pyroxenes. (a) Rhodes diagram for orthopx-liquid equilibrium from Putirka (2008) with K_D(Fe-Mg) = 0.29 ±0.2 using the andesite bulk rock. (b and c) Predicted vs observed clinopx components (Putirka, 1999) using the Gramado basalt bulk rock for Jacuí (b) and the andesite bulk rock for Caxias do Sul augite (c). Resulting K_D(Fe-Mg) values are 0.27 ±0.2.

The K_D(An-Ab) for plagioclase considered here were of 0.10 ±0.03 for ATC and 0.10 ±0.02 for ATP samples with 2σ of thermometer errors, hence yielding in very tight ranges of temperature and pressures with no systematic difference between cores and rims. Thermobarometry-hygrometry mean estimates for each sample are displayed in table 4 and P-T data in Fig. 15. Mean estimates for Chapecó (ATC) plagioclase (Fig.15b) (Guarapuava + Tamarana subgroups) are 1030°C, 4.1-4.3 kbar and 0.6-1.3% H_2O. For Palmas (ATP) flows, plagioclase resulted in overall mean estimates of 1040-976°C, 2.6-0.7 kbar and 0-1.8% H_2O. As pyroxene are not in equilibrium with the host bulk rock, its rims may result in unreliable estimates and so they were discarded. Nevertheless, it should be noted that pyroxenes yielded wider ranges in P estimates and clinopx exceeded the barometer error in the KMA1183 (1.8 kbar) and the KS1329 samples (2.3 kbar). Mean estimates for Chapecó clinopyroxene (Fig. 15b) are 965-973°C and 3.6-2 kbar (Guarapuava and Tamarana respectively). Palmas pyroxene resulted in mean values of 1136-1094°C, 2.9-1 kbar (clinopx), 1113-1094°C and 2.8-1.3 kbar (orthopx).

Between the different ATP subgroups, Caxias do Sul is represented by the lower

pitchstone domes (PEV25 and MA11b), an upper devitrified flow (PEV26), all from the eastern border of PMP, and a pitchstone sample (KLS1105) which lies westward, between Lageado and Soledade towns. PEV25 orthopyroxene resulted in 1106-1094°C and 2.2-2.8 kbar (anhydrous base and with 1% H_2O respectively) and 1094°C – 2.8 kbar as mean estimates with clinopyroxene returning no value. PEV25-MA11b plagioclase yielded 1016°C, 1.4 kbar and 0.8-1.8% H_2O. PEV26 clinopyroxene with 1094°C and 1.0 kbar, an orthopyroxene with 1107-1096°C and 1.3-1.9 kbar (anhydrous base and with 1% H_2O respectively), and plagioclase resulting 995°C, 0.7 kbar and 0.8-1.8% H_2O as mean values. KLS1105 orthopyroxene yielded mean estimates of 1113-1100°C and 1.7-2.3 kbar (anhydrous base and with 1% H_2O respectively), and plagioclase 1001°C, 0.8 kbar and 1.1-1.9% H_2O.

Santa Maria samples (Fig. 15d) are represented by lower pitchstones (KSO1374 and JM12) and upper devitrified rocks (KSO1374 and MA5). Its plagioclase resulted mean values of 1012-1028°C, 1.7-1.0 kbar and 0.4-1.3% H_2O.

Jacuí (Fig. 15e) clinopyroxene resulted mean estimates of 1134°C and 2.7 kbar, while plagioclase from pitchestone domes samples (KSO1095 and 1373) resulted mean values of 1039°C, 1.7 kbar and 0.5-1.3% H_2O and 976°C, 1.1 kbar and 1.3-2.1% H_2O for the KSO1091, from an upper devitrified flow.

Anita subtype plagioclase (Fig. 15e) resulted mean values of 1040°C, 2.6 kbar and 0-0.9% H2O for KS1329 sample, from the southern region, and 1034°C, 2.6 kbar and 0.6-1.4% H_2O for KPM1168, from the central region of PMP. KS1329 clinopyroxene resulted mean values of 1117°C and 2.4 kbar.

Table 4 – P, T and H_2O estimates.

Type	Subtype	Sample	Mineral	N	T (°C)			P (kbar)			Putirka (2005)	Putirka (2008)
					Av.	Max.	Min.	Av.	Max.	Min.	H_2O (%)	H_2O (%)
Chapecó	Tamarana	KJC1150	clino	5	973	976	969	2.0	2.5	1.6		
			plag	8	1030	1031	1029	4.1	4.5	3.7	0.6 ±0.1	1.2 ±0.1
	Guarapuava	KMA1183	clino	8	965	978	951	3.3	5.1	1.6		
			plag	26	1032	1034	1031	4.3	4.7	3.6	0.6±0.2	1.2 ±0.1
		PEV19	clino	7	971	984	962	4.0	5.7	2.9		
			plag	16	1030	1032	1029	4.2	4.6	3.4	0.6 ±0.2	1.2 ±0.1
Palmas	Jacuí	KSO1373	clino	14	1134	1142	1130	2.7	3.6	2.1		
			plag	33	1039	1041	1037	1.7	2.1	1.3	0.5 ±0.2	1.4 - 1.3
		KSO1095	clino	5	1136	1143	1131	2.9	3.9	2.2		
			plag	26	1039	1041	1037	1.8	2.3	1.3	0.5 ±0.2	1.4 - 1.3
		KSO1091	clino	14	1133	1144	1116	2.5	3.8	0.3		
			plag	28	976	977	974	1.1	1.5	0.8	1.3 ±0.2	2.1
	Caxias do Sul	KLS1105	ortho (anhydrous)	15	1113	1118	1107	1.7	3.0	0.8		
			ortho (1% H_2O)		1100	1105	1094	2.3	3.6	1.4		
			plag	22	1001	1010	992	0.8	2.0	0.4	1.1 ±0.3	1.9 ±0.1
		PEV25	ortho (anhydrous)	8	1106	1108	1104	2.2	2.9	1.1		
			ortho (1% H_2O)		1094	1096	1091	2.8	3.5	1.7		
			plag	19	1016	1032	1001	1.4	2.0	0.8	0.8 ±0.5	1.2-1.8
		MA11b	plag	28	1016	1032	1000	1.4	2.6	0.7	0.8 ±0.5	1.2-1.8
		PEV26	clino	23	1094	1103	1089	1.0	2.0	0.4		
			ortho (anhydrous)	1		1107			1.3			
			ortho (1% H_2O)			1096			1.9			
			plag	25	995	1001	990	0.7	1.1	0.3	0.8 ±0.2	1.8 ±0.1
	Santa Maria	JM12	plag	38	1027	1034	1020	1.7	2.4	1.0	0.4 ±0.4	1.1 ±0.3
		MA5	plag	19	1028	1034	1021	1.7	2.4	1.1	0.4 ±0.3	1.2 ±0.2
		KSO 1374	plag	31	1012	1014	1010	1.0	1.3	0.6	0.7 ±0.1	1.4-1.3
		KSO1376	plag	24	1017	1025	1009	1.2	1.9	0.6	0.6 ±0.3	1.3 ±0.1
	Anita	KS1329	clino	12	1117	1138	1098	2.4	4.5	0.1		
			plag	16	1040	1042	1038	2.6	3.3	2.2	0-0.1	0.9 ±0.1
		KPM1168	plag	18	1034	1036	1033	2.6	2.9	2.2	0.6 ±0.1	1.3-1.4

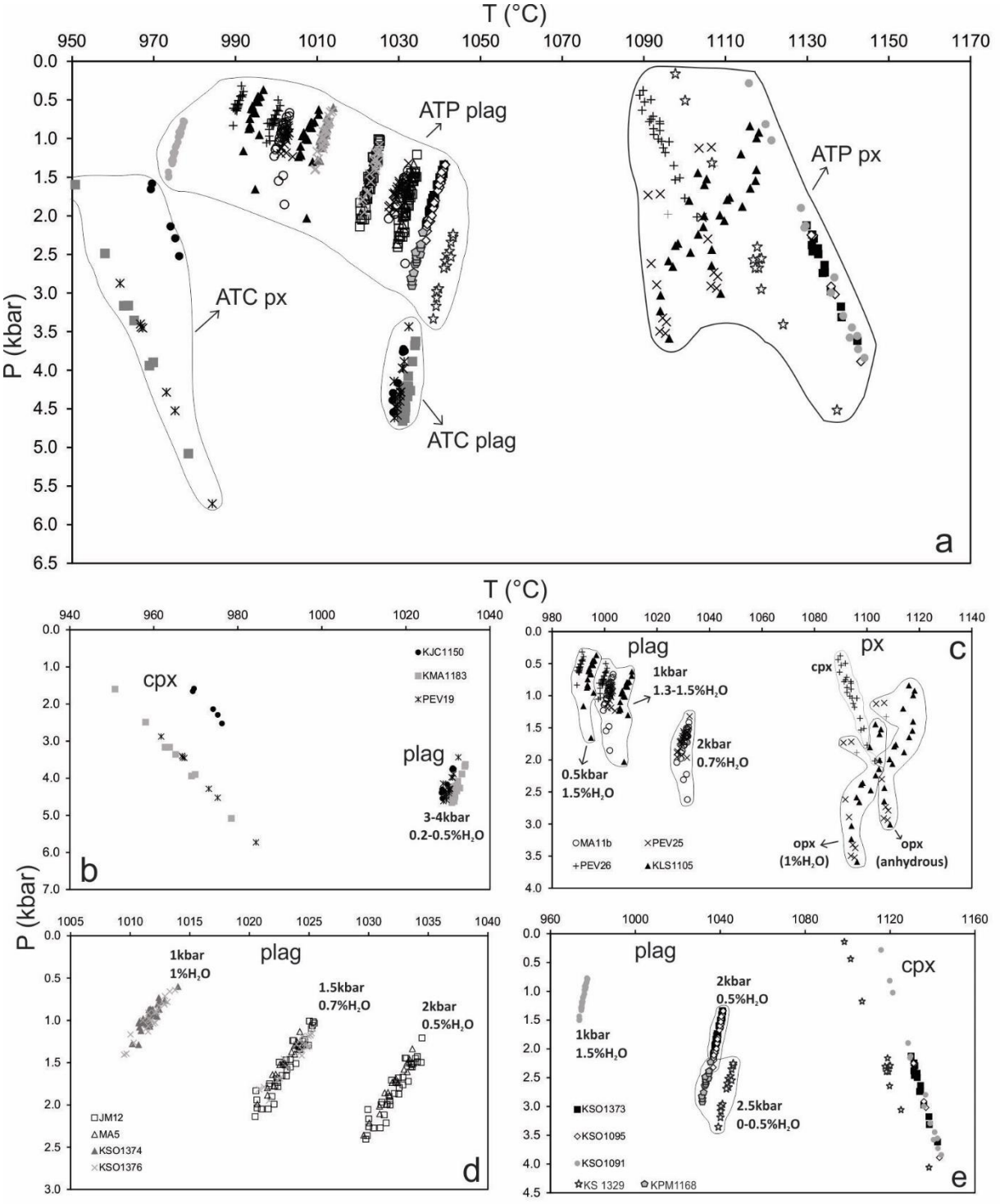

Fig. 15 – Temperature (T) vs pressure (P) diagrams with resulting plagioclase (plag), clinopyroxene (cpx) and orthopyroxene (opx) estimates for silicic volcanics from PMP. (a) Overall diagram with all results for ATC and ATP rocks. (b) Diagrama for ATC samples. (b-e) Diagrams for ATP subgroups samples, Caxias do Sul (c), Santa Maria (d), Jacuí and Anita (e). Marked values were used as input data.

7.2 Crystal Size Distribution (CSD)

CSD studies have been widely applied in order to characterize cooling magma crystallization histories, as well as the dynamics involved in magma storage and transport to the earth's surface (e.g. MARSH, 1988, 1998; CASHMAN AND MARSH, 1988; ARMIENTI et al., 1994; ARMIENTI, 2008; BINDEMAN, 2003; BLUNDY & CASHMAN, 2008; CASHMAN, 1992; CASHMAN AND MCCONNELL, 2005; HAMMER et al., 1999; LENTZ & MCSWEEN, 2000; PAMUKCU et al, 2012). The theory assumes the crystal population density from a melt crystallizing in steady-state condition (continuous nucleation and growth rates) yields a log-linear plot, ln(n) vs. crystal size, with a slope = $-1/G\tau$ and intercept = n^0, where G represents the growth rate, τ is the residence time and n^0 is the final nucleation density (MARSH, 1988; CASHMAN & MARSH, 1988). Straight CSDs lines, plotted on the 'classical' diagram of ln(population density) versus size, are characteristic of steady-state systems, however geological processes, such as magma mixing (HIGGINS, 1996; VINET & HIGGINS, 2010), polybaric crystallization (ARMIENTI et al.,1994), crystal settling (MARSH, 1998; BINDEMAN, 2003), textural coarsening or annealing or Ostwald ripening (HIGGINS, 1998, 1999; HIGGINS AND ROBERGE, 2003), can generate kinked or curved plots.

The current study reports the first CSDs from PMP rocks, specially for the silicic ones. For this purpose, quantitative analysis were extracted from x-ray maps and the EBSD method was also tested (see Analytical Methods section). Plagioclase was the main phase chosen as representing the vast majority of phenocrysts found in these rocks followed by pyroxene and then Fe-Ti oxides. PEV19 (ATC – Guarapuava subgroup) and PEV26 (ATP – Caxias do Sul subgroup) samples were selected for the EBSD method and KLS1105, PEV25 (Caxias do Sul subgroup), KSO1094, KSO1095 (Jacuí subgroup) and JM12 (Santa Maria subgroup) for x-ray maps as well also PEV19.

As many pyroxene crystals from PEV26 are altered, affecting their acquisitions by EBSD, only x-ray maping data were considered for this sample for its pyroxenes. Due to image resolutions smaller crystals which could be measured in the EBSD maps range from ~0.06 mm to ~0.1 mm in the x-ray maps. However, it should be noted they do not represent the smallest crystals in the samples. CSDCorrections bins with fewer

than five crystals should be removed from the CSD as they are not precise (MARSH, 1988; HIGGINS & ROBERGE, 2007). This usually happens with larger crystals, since they are not numerous in thin sections yielding significant errors in phase proportion estimated from CSDs (HIGGINS, 2002). In the ATC rocks (PEV19) even with four thin sections imaged, size crystals > 4 mm amounted to four specimens. However as the upper-lower error limits of ln(pop. density) for these large crystals are lower than 1, so they were considered. Pyroxene phenocrysts in the KLS1105 and PEV25 samples accounted for less than 100 crystals and therefore they were not considered in the CSD analysis. The resulting CSDs data is shown in Table 5 and CSD plots in Figures 16 and 17.

The resulting CSDs for ATC plagioclase and pyroxene using EBSD method are similar to those using x-ray maps + ImageJ (Fig. 16). Accordingly EBSD proved to be valid in the extraction of crystal quantitative analysis with the advantage of no need to separate touching crystals, difficult to identify under the optical microscope. The disadvantage is the fairly flat and smoothly polished sample/thin section surface and the long data acquisition time required to cover large areas with a suitable image resolution (~ one day for a half of a thin section = 9 x 35 mm).

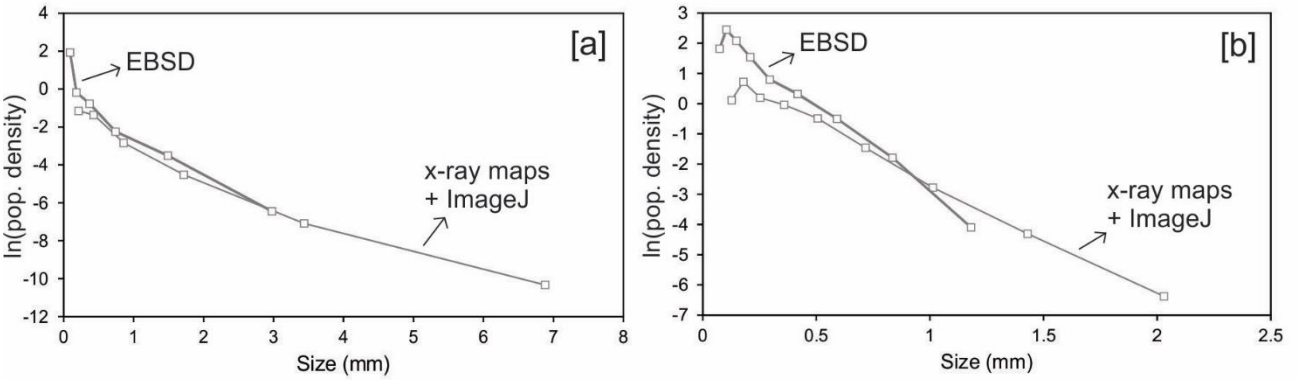

Fig. 16 – CSDs for ATC plagioclase (a) and pyroxene (b) comparing the two methods used for acquisition and processing of crystal quantitative analysis, EBSD and x-ray maps + ImageJ. The patterns are similar. In the plagioclase, CSD extending for larger sizes (right part) in x-ray maps is due to four thin sections compared to only two used in the EBSD, resulting in insufficient amount of crystals > 4 mm long obtained by latter. Instead, EBSD captured larger amounts of small crystals < 0.1 mm (left end).

The ATC porphyritic texture clearly stands out on the fine-grained ATP rocks in the plagioclase CSDs (Fig. 17a). The lognormal size distributions are verified by the

cumulative distribution function (Fig. 17c and e). Overall the ATC pyroxene, ATP plagioclase and KSO1095 pyroxene have straight line CSDs, with some deviations, and a turn-down in the smallest sizes measured. Slope\intercept values are -3.85\1.3, R^2 = 0.997, and -5.80\2.84, R^2 = 0.993 (x-ray maps + ImageJ and EBSD respectively) for ATC pyroxene; -7.29- -4.51\2.11-4.16, R^2 = 0.974-0.998, for ATP plagioclase; -6.47\1.98, R^2 = 0.996, and -4.67\1.26, R^2 = 0.95, for KSO1095 and KSO1094 pyroxene respectively.

ATC plagioclase and PEV26 pyroxene (ATP) show a concave-up CSD. Slopes\intercepts for ATC plagioclase are of -1.42\-1.26, R^2 = 0.96, for crystal sizes from 0.107 to 6.85 mm, and -47.76\4.23, R^2 = 1, for crystal sizes from 0.053 to 0.107 mm (Fig 18a). However, assuming three different populations in the size interval of 0.107 to 6.85 mm (Fig. 18b), the resulting slope\intercept values are of -0.94\-3.85, R^2 = 1 (size > 3.43 mm), -1.62\-1.56, R^2 = 0.995 (0.857 < size < 3.43 mm), and -2.58\-0.52, R^2 = 0.96 (0.107 < size < 0.857) (Fig. 14b). Slopes\intercepts for PEV26 pyroxene are of -1.18\-4.8, R2 = 1 (size > 1.57 mm), and -4.8\0.61, R2 = 0.98 (0.098 < size < 1.57 mm).

Table 5 – Resulting CSD parameters for ATC and ATP rocks.

Plagioclase Sample	N	Vol. Phase	Total number from CSD	Total vol. (%) from CSD	1σ	size interval	Slope (S)	Intercept (n^0)	R^2	Max CL[a] (mm)	L_{max}[b] (mm)	τ (-1/GS)	τ (CL/G)	τ (L_{max}/G)
						0.107-6.85 mm	-1.42	-1.26	0.96			2233		
						> 3.43 mm	-0.94	-3.85	1			3367	3361	15823
PEV19	503	7.29	0.404	7.36	1.67	0.857-3.43 mm	-1.62	-1.56	0.995	1.06	4.990			
						0.107-0.857 mm	-2.58	-0.52	0.959					
						0.053-0.107 mm	-47.76	4.23	1					
JM12	407	1.45	0.67	1.51	0.3		-6.35	2.44	0.985	0.231	1.178	499	732	3735
KLS1105	465	2.38	0.99	2.42	0.37		-4.51	2.68	0.993	0.423	1.251	703	1341	3967
KSO1095	255	1.78	0.683	1.79	0.36		-4.97	2.36	0.995	0.308	0.856	638	977	2714
PEV25	376	3.13	1.36	3.16	0.53		-5.33	3.23	0.998	0.225	0.916	595	713	2905
KSO1094	273	2.05	0.617	2.02	0.36		-4.87	2.11	0.974	0.521	0.904	651	1652	2867
PEV26	297	2.75	1.6	2.72	0.47		-7.29	4.16	0.995	0.15	0.956	435	476	3031
Pyroxene														
PEV19	589	3.5	0.594	3.52	0.64		-3.85	1.30	0.997	0.46	1.842			
PEV26	308	0.93	0.235	0.94	0.27	> 1.57 mm	-1.18	-4.80	1	0.76	2.634			
						0.098-1.57 mm	-4.80	0.61	0.985					
KSO1095	151	1.035	0.593	1.04	0.3		-6.47	1.98	0.996	0.239	0.794			
KSO1094	117	1.16	0.24	1.17	0.32		-4.67	1.26	0.95	0.358	1.297			

[a]Maximum characteristic length; [b]average of the four largest grains from the crystal population; τ = residence time in years.

Table 5 (continued).

Plagioclase Sample	N	Vol. Phase	Total number from CSD	Total vol (%) from CSD	1σ	size interval	Slope (S)	Intercept (n^0)	R^2	Max CL (mm)
						Large	-1.89	-0.78	0.999	
PEV19 (EBSD)	209	5.87	0.765	5.86	1.34	Int.	-3.74	0.56	0.997	0.588
						small	-22.64	4.04	1	
PEV19						Large	-0.94	-3.85	1	
(x-ray maps +	438	7.28	0.173	7.33	1.67	Int.	-1.62	-1.56	0.995	1.06
ImageJ)						Small	-2.58	-0.52	0.959	
Pyroxene										
PEV19 (EBSD)	477	3.14	1.92	3.12	0.55		-5.80	2.84	0.993	0.26

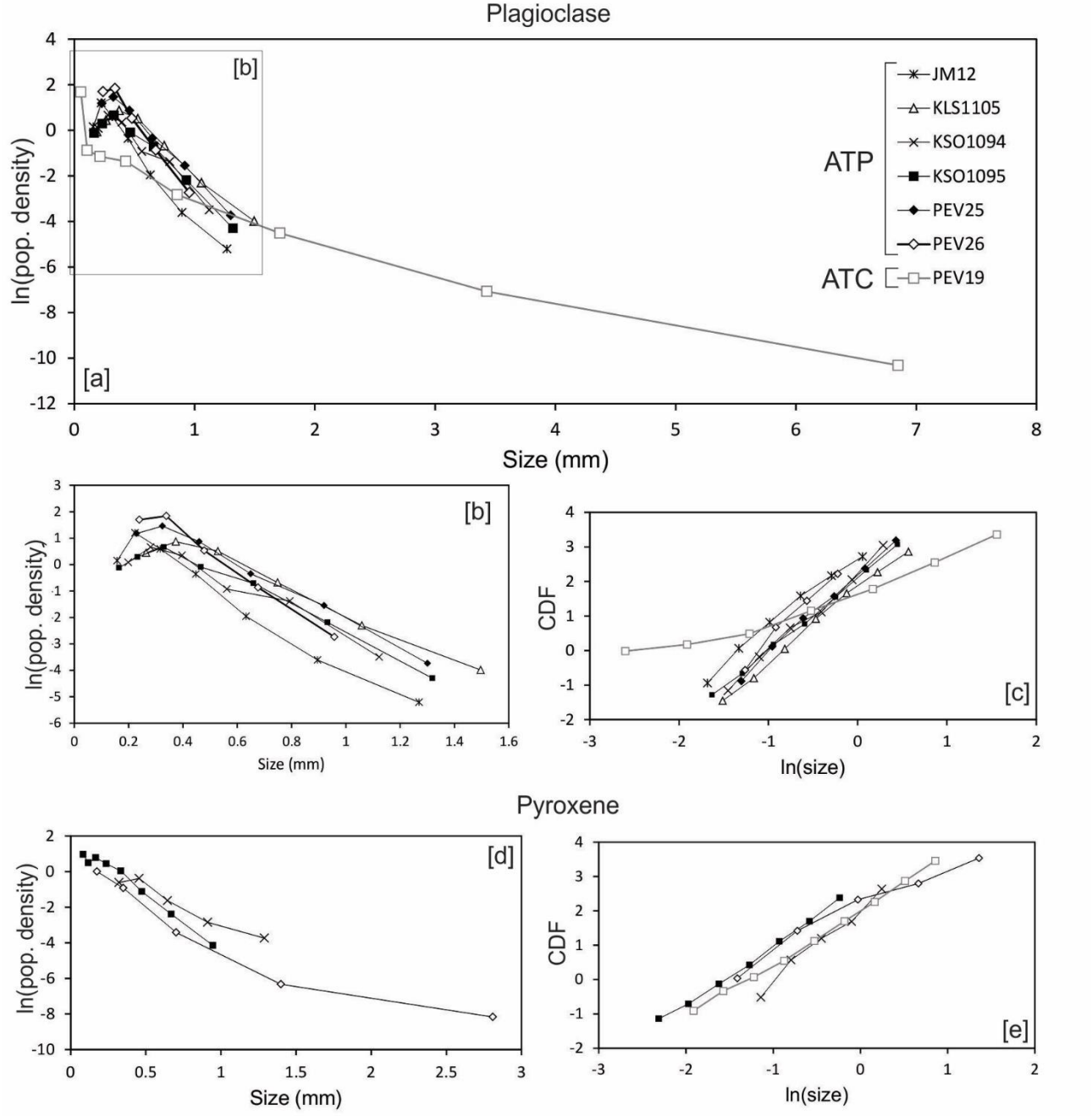

Fig. 17 – Plagioclase and pyroxene CSDs. (a) Plagioclase from ATC (EBSD + x-ray maps) and different subgroups of ATP rocks. The porphyritic nature of ATC is highlighted relatively to ATP. (b) CSD close-up for ATP shown in (a). (c, e) Cumulative distribution function (CDF) diagrams displaying lognormal size distributions for all samples. (d) pyroxene CSDs for ATP rocks. PEV19 = Guarapuava subgroup (ATC); ATP subgroup samples: JM12 = Santa Maria; KLS1105, PEV25 and PEV26 = Caxias do Sul; KSO1094 and KSO1095 = Jacuí.

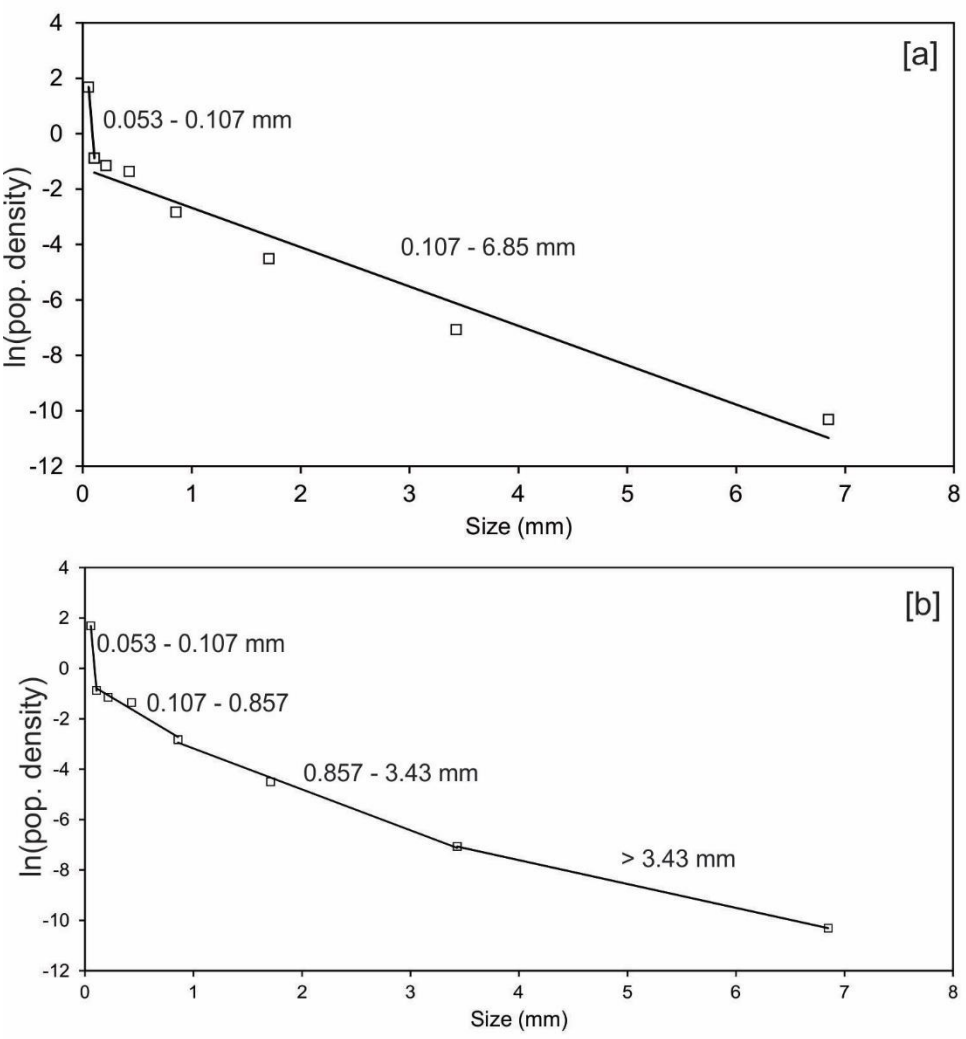

Fig. 18 - Best-fit segmentations (linear regressions) for ATC plagioclase CSD defined by distinct slopes and intercepts. (a) best-fit segments yielding two plagioclase size populations, 0.107 - 6.85 mm and 0.053 – 0.107 mm; (b) best-fit segments in the size interval of 0.107-6.85 mm yielding three other plagioclase size populations, > 3,43 mm, 0,857-3,43 mm and 0,107-0,857 mm.

8 DISCUSSION

8.1 Crystallization temperatures and depths

Temperatures calculated for ATC and ATP rocks are high (> 950°C). In the ATC samples plagioclase shows higher T (1030°C ±4°C) than augite (969°C ±18°C) indicating that plagioclase crystallized first. This is also consistent with simulations in Rhyolite-MELTS software (GUALDA & GHIORSO, 2015). In contrast, ATP pyroxenes show the highest T, in equilibrium with basaltic-to-andesitic liquids (1134 ±18°C and 1100 ±11°C averages, respectively), whereas plagioclase, with 976 ±2°C to 1040 ±2°C, in equilibrium with dacitic liquids, indicating that pyroxene (augite-orthopx) crystallized first, which is also consistent with simulations in Rhyolite-MELTS software (GUALDA & GHIORSO, 2015). The orthopx and augite T overlap to orthopx higher T suggest a co-precipitation of these phases or augite closely following orthopx crystallization. These data are also consistent with petrographyc observations in which pyroxene crystals show disequilibrium features such as rounding, corroded edges and reaction edges.

Pyroxene resulted in wider ranges in crystallization depths. Orthopx P estimates are within the model error which is high (SEE = 2.6 kbar, PUTIRKA, 2008). However augite P estimates in a single sample range up to 1.8 kbar in the ATC and 2.3 kbar in the ATP (KSO1091-Jacuí and KS1329-Anita) (SEE = 1.7 kbar, PUTIRKA et al., 2003). Augites with lightly lower Na_2O content resulted the lowest depths (P), but also the highest ones. It is not entirely clear why the Putirka et al. (2003) barometer does not accurately recover the pressures for shallow systems (≤ 3 kbar) (PUTIRKA, 2008). According to Putirka et al. (2009) this problems may be related to diffusion rates in clinopyroxene. Augites P estimates from KS1329 sample (Anita subtype) are questionable as they may not be intratelluric crystals, and in increasing cooling conditions rate the K_D(Fe-Mg) between clinopyroxene and melt is not suitable to prove the (dis)equilibrium (MOLLO et al., 2010). Nevertheless, P estimates calculated for pyroxene are low (upper crust) and this is consistent with its very low Na and Al^{VI} contents. Unlike pyroxenes, plagioclases show narrower ranges in calculated P for each sample.

Despite the limited condition of the resulting data, comparisons are rightful. ATC rocks show higher storage depths, 4-2 kbar for clinopyroxene and 4.3-4.1 kbar for plagioclase (Guarapuava and Tamarana subtypes respectively). ATP rocks show even shallower storage levels, 2.7-1 kbar for pyroxenes and 2.6-0.7 kbar for plagioclase.

Between the different ATP subgroups the Anita subgroup shows crystallization temperatures and depths slightly higher (1040°C – 2.6 kbar averages - plagioclase) than the other ones. These resulting higher depths for plagioclase, as also for ATC ones, reflect its lower An content (Anita = An_{41-54}, ATC = An_{30-49}, ATP rest = An_{48-74}) as the plagioclase-liquid barometer is based on experimental observations that the anorthite concentration in plagioclase decreases with increasing pressure (LANGE et al., 2009). Jacuí augites have crystallized at higher mean T-P (1133-1136°C-2.9-2.5 kbar averages) when compared to Caxias do Sul subgroup ones (1094°C-1 kbar averages). Furthermore, within these two groups, most evident in the Jacuí subgroup, the upper unit plagioclases show an overlap at lower T-P (Jacuí = 976°C-1.1 kbar vs 1039°C-1.8 kbar; Caxias do Sul = 995°C-0.7 kbar vs 1016°C-1.4 kbar). As these upper units have larger volumes, this can point to an increase in magma chamber size (Fig. 19), in which these magmas would be stored in the uppermost level.

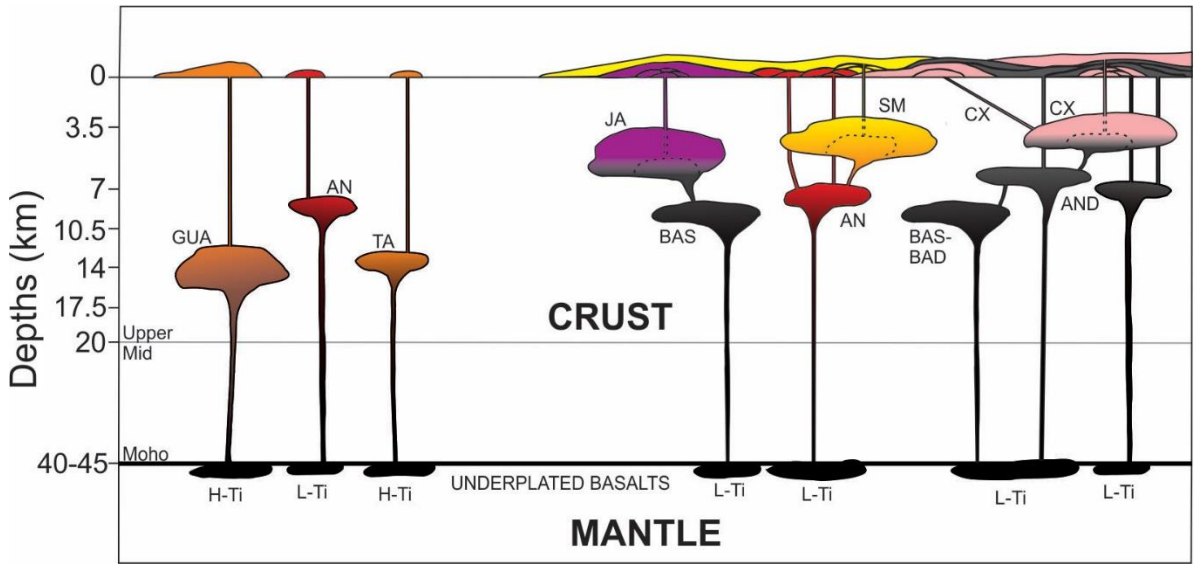

Fig. 19 – Schematic illustration (not to scale) of the magmatic plumbing system beneath Paraná Basin for PMP silicic volcanic rocks. Dashed lines represent early smaller volume magma bodies feeding lava domes. Moho depths of 40-45 km are from Snoke & James (1997), An & Assumpção (2006) and Bianchi (2008), and the upper-mid crustal boundary from Snoke &

James (1997). ATC subtypes: GUA = Guarapuava, TA = Tamarana; ATP subtypes: AN = Anita, JA = Jacuí, CX = Caxias do Sul, SM = Santa Maria. BAS = basalt; BAD = basaltic andesite; AND = andesite.

8.2 Water Content

Amphibole is stable in melts containing at least 4wt % H_2O (RUTHERFORD & HILL, 1993); while Barclay & Carmichael (2004) experiments showed that amphibole can crystallize at relatively low water contents (c. 2wt % at P < 50 to 300 MPa), and amphibole is stable down to at least 2.5wt % H_2O at 1000-1050°C. As there is no amphibole in any ATC or ATP rocks the maximum water content must be lower than 2 wt%.

Both hygrometers provided low water contents (≤ 2%), with SEE = ±1% (PUTIRKA, 2005, 2008). The plagioclase hygrometer of Putirka (2005) yielded mean water contents of 0.6wt % for ATC rocks and 0-1.3wt % for ATP rocks, whereas the hygrometer of Putirka (2008) yielded higher mean water contents, 1.2wt % for ATC and 0.9-1.9wt % for ATP rocks. Thus, these estimates are consistent with the anhydrous mineralogy and the high T calculated for these rocks.

8.3 Rheological and eruptive aspects

Factors determining eruptive styles (explosive-effusive) are the rheological properties of magma, magma supply and syn-eruptive ascent rates and magma degassing in the conduit (e.g. EICHELBERGER et al., 1986; JAUPART & ALLEGRE, 1991; WOODS & KOYAGUCHI, 1994; EICHELBERGER, 1995; DINGWELL, 1996; MARTEL et al., 1998; GONNERMANN & MANGA, 2003; PARFITT & WILSON, 2008). Magma rheology can be considered as a function of the melt viscosity, which is governed by major element composition, H_2O content and temperature (Giordano et al. 2008), since crystals would have had little effect on the bulk viscosity (ATP magmas < 5 % phenocrysts and ATC magmas with up to 20% of phenocrysts) (PETFORD, 2009).

Magma viscosities for ATC and ATP magmas were calculated by using the model of Giordano et al. (2008) with 0 to 1.2wt % H_2O for ATC and 0 to 1.5wt % H_2O for ATP

whole rock compositions (Fig. 20). The resulting values at 1000°C, $10^{4.31 - 6.39}$ Pa s for ATC and $10^{4.27 - 7.22}$ Pa s for ATP magmas, comprise almost 3 orders of magnitude with water increase. The highest values are for Clevelândia and Santa Maria magmas in anhydrous base, owing to its higher silica content (70-72% SiO_2). Nevertheless, these viscosities are considered low for silicic magmas (~$10^{\geq 8}$) even approaching to basic magmas viscosities (10^{2-3}) (FRANCIS and OPPENHEIMER, 2004). Solubilities were also calculated using the Zhang et al. (2007) method showing these silicic magmas would reach water saturation at very shallow levels from 25 MPa (~1 km) for 1.5wt % H_2O to shallower levels for lower H_2O contents (Fig. 20).

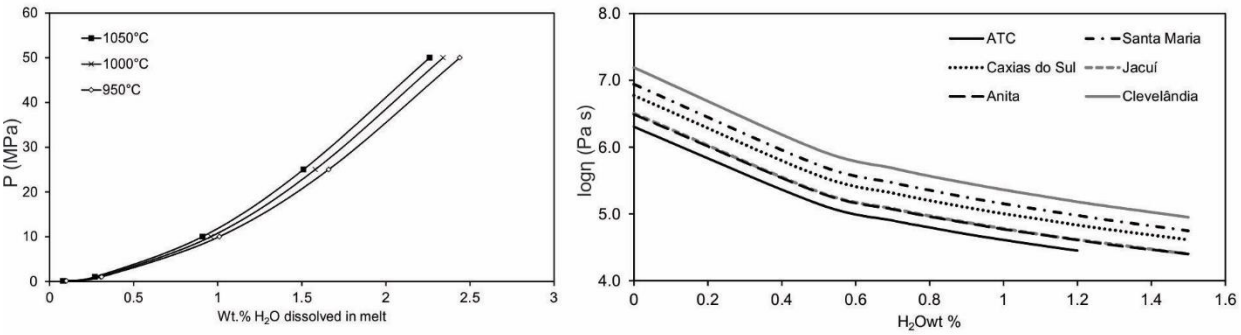

Fig. 20 – Solubilities by Zhang et al. (2007) method (left) and mean viscosities by Giordano et al. (2008) model (right) for ATC and ATP (Caxias do Sul, Anita, Santa Maria, Jacuí and Clevelândia subtypes) magmas.

Lava flows are degassed magma (e.g. EICHELBERGER et al., 1986; JAUPART & ALLEGRE, 1991; GONNERMANN & MANGA, 2003) and the same magma, with homogeneous volatile concentrations, can display contrasting eruption styles, typically explosive activity followed by effusive, although the reverse is also observed (HILDRETH & DRAKE, 1992; EICHELBERGER 1995). Proposed models invoke degassing in a closed-system for explosively erupted magma, in which gas bubbles remain in contact with the melt until it fragments (e.g. SPARKS, 1978; DINGWELL, 1996). In contrast, a degassing in open-system, with exsolved volatiles separating from melt through a permeable foam (EICHELBERGER et al., 1986) or fragmented (brecciated) magma (GONNERMANN & MANGA, 2003), is assigned for effusively erupted magma. Hence there seems to be a link between degassing and ascent rate, as degassing will be efficient in slower (cm/s^{-1}) and inefficient in faster ascent speeds (m/s^{-1}) (e.g. GONNERMANN & MANGA, 2007; BROWNE & SZRAMEK, 2015).

Assumptions arising from Jaupart & Allegre (1991) and Eichelberger et al. (1986) models and discussed in Eichelberger (1995) implicate nonexplosive degassing would be enhanced by low ascent rate resulting, in turn, from higher magma viscosity. Conversely magmas with lower viscosities would ascend more rapidly. With this bias more detailed studies, such as syn-eruptive microlites textures (e.g. BLUNDY & CASHMAN, 2001), are required in these rocks to constrain its ascent-driven crystallization histories.

Another factor is the strong dependence of degassing rate upon the mass flux (JAUPART & ALLEGRE, 1991; EICHELBERGER et al., 1986), since most large volume eruptions (≥ 10 km^3) are explosive, and long-term effusions may be the principle for large-volume silicic flows. However, small volume effusions (0.01-0.1 km^3) would be more typical (EICHELBERGER, 1995). That seems fairly consistent with the silicic volcanism in question, especially in the southern region, where lava domes represent small-volume flows and would express effusion rates limited by small magma chambers. Whereas large-volume ignimbrites reflect high magma supply rates tapping larger magma chambers. The explosive mechanism would be governed by shallow processes in response to sudden decompressions. Something similar to what happens in Vulcanian eruptions initiated from the top down and fueled by shallow degassing and pressurization (CASTRO & GARDNER, 2008; MORRISSEY & MASTIN, 2015). This mechanism is even enhanced in dike-like feeder systems (fissures), which seems to be the case, by providing the magma rapidly travel shorter distances from storage (BLAKE & FINK, 1987; CASTRO et al., 2013). Eruptions would be characterized by low collapse heights and little heat loss during collapse (‘boil over’) due to the high temperatures, low water content and low viscosities (SPARKS et al., 1978; HENRY & WOLF, 1992).

8.4 Crystal size distributions (CSDs)

ATC and ATP CSDs can be summarized as shown in Fig. 21, where it is possible to recognize three parts (segments). Part (1) slopes represent crystal population developed during the storage of magma before the eruption. They can be straight, with some deviations (Fig 21a), shallower and slightly curved upward (Fig 21b); or have a

pronounced upward concavity (Fig. 21c).

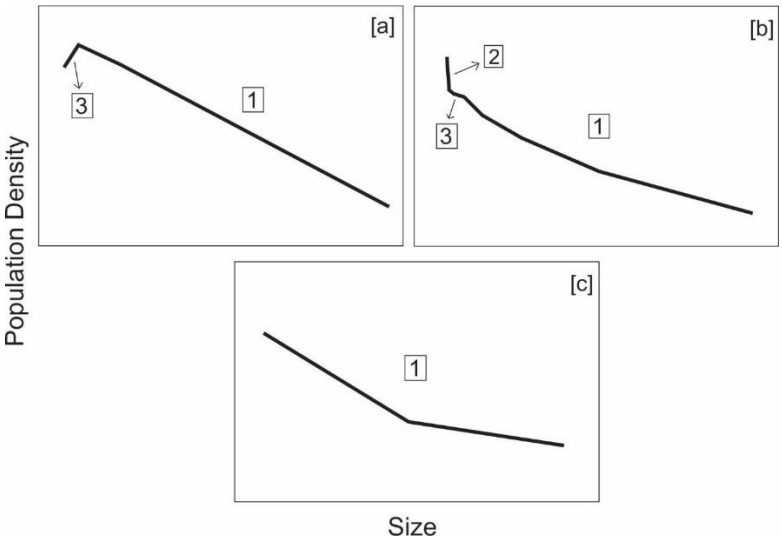

Fig. 21 – Resulting CSDs for ATP and ATC rocks, bearing in mind they can vary from sample to sample in the ATP. [a] = ATP plagioclase-pyroxene and ATC pyroxene; [b] = ATC plagioclase; [c] PEV26 pyroxene; Numbers represent crystallization stages (explanation in the text).

Part (2) corresponds to the small crystals (<0.1 mm) and, as mentioned earlier, these crystals do not represent the smallest sizes found in the samples, but the smaller size allowed by the image resolutions. Its steep slopes are assigned by high population densities concentrated in small bin sizes.

A drop in the number density generates a turn-down shown by Part (3).
As in the ATP samples only plagioclase crystals ≥ 0.1 mm were measured and high densities of smaller crystals are observed in the groundmass, it can be considered that they also have the Part (2).

The linear character of Part (1) shown by fine-grained ATP rocks (Fig. 21a) reflects a simple crystal nucleation and growth (constant rates) in a batch system (MARSH, 1988, 1998) and this common characteristic to all ATP samples suggests that, despite distinct evolution histories, their phenocrysts share a common cooling history. Whereas the shallower slope coupled with upward curvature in the ATC plagioclase (Fig 21b) represent a broad range in crystal sizes, megaphenocrysts, phenocrysts and microphenocrysts. Two populations of pyroxene (large and intermediate) of augite+orthopx, resulted in the more pronounced upward curvature (Fig 21c) in the PEV26 sample, with long orthopx crystals comprising the largest sizes.

Mechanisms have been described in the literature to explain curved CSDs, such as accumulation (MARSH, 1988, 1998), magma mixing (HIGGINS, 1996) or cycles of nucleation-growth alternating with coarsening periods (HIGGINS & ROBERGE, 2003) by temperature oscillations (SIMAKIN & BINDEMAN, 2008). Accumulation can be ruled out for ATC plagioclase, since geochemical data show negative Eu anomalies. However, this can be considered for PEV26 pyroxene. The long orthopx and some large augite crystals may represent 'antecrysts', stored in a crystal accumulation and reincorporated by the emplacement event (MARSH, 1998; JERRAM & MARTIN, 2008), since they derive from more mafic melts as shown by equilibrium tests for the thermobarometry.

An content in the ATC plagioclase does not vary significantly between microphenocrysts to megaphenocrysts and neither mafic enclaves or compositional layering are observed, therefore ruling out a magma mixing hypothesis. Coarsening is a process by which small crystals are resorbed while the larger crystals grow so that the total surface energy is minimized. It occurs when magmas are held near their liquidus temperature for a long period (e.g. HIGGINS, 1998, 1999, 2009). For Simakin & Bindeman (2008) crystal dissolution–precipitation processes or annealing are driven by temperature oscillations present in natural magma chambers. These oscillations are expected owing the thermal and compositional convection induced by fresh hot magma recharge or heating from below with no influxes into the chamber, but yet a fresh hot magma heating the lower level of the magma chamber is required (COUCH et al., 2001). This mechanism also accounts for the turn down shown by Part 3 which represents a disappearance of the small crystals, and it appears to be consistent with the studied silicic rocks, given its high temperatures, plagioclase with oscillatory zoning and plagioclase and pyroxene crystals with resorption textures, such as embayment, irregular outlines and course sieve.

Steep crystal size distributions for small sizes, as represented by Part (2), are commonly observed in volcanic rocks, implying higher rates of nucleation associated with higher degrees of undercooling (MARSH, 1988). They correspond to the groundmass grown under syn-eruptive conditions, in which a magma is rising through a conduit (e.g. CASHMAN,1988; ARMIENTI et al., 1994; PIOCHI et al., 2005; SALISBURY et al., 2008).

8.4.1 Timescales of crystallization

Several works have used CSD to constrain timescales of crystal growth in magmatic systems (e.g. HIGGINS, 1996; MANGAN, 1990; NOGUCHI et al., 2006; PIOCHI et al., 2005; RESMINI & MARSH, 1995; PAMUCKU et al. 2012). If growth rates are assumed to be linear and independent of crystal size or time (MARSH, 1988, 1998): (1) the largest crystal gives the maximum crystallization time of the system by $\tau_{max} = L_{max}/G$, where G is growth rate, τ is time and L is crystal size; (2) CSD slope, $-1/(G\tau)$, is related with the growth time of a population of crystals on a log-linear plot of population density vs crystal size (CASHMAN & MARSH, 1988; MARSH, 1988, 1998). Moreover Cashman (1988) estimated growth rates for plagioclase phenocryst in the range 10^{-13} – 10^{-14} m s^{1}.

Thus, a growth rate of 10^{-14} m s^{-1} was used to calculate residence times for plagioclase phenocrysts from ATC and ATP rocks, as well as maximum characteristic lengths (max CL) as L. The residence times estimated for ATC plagioclase are of ~3,360 years (from max CL) or 2,233-3,367 years (from CSD slope). However, if we assume L_{max} as the average of the four largest grains from the crystal population of each sample (e.g. BOORMAN et al., 2004; O'DRISCOLL et al., 2007, 2008), the residence time is much longer, ~15,800 years or, even greater, 31,710 to 63,420 years, if we assume largest sizes reported by the literature of 1-2 cm long respectively (GARLAND et al. 1995; NARDY et al. 2002; 2008) as L_{max}. This huge difference in the residence times from CSD slope vs L_{max} is probably due to a CSD slope for largest crystals based on a small number of measured crystals (4 crystals) which will not result a true CSD at those crystal sizes (CASHMAN & MARSH, 1988, CASHMAN, 1990). Other methods (e.g. thermal ionization mass spectrometry measurements) are necessary to better constrain the timescales and comparing with CSD data.

Fine-grained ATP plagioclase yielded shorter residence times ranging from 435 to 703 years (CSD slopes) and 476 to 1652 years (max CL), with longer times for L_{max}, ~2,700 to 4,000 years. These timescales are within of ranges calculated for other systems, such as 5,000 (L_{max}) and 400 to 2,500 years (CSD slopes) for the Bishop Tuff (PAMUCKU et al. 2012) and 15.2 ± 2.9 ka for the rhyolite magma generation from

basalts in shallow depths and its subsequent crystallization at the Alid volcanic center (LOWENSTERN et al., 2006). Nevertheless they are considered short, since large-volume volcanic systems are products of extensive and persistent melting. This may reflect efficient thermal conditions coupled with crustal assimilation (LOWENSTERN et al., 2006; ZELLMER & ANNEN, 2008) which is consistent with the high thermal gradients found for ATC and ATP magmas (present work) and crustal assimilation by ATP magmas (BELLIENI et al., 1996; GARLAND et al., 1995; NARDY et al., 2008).

9 CONCLUSIONS

The main conclusions of the present study are as follows:

- Thermobarometric studies indicate a well developed plumbing system with silicic magmas characterized by high T and low water contents in shallow storage depths (upper crust levels). ATC magmas show mean crystallization T of 1030°C ±4°C for plagioclase and 969 ±18°C for augite and deeper storages at ~4 kbar for Guarapuava-Tamarana plagioclase and 4-3.3 kbar (Guarapuava) and 2 kbar (Tamarana) for augite. ATP magmas show mean crystallization T of 976 ±2°C and 1040 ±2°C for plagioclase, 1113 to 1094°C for orthopyroxene and 1136 to 1094°C for augite, with pyroxenes in equilibrium with basalt-to-andesite liquids. Storage depths are upper crustal, 2.8 to 1 kbar for pyroxene and 2.6 to 0.7 kbar for plagioclase. Anita subgroup shows the deepest storage averages for plagioclase, whereas Jacuí-Caxias do Sul lower units show deeper storage than its upper units.
- Water contents are low, from 0.6 to 1.2wt % for ATC rocks and 0 to 1.9wt % for ATP rocks, consistent with the anhydrous mineralogy and high T.
- Lava domes represent degassed small-volume flows and would express effusion rates limited by small magma chambers. Whereas large-volume ignimbrites reflect high eruption rates tapping larger magma chambers. The explosive mechanism would be governed by shallow processes in response to sudden decompressions. Something similar to what happens in Vulcanian eruptions initiated from the top down and fueled by shallow degassing and pressurization (MORRISSEY & MASTIN, 1999; CASTRO & GARDNER, 2008). This mechanism is even enhanced in dike-like feeder systems (fissures), which is the case, by providing the magma rapidly to travel shorter distances from storage (BLAKE & FINK, 1987; CASTRO et al., 2013). Eruptions would be characterized by low collapse heights and little heat loss during collapse (‘boil over’) due to the high temperatures, low water content and low viscosities (SPARKS et al., 1978; HENRY & WOLF, 1992).
- Crystal size distributions indicate different thermal regimes characterized by crystallizations in a magma chamber and during ascent in a conduit (syn-

eruptive). ATC intratelluric plagioclase represent a prolonged and varied crystallization, with changing nucleation-coarsening regimes driven by temperature oscillations present in natural magma chambers (e.g. HIGGINS & ROBERGE, 2003; HIGGINS, 2009; SIMAKIN & BINDEMAN, 2008). Whereas ATC pyroxene and ATP plagioclase-pyroxene show a simple crystal nucleation and growth under conditions of linearly increasing undercooling with a pre-eruptive coarsening. An augite+orthopx CSD (Caxias do Sul subtype), display the more pronounced upward curvature, with long orthopx crystals compraising the largest sizes. These long crystals may represent 'antecrysts', stored in a crystal accumulation and reincorporated in the magma by the emplacement event.

- Residence times from CSD slopes and maximum crystal sizes are of ~2,200 to 15,800 years, respectively, for ATC crystallization, or longer, in the order of 31,710 to 63,420 years, if we assume the largest sizes reported in the literature of 1-2 cm long respectively (GARLAND et al. 1995; NARDY et al. 2002, 2008). Fine-grained ATP plagioclase yielded shorter residence times ranging from 435 to 703 years (CSD slopes) and 476 to 1652 years (max CL), with longer times for L_{max}, ~2,700 to 4,000 years. These timescales are within of ranges calculated for other systems, such as 5,000 (L_{max}) and 400 to 2,500 years (CSD slopes) for Bishop Tuff (PAMUCKU et al. 2012) and 15.2 ± 2.9 ka for the rhyolite magma generation from basalts in shallow depths and its subsequent crystallization in Alid volcanic center (LOWENSTERN et al., 2006). Nevertheless these are considered short, since large-volume volcanic systems are products of extensive and persistent melting. This may reflect efficient thermal conditions coupled with crustal assimilation (LOWENSTERN et al., 2006; ZELLMER & ANNEN, 2008) which is consistent with the high thermal gradients found for ATC and ATP magmas (present work) and crustal assimilation by ATP magmas (BELLIENI et al., 1996; GARLAND et al., 1995; NARDY et al., 2008).

REFERENCES

ALBERTI, A.; PICCIRILLO, E.M.; BELLIENI, G.; CIVETTA, L.; COMIN-CHIARAMONTI, P.; MORAIS, E.A.A. Mesozoic acid volcanics from Southern Angola: petrology, Sr-Nd

isotope characteristics, and correlation with the acid stratoid volcanic suítes of the Paraná Basin (south – eastern Brazil). Eur. J. Mineral, 4, 597-604, 1992.

ARMIENTI, P., PARESCHI, M.T., INNOCENTI, F., POMPILIO, M. Effects of magma storage and ascent on the kinetics of crystal growth: the case of the 1991–1993 Mt. Etna eruption. Contrib. Mineral. Petrol. 115, 402–414, 1994.

ARMIENTI, P. Decryption of igneous rock textures: crystal size distribution tools In: Minerals, Inclusions and Volcanic Processes. Rev. Mineral. Geochem. 69, 623–648, 2008.

BARCLAY, J. & CARMICHAEL, I. S. E. A hornblende basalt from western Mexico: water-saturated phase relations constrain a pressure-temperature window of eruptibility. J. Petrol., 45, 485-506, 2004.

BARKER, A. K.; HOLM, P. M.; PEATE, D.W.; BAKER, J. A. Geochemical Stratigraphy of Submarine Lavas (3-5 Ma) from the Flamengos Valley, Santiago, Southern Cape Verde Islands. J. Petrol., 50, 169-193, 2009.

BEATTIE, P. Olivine-melt and orthopyroxene-melt equilibria. Contrib. Mineral. Petrol., 115, pp. 103-111, 1993.

BELLIENI, G.; BROTZU, P.; COMIN-CHIARAMONTI, P.; ERNESTO, M.; ERNESTO, M.; MELFI, A. J.; PACCA, I. G.; PICCIRILLO, E. M.. Flood basalt to rhyolites suites in the southern Paraná plateau (Brazil): paleomagnetism, petrogenis and geodynamic implications. J. Petrol, 25: 579-618, 1984.

BELLIENI, G.; COMIN-CHIARAMONTI, P.; MARQUES, L. S.; MELFI, A. J.; NARDY, A. J. R.; PAPATRECHAS, C.; PICCIRILLO, E. M.; ROISENBERG, A. Petrogenetic aspects of acid and basaltic lavas from the Paraná plateau (Brazil): geological, mineralogical and petrochemical relationships. J. Petrol, 27: 915-944, 1986.

BERGER, J.; ENNIH, N.; LIEGEOIS J.-P.; NKONO, C.; MERCIER, J.-C. C.; DEMAIFFE, D. A complex multi-chamber magmatic system beneath a late Cenozoic volcanic field: evidence from CSDs and thermobarometry of clinopyroxene from a single nephelinite flow (Djbel Saghro, Morocco). In: ENNIH, N. & LIEGEOIS, J.-P. (Eds). The Boundaries of the West African Craton. London: Geological Society, 2008. 297, 509–524. Special Publications.

BEST, M. G. & CHRISTIANSEN, E. H. Origin of broken phenocrysts in ash-flow tuffs. Geol. Soc. Am. Bull., 109, 63-73, 1997.

BINDEMAN, I. N. Crystal sizes in evolving silicic magma chambers. Geology 31, 367-370, 2003.

BLAKE, S. & FINK, J. H. The dynamics of magma withdrawal from a density stratified dyke. Earth Plan Sci Lett 85, 516-524, 1987.

BLUNDY, J. & CASHMAN, K. Magma ascent and crystallization at Mount St. Helens, 1980-1986. Contrib. Mineral. Petrol. 140, 631-650, 2001.

BLUNDY, J. & CASHMAN, K. Petrologic reconstruction of magmatic system variables and processes In: Minerals, Inclusions and Volcanic Processes. Rev. Mineral. Geochem. 69, 179-239, 2008.

BOORMAN, S.; BOUDREAU, A.; KRUGER, F. J. The Lower Zone-Critical Zone transition of the Bushveld Complex: A quantitative textural study. J. Petrol. 45, 1209-1235, 2004.

BROWNE, B. & SZRAMEK, L. Rates of magma ascent and store. In: SIGURDSSON, H. The Enclyclopedia of Volcanoes. Second edition. San Diego: Academic Press, 2015. p. 203-214.

CAPRARELLI, G. & RIEDEL, S. P. A clinopyroxene–basalt geothermobarometry perspective of Columbia Plateau (NW-USA) Miocene magmatism. Terra Nova, 17, 265–277, 2005.

CASHMAN, K. V. Crystallization of Mount St. Helens 1980–1986 dacite: a quantitative textural approach. Bull. Volcanol. 50, 194–209, 1988.

CASHMAN, K. V. Textural constraints on the kinetics of crystallization of igneous rocks. Rev. Mineral. 24, 259–314, 1990.

CASHMAN, K. V. Groundmass crystallization of Mount St. Helens dacite, 1980– 1986: a tool for interpreting shallow magmatic processes. Contrib. Mineral. Petrol. 109, 431–449, 1992.

CASHMAN, K. V. & MARSH, B. D. Crystal size distribution (CSD) in rocks and the kinetics and dynamics of crystallization II: Makaopuhi lava lake. Contrib. Mineral. Petrol. 99, 292–305, 1988.

CASHMAN, K. V. & MCCONNELL, S. M. Multiple levels of magma storage during the 1980 summer eruptions of Mount St. Helens, WA. Bull. Volcanol, 68, 57-75, 2005.

CASTRO, J. M. & GARDNER, J.E. Did magma ascent rate control the explosive-effusive transition at the Inyo volcanic chain, California? Geology, 36 (4), 279-282, 2008. doi: 10.1130/G24453A.1

CASTRO, J. M.; SCHIPPER, C. I.; MUELLER, S. P.; MILITZER, A. S.; AMIGO, A.; PAREJAS, C. S.; JACOB, D. Storage and eruption of near-liquidus rhyolite magma at Cordón Caulle, Chile. Bull. Volcanol., 75, 702. 2013. doi: 10.1007/s00445-013-0702-9

CORDANI, U. G.; CIVETTA, L.; MANTOVANI, M. S. M.; PETRINI, R.; KAWASHITA, K.; HAWKESWORTH, C. J.; TAYLOR, P.; LONGINELLI, A.; CAVAZZINI, G.; PICCIRILLO, E. M. Isotope geochemistry of flood volcanics from the Paraná basin (Brazil). In: PICCIRILLO, E. M. & MELFI, A. J. (Eds). The Mesozoic flood volcanism of the Paraná

basin: petrogenetic and geophysical aspects. IAG-USP press, 1988. p. 157-178.

COUCH, S.; SPARKS, R. S. J.; CARROLL, M. R. Mineral disequilibrium in lavas explained by convective self-mixing in open magma chambers. Nature, 411, 1037-1039, 2001.

DAY, A., MEHNERT, K., NEUMANN, B. Channel 5 User Manual, HKL Technology A/S, Hobro, Denmark, 2001.

DINGWELL, D. B. Volcanic dilemma: Flow or blow? Science, 273, 1054-1055, 1996.

EICHELBERGER, J. C.; CARRIGAN, C. R.; WESTRICH, H. R.; PRICE, R. H. Non-explosive silicic volcanism: Nature, 323, 598-602, 1986. doi: 10.1038/ 323598a0.

EICHELBERGER, J. C. Silicic Volcanism: Ascent of Viscous Magmas from Crustal Reservoirs. Annu. Rev. Earth Planet. Sci., 23, 41-63, 1995.

FRANCIS, P. & OPPENHEIMER, C. Volcanoes. Second Edition. New York: Oxford University Press, 2003.

GALIPP, K.; KLÜGEL, A.; HANSTEEN, T.H. Changing depths of magma fractionation and stagnation during the evolution of an oceanic island volcano: La Palma (Canary Islands). J. Volcanol. Geotherm. Res., 155, 258-306, 2006.

GARLAND, F.; HAWKESWORTH, C. J.; MANTOVANI, M. S. M. Description and Petrogenesis of the Paraná Rhyolites, Southern Brazil. J. Petrol, 36(5), 1193-1227, 1995.

GIORDANO, D, RUSSELL J.K, & DINGWELL, D.B. Viscosity of Magmatic Liquids: A Model. EPSL, 2008.

GONNERMANN, H. M., & MANGA, M. Explosive volcanism may not be an inevitable consequence of magma fragmentation: Nature, 426, 432–435, 2003. doi: 10.1038/nature02138.

GUALDA, G. A. R.; GHIORSO, M. S.; LEMONS, R. V.; CARLEY, T. L. Rhyolite-MELTS: A modified calibration of MELTS optimized for silica-rich, fluid-bearing magmatic systems. J. Petrol., 53, 875-890, 2012.

HAMMER, J. E.; CASHMAN, K. V.; HOBLITT, R. P.; NEWMAN, S. Degassing and microlite crystallization during pre-climactic events of the 1991 eruption of Mt. Pinatubo, Philippines. Bull. Volcanol, 60, 355-380, 1999.

HENRY, C. D. & WOLFF, J. A. Distinguishing strongly rheomorphic tuffs from extensive silicic lavas. Bulletin of Volcanology, 54: 171-186, 1992.

HIGGINS, M. D. Crystal size distributions and other quantitative textural measurements in lavas and tuff from Egmont volcano (Mt. Taranaki), New Zealand. Bull. Volcanol. 58,

194–204, 1996.

HIGGINS, M. D. Origin of anorthosite by textural coarsening: quantitative measurements of a natural sequence of textural development. J. Petrol. 39, 1307–1323, 1998.

HIGGINS, M. D., 1999. Origin of megacrysts in granitoids by textural coarsening: a crystal size distribution (CSD) study of microcline in the Cathedral Peak Granodiorite, Sierra Nevada, California. In: CASTRO, A.; FERNANDEZ, C.; VIGNERESSE, J. L. (Eds.). Understanding Granites: Integrating New and Classical Techniques. London: Geological Society, 1999. 168, 207-219. Special Publication.

HIGGINS, M. D. Measurement of crystal size distributions. Am. Mineral. 85 (9), 1105–1116, 2000.

HIGGINS, M. D. A crystal size-distribution study of the Kiglapait layered mafic intrusion, Labrador, Canada: evidence for textural coarsening. Contrib. Mineral. Petrol. 144, 314–330, 2002.

HIGGINS, M.D. Quantitative Textural Measurements in Igneous and Metamorphic Petrology. Cambridge University Press, Cambridge, UK, 2006.

HIGGINS, M. D. & ROBERGE, J. Crystal size distribution of plagioclase and amphibole from Soufrière Hills Volcano, Montserrat: evidence for dynamic crystallization- textural coarsening cycles. J. Petrol. 44, 1401–1411, 2003.

HIGGINS, M. D. & ROBERGE, J. Three magmatic components in the 1973 eruption of Eldfell Volcano, Iceland: evidence from plagioclase crystal size distribution (CSD) and geochemistry. J. Volcanol. Geotherm. Res. 161, 247–260, 2007.

HIGGINS, M. D. & MEILLEUR, D. Development and emplacement of the Inyo Domes Magmatic Suite, California: Evidence from geological, textural (CSD) and geochemical observations of ash and lava. J. Volcanol. Geotherm. Res. 186, 280-292, 2009.

HILDRETH, W. & DRAKE, R. E. Volcan Quizapu, Chilean Andes. Bull. Volcanol., 54, 93-125, 1992.

ISHII, T. The relations between temperature and composition of pigeonite in some lavas and their application to geothermometry. Mineral. Journal, 8, 48-57, 1975.

JAUPART, C. & ALLEGRE, C. J. Gas content, eruption rate and instabilities of eruption regime in silicic volcanoes: Earth and Planetary Science Letters, 102, 413-429,1991. doi:10.1016/0012-821X(91)90032-D.

KLÜGEL, A.; HANSTEEN, T. H.; GALIPP, K. Magma storage and underplating beneath Cumbre Vieja volcano, La Palma (Canary Islands). EPSL, 236, 211– 226, 2005.

KRETZ, R. Transfer and exchange equilibria in a portion of the pyroxene quadrilateral as deduced from natural and experimental data. Geochimica et Cosmochimica Acta 46, 411-421, 1982.

KUDO, A. M. & WEILL, D. F. An igneous plagioclase thermometer. Contrib. Mineral. Petrol., 26, p. 52-65, 1970.

LANGE, R. A.; FREY, H. M.; HECTOR, J. A thermodynamic model for the plagioclase-liquid hygrometer/thermometer. Am. Mineral., 94, 494-506, 2009.

LE BAS, M. J.; LE MAITRE, R. W., STRECKEISEN, A.; ZANETTIN, B. A chemical classification of volcanic rocks based on the total alkali-silica diagram. J. Petrol., 27, 745-750, 1986.

LENTZ, R. C. F. & MCSWEEN, H. Y. J. Crystallization of the basaltic shergottites: insights from crystal size distribution (CSD) analysis of pyroxenes. Meteorit. Planet. Sci. 35 (5), 919-927, 2000.

LINDSLEY, D. H. Pyroxene thermometry. American Mineralogist, 68, 477-493, 1983.

LONGPRÉ, M. A.; TROLL, V. R; HANSTEEN, T. H., Upper mantle magma storage and transport under a Canarian shield-volcano, Teno, Tenerife (Spain). J. Geophys. Res., 113, 2008.

LOWENSTERN J. B., CHARLIER B. L. A., CLYNNE M. A., WOODEN J. L. Extreme U–Th disequilibrium in rift-related basalts, rhyolites and granophyric granite and the time scale of rhyolite generation, intrusion and crystallization at Alid Volcanic Center, Eritrea. J. Petrol, 47, 2105–2122, 2006. DOI: 10.1093/petrology/egl038.

MAITLAND, T. & SITZMAN, S. Electron Backscatter Diffraction (EBSD) Technique and Materials Characterization Examples. In: ZHOU, W. & WANG, Z. L. (Eds). Scanning Microscopy for Nanotechnology: techniques and applications. New York: Springer-Verlag, 2007. Ch. 2, p. 41-75**.**

MANGAN, M. T. Crystal size distribution systematics and the determination of magma storage times: the 1959 eruption of Kilauea Volcano, Hawaii. J. Volcanol. Geotherm. Res. 44, 295–302, 1990.

MANTOVANI, M. S. M.; CORDANI, U. G.; ROISENBERG, A. Geoquímica isotópica em vulcânicas ácidas da Bacia do Paraná e implicações genéticas associadas. Rev. Bras. Geoc., 15, 61-65, 1985.

MARSH, B. D. Crystal size distribution (CSD) in rocks and the kinetics and dynamics of crystallization; I. Theory. Contrib. Mineral. Petrol. 99, 277–291, 1988.

MARSH, B.D. On the interpretation of crystal size distributions in magmatic systems. J. Petrol. 39, 553–599, 1998.

MARTEL, C.; PICHAVANT, M.; BOURDIER, J.-L; TRAINEAU, H.; HOLTZ, F.; SCAILLET, B. Magma storage conditions and control of eruption regime in silicic volcanoes: experimental evidence from Mt. Pelée Earth Planet. Sci. Lett., 156, 89-99, 1998.

MATHEZ, E. A. Refinement of the Kudo & Weill plagioclase discrimination thermometer and its application to basaltic rocks. Contrib. Mineral. Petrol., 41, 61-72, 1973.

MOLLO, S.; DEL GAUDIO, P.; VENTURA, G.; IEZZI, G.; SCARLATO, P. Dependence of clinopyroxene composition on cooling rate in basaltic magmas: Implications for thermobarometry. Lithos, 118, 302-312, 2010. doi:10.1016/j.lithos.2010.05.006

MORDICK, B. E. & GLAZNER, A. F. Clinopyroxene thermobarometry of basalts from the Coso and Big Pine volcanic fields, California. Contrib. Mineral. Petrol., 152, 111-24, 2006.

MORGAN, D. J., JERRAM, D. A. On estimating crystal shape for crystal size distribution analysis. J. Volcanol. Geotherm. Res. 154, 1–7, 2006.

MORRISSEY, M. M. & MASTIN, L. G. Vulcanian eruptions. In: Sigurdsson, H., (Ed). Encyclopedia of volcanoes (Second Edition). San Diego: Academic Press, 2015. p. 463–475.

NARDY, A. J. R. Geologia e petrologia do vulcanismo mesozóico na região central da Bacia do Paraná, Tese de Doutoramento, Instituto de Geociências e Ciências Exatas, UNESP, 316 p, 1995.

NARDY A. J. R., ENZWEILER J., BAHIA F O. O., OLIVEIRA M.A.F., PENEREIRO M. A. V. Determinação de elementos maiores e menores em rochas silicáticas por espectrometria de fluorescência de raios-X: Resultados Preliminares. In: SBGq, Congresso Brasileiro de Geoquímica, 6, Resumo, p. 346-348, 1997.

NARDY, A. J. R.; OLIVEIRA, M. A. F.; BETANCOURT, R. H. S.; VERDUGO, D. R. H.; MACHADO, F. B. Geologia e estratigrafia da Formação Serra Geral. SP, UNESP, Geociências, 21: 15-32, 2002.

NARDY, A. J. R.; MACHADO, F. B.; OLIVEIRA, M. A. F. As rochas vulcânicas mesozóicas ácidas da Bacia do Paraná: litoestratigrafia e considerações geoquímico-estratigráficas. Revista Brasileira de Geociências, 38(1): 178-195, 2008.

NARDY, A. J. R.; ROSA, M. C.; LUCHETTI, A. C. F.; FERREIRA, M. L. C.; MACHADO, F. B.; OLIVEIRA, M. A. F. Parâmetros Físicos Pré-Eruptivos do Magmatismo Ácido da Província Magmática do Paraná: Resultados Preliminares. Geociências (UNESP. Impresso), 30, 575-588, 2011.

NATHAN, H. D. & VAN KIRK, C. K. A model of magmatic crystallization. J. Petrol, 19, 66-94, 1978.

NOGUCHI, S.; TORAMARU, A.; SHIMANO, T. Crystallization of microlites and degassing during magma ascent: constraints on the fluid mechanical behavior of magma during the Tenjo eruption on Kozu Island, Japan. Bull. Volcanol. 68, 432–449, 2006.

O'DRISCOLL, B.; DONALDSON, C. H.; TROLL, V. R.; JERRAM, D. A.; EMELEUS, C. H. An origin for harrisitic and granular olivine in the Rum Layered Suite, NW Scotland: a crystal size distribution study. J. Petrol. 48, 253-270, 2007.

O'DRISCOLL, B.; STEVENSON, C. E.; TROLLY, V. R. Mineral lamination development in layered gabbros of the British palaeogene igneous province: A combined anisotropy of magnetic susceptibility, quantitative textural and mineral chemistry study. J. Petrol. 49, 1187-1221, 2008.

PAMUKCU, A. S., GUALDA, G. A. R. & ANDERSON, A. T. Crystallization stages of the Bishop Tuff magma body recorded in crystal textures in pumice clasts. J. Petrol, 53, 589-609, 2012.

PARFITT, L.; WILSON L. Fundamentals of Physical Volcanology. First edition. Blackwell Publishing Ltda, 2008.

PETFORD, N. Which effective viscosity?, Mineral. Mag., 73, 167–191, 2009. doi:10.1180/minmag.2009.

PICCIRILLO, E. M.; RAPOSO, M. I. B.; MELFI, A.; COMINCHIARAMONTI, P.; BELLIENI, G.; CORDANI, U. G.; KAWASHITA, K. Bimodal fissural volcanic suites from the Paraná Basin (Brazil): K-Ar age, Sr-isotopes and geochemistry. Geochim. Brasil., 1, 53-69, 1987.

PIOCHI, M., MASTROLORENZO, G., PAPPALARDO, L. Magma ascent and eruptive processes from textural and compositional features of Monte Nuovo pyroclastic products, Campi Flegrei, Italy. Bull. Volcanol. 67, 663–678, 2005.

POLO, L. A., 2014. O vulcanismo ácido da Província Magmática Paraná-Etendeka na região de Gramado Xavier, RS: estratigrafia, estruturas, petrogênese e modelo eruptivo. 340 p. Tese (Doutorado), IGc, Universidade de São Paulo, São Paulo, 2014.

PRADO, J. C. 2015. Estratigrafia do vulcanismo mesozóico ácido da Província Magmática do Paraná. 97 p. Trabalho de conclusão de curso, IGCE, Universidade Estadual Paulista, Rio Claro, 2015.

PUTIRKA, K. Magma transport at Hawaii: inferences from igneous thermobarometry. Geology, 25, 69-72, 1997.

PUTIRKA, K. Igneous thermometers and barometers based on plagioclase + liquid equilibria: tests of some existing models and new calibrations. Am. Mineral., 90, 336-346, 2005.

PUTIRKA, K.; RYERSON, F. J.; MIKAELIAN, H. New igneous thermobarometers for mafic and evolved lava compositions, based on clinopyroxene + liquid equilibria. Am. Mineral., 88, 1542-1554, 2003.

PUTIRKA, K. & Condit, C. A cross section of a magma conduit system at the margins of the Colorado Plateau. Geology, 31, 701-704, 2003.

PUTIRKA, K. Thermometers and barometers for volcanic systems. Rev. Mineral. Geochem., 69, 61-120, 2008.

PUTIRKA, K.; KUNTZ, M. A.; UNRUH, D. M.; VAID, N. Magma Evolution and Ascent at the Craters of the Moon and Neighboring Volcanic Fields, Southern Idaho, USA: Implications for the Evolution of Polygenetic and Monogenetic Volcanic Fields. J. Petrol., 00, 1-27, 2009. doi:10.1093/petrology/egp045

RESMINI, R. G. & MARSH, B. D. Steady-state volcanism, paleoeffusion rates, and magma system volume inferred from plagioclase crystal size distributions in mafic lavas; Dome Mountain, Nevada. J. Volcanol. Geotherm. Res. 68 (4), 273–296, 1995.

RHODES, J. M.; DUNGAN, M. A.; BLANCHARD, D. P.; LONG, P. E. Magma mixing at mid-ocean ridges: evidence form basalts drilled near 22°N on the mid-Atlantic ridge. Tectonophys, 55, 35-61, 1979.

RUTHERFORD, M. & HILL, P. Magma ascent rates from amphibole breakdown: An experimental study applied to the 1980–1986 Mount St. Helens eruptions. J. Geophys. Res., 98(B11), 19667-19685, 1993.

SALISBURY, M. J.; BOHRSON, W. A.; CLYNNE, M. S.; RAMOS, F. C.; HOSKIN, P. Multiple plagioclase crystal populations identified by crystal size distribution and in situ chemical data: implications for timescales of magma chamber processes associated with the 1915 eruption of Lassen Peak, CA. J. Petrol. 49, 1755-1780, 2008.

SCHWARZ, S.; KLÜGEL, A.; WOHLGEMUTH-UEBERWASSER, C. Melt extraction pathways and stagnation depths beneath the Madeira and Desertas rift zones (NE Atlantic) inferred from barometric studies. Contrib. Mineral. Petrol., 147, 228–240, 2004.

SIMAKIN, A. G. & BINDEMAN, I. N. Evolution of crystal sizes in the series of dissolution and precipitation events in open magma systems. J. Volcanol. Geotherm. Res., 177, 997-1010, 2008.

SPARKS, R. S. J.; WILSON, L.; HULME, G. Theoretical modeling of the generation movement and emplacement of pyroclastic flows by column collapse. J. Geophys. Res. 83, 1727-1739, 1978.

VINET, N. & HIGGINS, M. D. Magma solidification processes beneath Kilauea Volcano, Hawaii: a quantitative textural and geochemical study of the 1969-1974 Mauna Ulu Lavas. J. Petrol., 51 (6), 1297-1332, 2010.

WHITTINGHAM, A. M., 1991. Stratigraphy and petrogenesis of the volcanic formations associated with the opening of the South Atlantic, southern Brazil. Ph.D. Thesis, Oxford University, Oxford, 1991.

WOODS, A. M. & KOYAGUCHI, T. Transitions between explosive and effusive eruption of silicic magmas: Nature, 370, 641-644, 1994. doi:10.1038 /370641a0.

ZELLMER, G. F. & ANNEN, C. An introduction to magma dynamics. Geological Society, London, Special Publications, 304, 1-13, 2008.

ZHANG, Y.; XU, Z.; ZHU, M.; WANG, H. Silicate Melt Properties and Volcanic Eruptions. Rev. Geophy., 45, 1-27, 2007.